UNIVERSITÀ
DEGLI STUDI
FIRENZE

DOTTORATO DI RICERCA TOSCANO IN NEUROSCIENZE

CICLO XXXI

COORDINATORE: Prof. Renato Corradetti

Bipolar Cells in Retinitis Pigmentosa: Influence of the Age of Phenotype Manifestation on the Nature and Severity of Remodeling

Settore Scientifico Disciplinare BIO/09

Dottorando

Dott.ssa Stefanov Antonia

(firma)

Tutore

Dott.ssa Enrica Strettoi

(firma)

Coordinatore

Prof. Corradetti Renato

(firma)

Prof.ssa Maria Concetta Morrone

(firma)

Anni 2015/2018

To my little brother,

without whom, probably, I would have never become a retinal scientist.

TABLE OF CONTENT

ABSTRACT

The majority of Retinitis Pigmentosa (RP) rodent models typically manifest a phenotype during various stages of retinal development, differing from what is usually observed in the human pathology, where the disease arises mostly during young adulthood, long after the completion of retinal development. This casts a shadow over the possibility of translating results gained from these developmental rodent models to the human retinopathy. Therefore, development of adult models of RP is of great need in this field of research.

Non-transgenic Tvrm4 mice, produced by chemical mutagenesis at the Jacksons Laboratory, bear a silent, photo-inducible point-mutation expressed on the 7th transmembrane domain of rhodopsin. The mutation can be activated in adulthood upon a short exposure to bright light, mimicking time of onset of typical human RP, in particular of a special form caused by rhodopsin mutations with focal, light sensitive phenotype and mild disease progression, often referred to as type B1 RP. Here we exploit Tvrm4 mice to gain insight into the nature, time-course and severity of inner retinal remodeling accompanying photoreceptor death, with a special attention to bipolar cells, key neurons for retinal repair strategies based on inner retinal integrity.

Specifically, this thesis focuses on inner retinal remodeling of adult Tvrm4 mice, also including observations carried on at developmental stages close to the time of eye-opening. Mice were photo-induced for 2 minutes with 12.000 lux irradiation and examined 3, 6 and 9 weeks following phenotype induction, to estimate long term effects of complete photoreceptor death in the central retina. Harvested retinal tissue was processed for immunohistochemistry or ultrastructural studies, imaged with the aid of Confocal and Transmission Electron Microscopy and analyzed in MetaMorph image analyzer and SigmaPlot.

High rate of bipolar cell survival despite regressive dendritic and axonal remodeling, considerable rate of horizontal cell death, ultrastructural remodeling of ribbon synapses and preservation of higher order neurons found in Tvrm4 mutants coincide with previously described characteristics of RP rodent models. Hence, we conclude that these remodeling features are independent of the age of disease onset and the underlying genetic mutation and are true hallmarks of RP.

In vivo photo-induction of Tvrm4 mice around the time of eye opening (P15 and P19) was possibly jeopardized by so far unidentified factors rescuing photoreceptors from light induced degeneration, possibly repressing oxidative stress and inflammation. And yet, when photoreceptor degeneration was successfully initiated, albeit at reduced rate, in young animals, the fundamental

features of the disease phenotype were similar to what found in the adults or in other RP mouse models. The reason of photoreceptor rosette formation surrounded by activated microglia in the retinal periphery is subject to further investigation.

The finding that remodeling in adult Tvrm4 mice is by no means more severe than in developmental models of the disease provides encouraging support for implementing retinal repair strategies for human RP. Furthermore, the inducible phenotype observed in Tvrm4 mice mimics faithfully type B1 human RP with focal photoreceptor senescence and moderate speed of disease progression. Therefore, we conclude, that the Tvrm4 mouse, a novel rhodopsin mutant with autosomal dominant inheritance pattern is a valuable and representative model of human RP.

1. INTRODUCTION

1.1. Bipolar cells of the mouse retina

A wide variety of light stimuli perceived by retinal photoreceptors (PRs), namely rod and cone cells undergoes complex processing before transmission to the next retinal and then brain station and eventually to the cerebral visual cortex. Retinal bipolar cells are second order neurons responsible for sorting, shaping and relaying "raw" visual signals received from PRs to highly specialized output neurons, the retinal ganglion cells (RGCs).

The mouse retina contains at least 11 different types of bipolar cells. This number becomes 13 if we consider 3a and 3b as well as 5a and 5b as different types (**Figure 1.1.**). The term 'bipolar cell' (BC) was first used by Tartuferi, a student of Camillo Golgi, who referred to those retinal interneurons projecting two protrusions, one towards the outer and one towards the inner retinal layers. Indeed, their bipolar morphology reflects well their function: they connect the outer retina, and in particular the PRs, to the inner retina, more precisely to the inner plexiform layer (IPL). The IPL is considered as a retinal 'switchboard': here the BC axonal endings stratify systematically at one or more different depths, known as "sublayers" or "strata", where they relay information to spatially segregated and functionally distinct amacrine and/or ganglion cell types. A fundamental blueprint of the vertebrate retinal architecture lies in the segregation of processes of cells which respond to light decrements (the so-called "OFF" cells in the most superficial part of the IPL (Layers 1-2), whereas cells mostly responsive to light increments (or "ON" cells) end in the deepest part of the IPL, composed by sublaminae 3-5. Based on stratification level of axonal arborizations, (right part of **Figure 1.**), we can distinguish between OFF (types 1-4) and ON (types 5-9) types of BCs which collect information from cones and are therefore known as cone bipolar cells (CBCs). However, there is only one type of rod bipolar cell (RBC), whose axonal arbors stratify in layer 5 and belongs to the retinal ON pathway (Strettoi, 1990; Wässle, 2004; Euler et al. 2014).

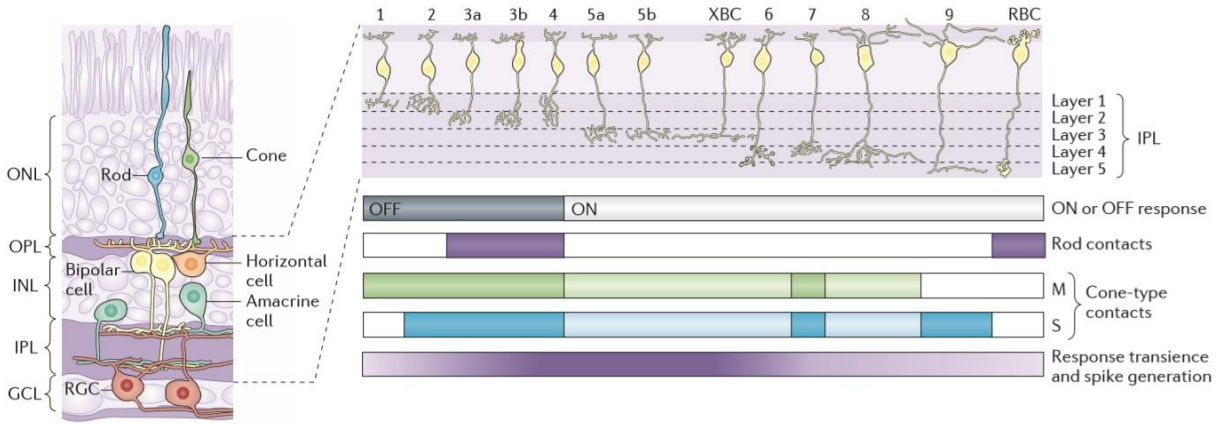

Figure 1.1. Schematic diagram of the distinct retinal bipolar cell types, their stratification properties and contacts (Euler et al., 2014)**.**

A complete classification of BCs based on morphological features has been possible using a combination of single-cell labeling techniques as well as exploiting the unique immuno-staining properties of distinctive populations of these neurons. Although some markers label homologous populations of BC types, for example the antibody against protein kinase C alpha (PKCα) labeling RBCs exclusively in the retinae of all mammalian species studied so far (Euler et al., 2014), other antibodies like calcium binding protein 5 (CaB5) stain heterogenous BC populations including RBCs and type 3 OFF BCs. The latter was subdivided into two additional types: type 3a, positive for the channels HCN4 and type 3b, positive for protein kinase A receptor subunit IIβ (PKARIIβ) (Mataruga et al., 2007). Finally, CaB5 antibodies also label type 5 ON cone BCs in the mouse retina (Haverkamp et al., 2008).

A panel of antibodies and transgenic markers largely used to label BCs in the mouse retina is summarized in **Figure 1.2.**: all ON type BCs are positively labeled by G0α and Gγ13 (Vardi, 1998; Huang et al., 2003); type 9 cells express Clomeleon in the Clomeleon 1 mouse line (Haverkamp et al., 2005); type 7 cells express green fluorescent protein (GFP) in the GFP-GUS mouse line (Huang et al., 2003); type 1 and 2 OFF cone BCs are immunoreactive for (NK3R) (Ghosh et al., 2004), but can only be distinguished by a co-staining for synaptotagmin/ZNP1, which is selective for type 2 whole cells and type 6 axonal endings (Wässle et al., 2009); type 4 OFF cone BCs express the calcium binding protein calsenilin (Csen), but there is no marker currently available to discriminate type 6 and 8 ON cone bipolars (Haverkamp et al., 2008). Additionally, another calcium binding protein, secretagogin (SCGN) was recently reported to label type 2, 3, 4, 5, 6 and probably type 8 cone BCs in the mouse retina (Puthussery et al., 2010). Finally, as reminded above, RBCs can be stained with PKCα antibodies.

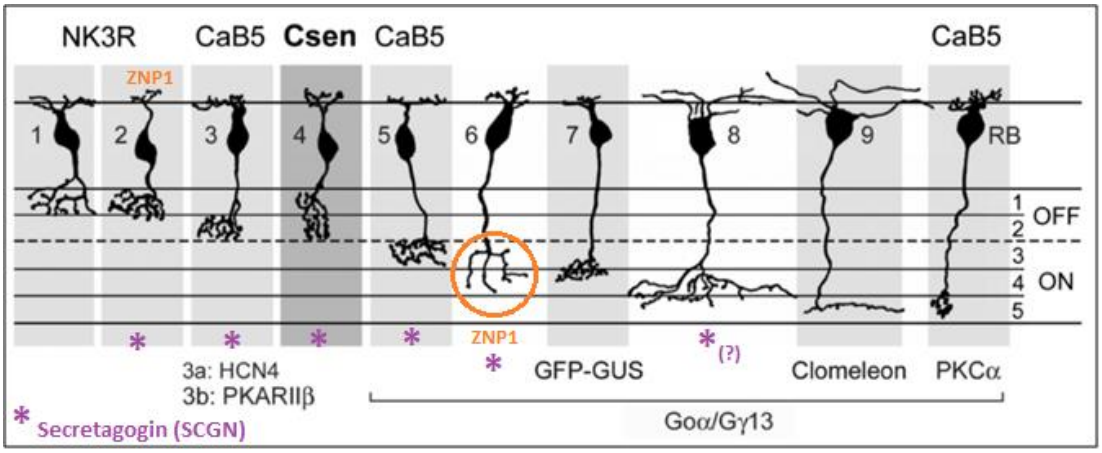

Figure 1.2. Summary of the available bipolar cell markers in the mouse retina. From Haverkamp et al. 2008, modified according to Wässle et al. 2009 and Puthussery et al. 2010.

As already mentioned rather than simply conveying the information from PRs to the next retina station, BCs are responsible for the primary, first-step processing of visual signals. Processing starts with sorting: in the mouse retina, 4 types of PRs (S-cones, M-cones, dual-cones, co-expressing S and M photo pigments, and rods) send signals to 11 types of BCs (10 types of cone and 1 type or rod BC), which are then further dividing the signals among at least 20 morphologically and functionally distinct ganglion cell (GC) types. Shaping of the PR input signals depends on a number of factors: these include the size and morphology of the BC dendritic tree and, more in general of the BC cell itself; the PR types contacted; the glutamate receptor subtypes expressed on the BC dendrites; the set and distribution of ion channels expressed by the BC. All these elements influence BC physiology and thus the operational properties. In addition, BC output at the axonal endings is influenced by targeted and selective inhibitory inputs from a large set of different amacrine cells (AC), and is dependent on the previous state (history of activity) of the BC itself, in the end resulting in unique and time-dependent patterns of glutamate release from BCs to postsynaptic ACs and GCs (Wässle, 2004; Euler et al. 2014).

It is well known that the dichotomy between ON and OFF responses is generated in the outer retina by the nature of the distinctive types of glutamate receptors expressed by BCs. OFF BCs express AMPA and kainate receptors, cation channels opened by glutamate. Since PRs are hyperpolarized by light, they decrease glutamate release. Hence, OFF BCs hyperpolarize too, as a result of reduced cations entering the cells. These photoreceptor-to-bipolar synapses are referred to as ’sign conserving’. Conversely, ON BCs express metabotropic glutamate receptors, which close the cation channel TRPM1 upon glutamate binding. This way ON BCs depolarize in response to PR

hyperpolarization, making the synapse 'sign inverting' (Morgans et al. 2009; Shen et al. 2009; Masland, 2012).

Another differentiation among BC types can be applied based on their sustained or transient response patterns, which depends on the expression of rapidly or slowly inactivating glutamate receptors (Awatramani and Slaughter, 2000; DeVries, 2000). Four functional classes of BCs are therefore created: ON-sustained, ON-transient, OFF-sustained and OFF-transient. These show a wide variety of differences in their light response waveforms, not only in the simple tonic-versus phasic temporal domain but because of the complex and versatile combinations of the two sets of receptors and channels (Wu et al., 2001). The functional outcome of the aforementioned waveforms is still actively studied. A possible, additional shaping factor might depend on the expression of different subsets of regulator of G-protein signaling (RGS) proteins, which act in ON BCs modulating the response to synaptic input kinetics (Cao et al., 2012).

1.2. Parallel processing in the mouse retina

Processing of the visual information begins with horizontal cells and BCs, sorting the primary signals sent by rods and cones (Masland, 2012).

Horizontal cells (HC) have a considerable lateral spread and are coupled through gap junctions, also known as electrical synapses, constituting channels between adjacent cells allowing the exchange of ions, second messengers and small metabolites. According to nowadays' leading theories, HCs measure and average the level of illumination falling upon a particular region of the retina and send an inhibitory output to rod and cone PRs and probably to the dendrites of BCs, overall exerting a so-called "local gain control". This is an extremely important role, since in an environment with objects of different brightness, a very bright object would dazzle vision like a bright object in dim light saturates a camera's chip. Therefore, it is of high importance to adjust the input to the inner retinal network keeping it within the optimal operating range of the circuit (Herrmann et al., 2011; Masland, 2012).

Synaptic terminals of rod PRs, called spherules, contain a highly specialized presynaptic machinery, the synaptic ribbon, a complex structure shaped like a bi-dimensional, protein sheet optimized to tethering synaptic vesicles, which in PRs contain glutamate as a neurotransmitter. A rod spherule typically possesses one single ribbon synapse, which is opposed to the invaginating processes of HCs and BCs. The dendritic processes of HCs, which are usually two, approach the ribbon laterally leaving space in the middle for one or two BC processes, invaginating in central position to contact the presynaptic terminal. Within the invagination, ionotropic glutamate receptors

(GluR - receptors that exert effects through modulation of ion channel activity) are expressed on the dendritic tips of HC processes, whereas BC processes express the metabotropic mGluR6 receptors. The latter is associated with G proteins and exert effects through enzymatic activation. RBCs depolarize upon light stimuli and therefore belong to the functional group of ON-bipolar cells. In a mouse, each RBC dendritic arborization contacts 20-80 rod spherules (Wässle, 2004), while the axon, emerging from the inner aspect of the cell body, terminates in large, bulbous endings reaching sublamina 5 of the IPL, close to the GC layer. RBCs, as a rule, do not make direct synaptic contacts with GCs dendrites, but instead synapse with inner dendrites of a bistratified amacrine cell, called AII (**Figure 1.3.**). Similar to RBCs, AIICs depolarize in response to a light stimulus. Converging inputs from multiple RBCs are collected by AII inner dendrites; at that point, a dichotomy is generated, insofar the AII AC makes electrical synapses/gap junctions with the axonal terminals of ON cone BCs (Fig. 2, ON1), also arborizing in the deepest half of the IPL; and inhibitory, chemical synapses on the axonal endings of OFF cone BCs in the outer half of the IPL(Fig. 2, OFF1). Finally, both ON and OFF CBCs establish direct synaptic contacts with dendrites of GCs (Strettoi et al. 1990, 1992, 1994). The described 5-neurons circuit represents the 'classical rod pathway' of the mammalian retina, a highly sensitive network capable of detecting the absorption of one single photon.

Alternative routes can transmit rod signals to GCs. An example of such alternative rod pathway is represented by gap junctions between rod and cone PR terminals, called pedicles (Fig. 2, OFF2). Another route is constituted by cone BCs contacting rod spherules directly (Fig. 2, OFF3), altogether demonstrating the existence of at least three circuits carrying the rod signals outside the retina (Wässle, 2004; Morgans et al. 2009; Shen et al. 2009).

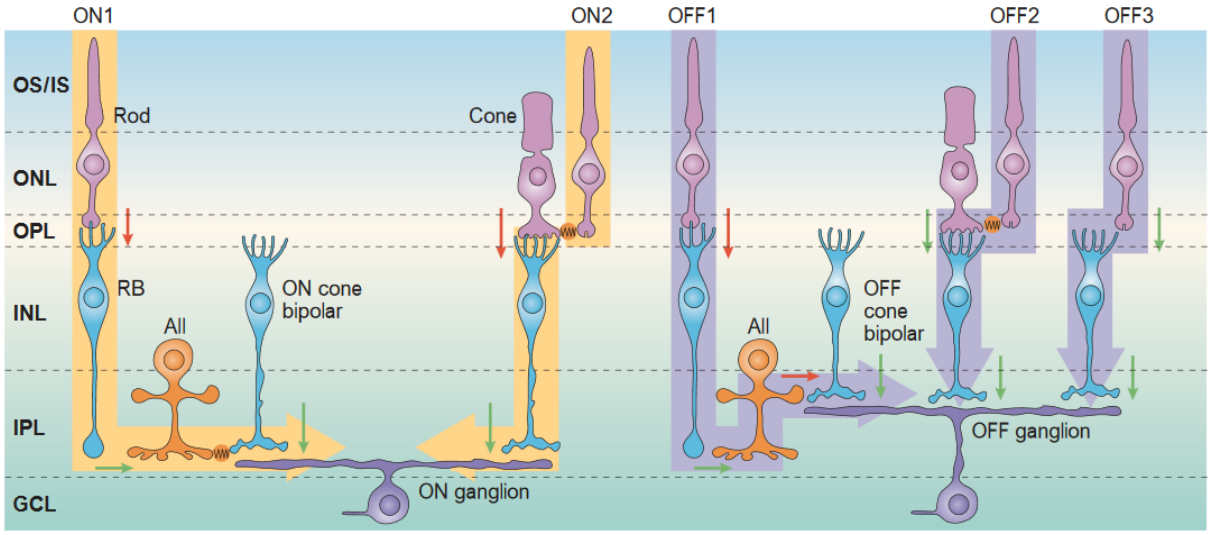

Figure 1.3. Summary of the rod pathways of the mammalian retina. Laminar distribution of the retina: OS/IS – outer and inner segments of photoreceptors; ONL – outer nuclear layer; OPL – outer plexiform layer; INL – inner nuclear layer; IPL – inner plexiform layer; GCL – ganglion cell layer. Red arrows represent sign inverting synapses, while green arrows stand for sign preserving synapses. (Wässle, 2004; modified from Demb et al. 2002)

Cone PRs – similarly to rods – release glutamate through their complex synaptic terminal, the pedicles, containing 20-50 ribbon synapses (Wässle, 2004). Like rods, they are depolarized in the dark, which therefore corresponds to the phase of maximum transmitter release and is reduced upon graded hyperpolarization induced by light. The synaptic ribbons are opposed to invaginating processes of HCs and ON cone BCs, while OFF cone BC processes synapse to the base of the cone pedicles. Pedicles are this way capable of making a very large number of contacts (up to 500 in the central retina of a primate) even though the number of types of postsynaptic cells is smaller. Each postsynaptic element (at least two types of HCs and eight different types of cone BCs) sends multiple processes to the same cone terminal.

As previously specified, postsynaptic neurons express different sets of glutamate receptors: HCs and OFF cone BCs, which hyperpolarize to light, express ionotropic AMPA and kainate glutamate receptors, while ON cone BCs, which depolarize upon exposure to light stimuli, express the metabotropic mGluR6 receptor. OFF cone BC axons stratify in the OFF layers of the IPL and transfer their signals onto OFF GCs, hence OFF GCs get excited by stimuli that are darker than the background. Conversely, ON cone BC axonal endings terminate in the ON layers – 3-5 sublaminae of the IPL – and synapse to ON GCs exciting them with signals brighter than the background (Wässle, 2004; Morgans et al. 2009; Shen et al. 2009).

BC responses, which are already selective, are further fine-tuned by ACs, whose dendrites form complex networks deputed to feedback and feedforward inhibition, ultimately contributing to the

establishment of highly specified GC subtypes. The second class of inhibitory interneurons (the first being represented by HCs) occupies a central but quite hardly accessible place in the retina: ACs are axonless neurons and it is sometimes challenging to recognize input and output sites on their dendritic arbors. They synapse not only onto GCs, but also with each other, and they send feedbacks to the same BCs that drive them (Strettoi et al. 1990; Lin et al., 2000; Jusuf et al., 2005; Eggers and Lukasiewicz, 2011; Masland, 2012). Their overwhelming morphological diversity, for which one can distinguish large, small and medium-field neurons of great variety and different frequency in the retina, is another factor making experimental targeting of specific AC types extremely daunting. Yet, continuous efforts are being made to extend our present knowledge on ACs physiology, especially for those exemplars for which a genetic marker or a specific staining method exist. The available repertoire of experimental tools is capable of distinguishing approximately 30 different types of ACs (Masland, 2012). Regarding their functions, three general principles have been identified:

- ACs are responsible for shaping motion detection sensitivity of a subset of GCs. In other words, ACs allow certain GCs to distinguish true motion of an object from overall movement of the scene or the observer, for example due to head and/or eye movements, when everything is shifting on the surface of the retina at the same time (Masland, 2012).
- Probably, most AC types (and in particular small-field ACs) carry out some sort of ’vertical integration’, intercommunicating among many, if not all, the layers of the IPL. An example is type 7 glycinergic AC, stretching across all the IPL layers and carrying OFF information into the ON laminae and vice versa (**Figure 1.4.**; Menger et al., 1998). This type of communication is termed as crossover inhibition, due to the fact that ACs release gamma aminobutyric acid (GABA) or glycine, both inhibitory neurotransmitters (Molnar et al., 2009).
- Most of the ACs have highly specific tasks. For example, A17 AC is a wide-field cell making synaptic contacts to the RBC axonal endings within reach, using electrically isolated synaptic boutons. These contacts provide an inhibitory feedback in return to the RBC input sent to the same A17 cell, supposedly improving the accuracy of RBC signaling (Strettoi et al. 1990; Grimes et al., 2010; Masland, 2012) and definitely enhancing the transient component of AII amacrine responses (Raviola and Dacheux, 1987).

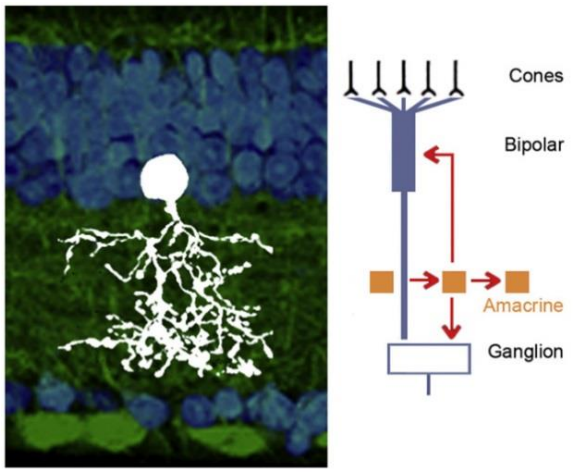

Figure 1.4. Image of type 7 glycinergic AC adapted from Menger et al. 1998 (left); schematic diagram (right) of AC connectivity and inhibitory activities, showing how ACs provide circuitry for lateral, feedforward and feedback inhibition across the retina (Masland, 2012).

The main characteristic according to which BCs are classified is the IPL layer corresponding to the level of their axonal arbor stratification. BCs dendrites collect input from all the cones within reach, but their axonal terminals are available only for a restricted set of postsynaptic partners. Restricted laminar stratification is generally true for all BCs and GCs types. They may stratify in a narrow layer, or a wider one or even in multiple ones, but always according to specific, stereotyped rules (Masland, 2012). The output signaling of BCs is selectively sampled by different sets of retinal GCs (**Figure 1.5.**); however, because BC signals combine with inputs from different ACs, the overall number of GC types in the retina exceeds the number of BC types (Taylor and Smith, 2011).

The number of retinal GC types is hard to estimate, for no universally standardized classification exists and new cell types, possibly occurring at low frequencies, are found constantly. According to the most widely accepted view, the overall number of different GC types lies close to 20 (Masland, 2012). This may sound like a high number of cell types projecting axons to the brain. We should keep in mind however, that there are nine modality-specific channels for touch, five for taste and over 300 for smell. Considering that the visual cortex occupies ~50% of the cortex in primates (Van Essen, 2004), it would have been unlikely for vision to possess only the two channels (ON and OFF) postulated in the early days of visual system physiology. Assuming the existence of 20 univocally distinguishable GC types, it has to be said that at least half of them have not yet been functionally characterized even for the retina of the rabbit, where GC studies are at the most advanced stages, while an even smaller fraction has been thoroughly described in the retina of rats, mice, cats or primates (Masland, 2012).

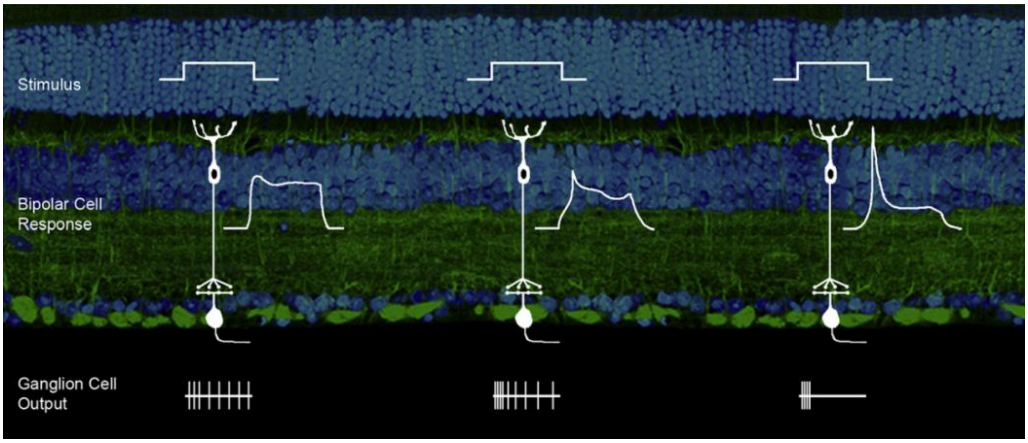

Figure 1.5. Schematic summary of how different BCs with diverse temporal properties contact different types of GCs with different response properties (Masland, 2012).

1.3. Retinal ribbon synapses

Years of research have elucidated the fine structure of synaptic ribbons, plate-like, proteinaceous bodies which appear dense in transmission electron microscopic (TEM) images, surrounded by a halo of synaptic vesicles. These specialized machineries are found in the presynaptic terminals of cochlear hair cells, pineal photoreceptors, retinal PRs as well as retinal bipolar neurons (**Figure 1.6.**). The output synapses of these sensory neurons share the necessity of providing fast signaling to follow rapidly changing stimuli, using graded signals to transmit information, and covering a wide range of stimulus intensities in a sustained manner (Sterling and Matthews, 2005). Moreover, they provide simultaneous output signals onto multiple, postsynaptic partners.

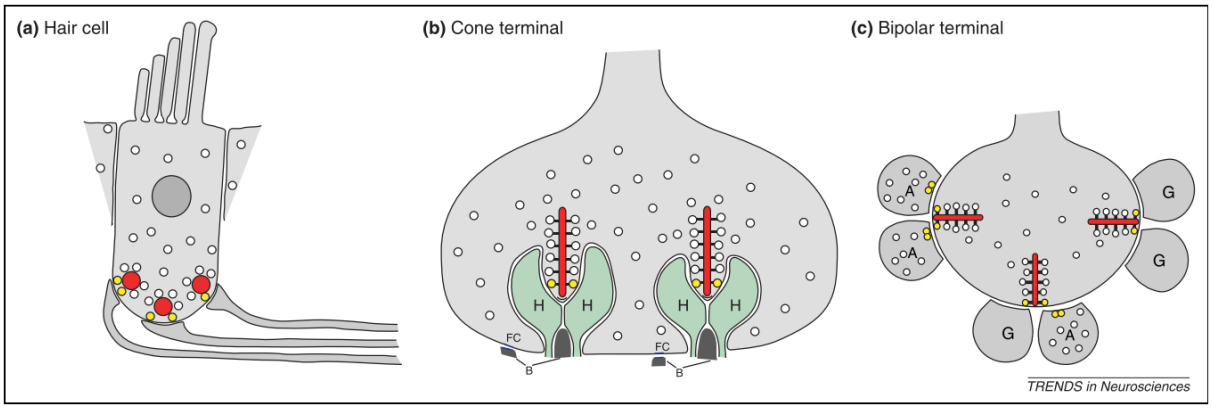

Figure 1.6. A schematic summary of the occurrence of synaptic ribbons in vertebrates by Sterling and Matthews, 2005.

Ribbons are heterogeneous organelles that vary in size, number and in the number of tethered vesicles depending on activity and cell type. Vesicles are tethered to the ribbon by fine filaments made of yet unknown components. Vesicle tethering occurs along all the possible dimensions and

the whole length of the ribbon except for the basal region, characterized by the so called arciform density, which in TEM pictures appears as an osmiophilic 'shadow', anchoring the ribbon to the active zone membrane (Sterling and Matthews, 2005).

Ribbon synapses are associated with numerous tasks within the output area of the presynaptic terminal. They are responsible for directing synaptic vesicles to the active zone, organizing them for priming and membrane fusion before release, as well as for synchronizing exo- and endocytosis. Photoreceptor ribbons exhibit activity-dependent dynamics. In darkness, due to depolarization induced by open cation channels, ribbons can support release of neurotransmitter (glutamate) continuously, at high rates; however, in light conditions, special protein interactions allow them to dissociate from the active zone and float freely in the cytoplasm (Lenzi and von Gersdorff, 2001; Parsons and Sterling, 2003).

A wide variety of proteins participate in the organization of these highly specialized ribbon synapses. RIBEYE is a ~120kDa complex constituting the majority of the ribbon's mass and specific for this organelle. By interacting with RIBEYE, another protein, named Bassoon, is responsible for the anchoring of ribbons at the active zone. Similar interactions with Guanylate-cyclase activating protein 1 (GCAP), on the other hand, result in the dissociation of ribbons from the active zone. RIBEYE is attached to the voltage-gated Ca2+ channels as well, probably through Munc119 and CaBP. A member of the kinesin-type motor proteins, KIF3A is also found in synaptic ribbons, however its function is still questioned. Several other proteins in the cytomatrix of the active zone (CAZ) like Piccolo (associated with BC ribbon anchoring and maintenance of its morphology), RIM (regulating synaptic vesicle fusion), Munc13-1 and CAST (playing a role in Ca-dependent exocytosis) help the fine synchronization of the ribbon's specific functions (Ohtsuka et al., 2002; Sterling and Matthews, 2005).

Defects in the synaptic ribbon morphology and function have been associated to specific alterations of neuronal communication in a variety of ocular diseases, such as X-linked congenital night blindness, rod-cone dystrophies, RP and glaucoma, which explains why special attention should be payed to these organelles in medical research (tom Dieck and Brandstätter, 2006).

1.4. Retinal gap junctions

The speed of communication between neurons is of crucial importance for the rapid integration and propagation of signals in the retina, just like in the brain. Although chemical synapses are the most common forms of inter-neuronal signal transmission, there are considerable differences in communication velocity between conventional and electrical synapses, also known as gap junctions.

Gap junctions are structurally assembled of two hemi channels called connexons, each one composed of six transmembrane protein subunits called connexins (**Figure 1.7.**). These form a channel between the cytoplasm of two adjoining cells, allowing intercellular diffusion of ions and small molecules of up to 1 kDa size. Most retinal neurons are electrically coupled, although research to map gap junctions in all retinal layers is still undergoing. Briefly, gap junctions couple cones-to-cones, cones-to-rods, rods-to-rods, HCs-to-HCs, AII ACs-to-AII ACs, AII ACs-to-cone BCs and ON direction-selective GCs to each other (Bloomfield and Völgyi, 2009).

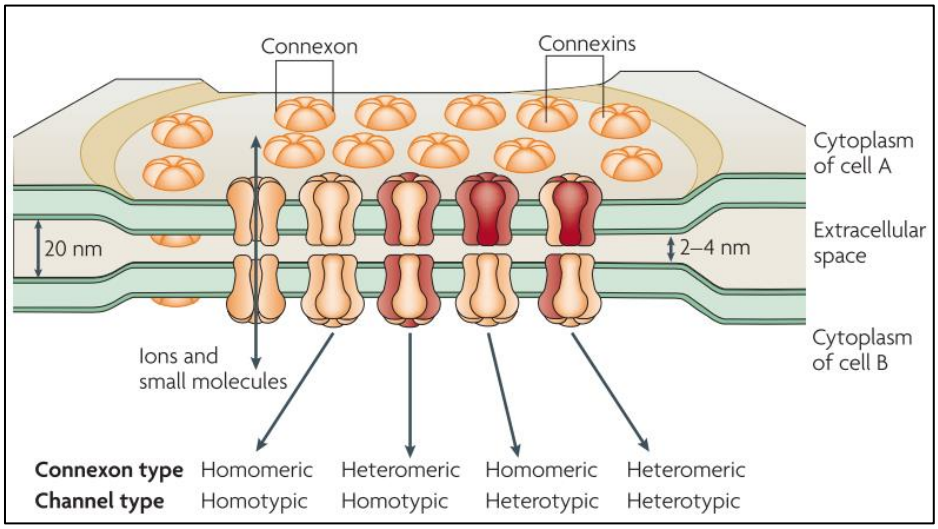

Figure 1.7. Schematic drawing showing the structure of gap junctions (Bloomfield and Völgyi, 2009).

Similarly to ionic channels, the conductance of gap junctions is controlled by numerous factors. Posttranslational modification by phosphorylation is one of them. Light activated neuromodulators, like dopamine and nitric oxide (NO), released by specialized AC subpopulations, trigger a number of intracellular signaling pathways activating cAMP- and cGMP-dependent protein kinases. These are responsible for the phosphorylation or dephosphorylation of gap junction connexins, increasing or decreasing their conductance in a light dependent manner, depending on the type and activity of the retinal neuron in which they are expressed (Witkovsky and Dearry, 1991; Bloomfield et al., 1997; Xin and Bloomfield, 1999; Xin and Bloomfield, 2000; Lampe and Lau, 2000; Lampe and Lau, 2004). Gap junction conductance is also dependent on cytosolic Ca^{2+} levels acting through calmodulin, a Ca-binding protein in direct contact with the connexins, causing gap junctions to close if Ca^{2+} levels rise above a certain threshold (Rose and Loewenstein, 1977; Peracchia, 1978; Peracchia et al., 1996; Török et al., 1997; Peracchia et al., 2000; Lurtz and Louis, 2007). Intracellular pH is another factor directly affecting the electrical coupling of two or more neurons in an activity dependent manner, since changes in proton levels reflect neuronal activity. An elevation

in proton levels most often results in reduced conductance of certain gap junctions, whereas a more basic environment usually increases the conductance rate. An exception, which however confirms the rule, is represented by the conductance of connexin36 (CX36) gap junctions, largely expressed in the retina, which decreases upon alkalosis in sharp contrast with others responding in the same way upon acidosis (Spray et al., 1981; González et al., 2008). Last but not least, gap junctions in most mammals are sensitive to the voltage differences of the cell membrane, a second example of activity-dependent conductance modulation. However, it is important to note that aperture and closure of gap junctions is a graded, rather than an all-or-none change (Spray et al., 1979; Moreno et al., 1991; Moreno et al., 1994).

A wide range of neuro-pathologies have been linked to defects in gap junctions both in the central and in the peripheral nervous system. Therefore, broadening our understanding of the functional role of gap junctions, their regulation and the dynamic connection between electrical and chemical signaling is an important future challenge for which the neural retina will definitely constitute an essential resource (Nakase and Nasus, 2004; Bloomfield and Völgyi, 2009).

1.5. Retinal degeneration and remodeling

Retinal and/or PR degeneration can be triggered by a large variety of genetic defects: rhodopsin gene mutations, defects in the retinal pigmented epithelium, in ciliary or transport proteins, abnormalities in the members of the phototransduction cascade or closure, like transducin or arrestin, mutations affecting metabotropic glutamate receptors, alterations of signal transduction components etc., just to mention a few. So far, hundreds of mutations in more than 70 different genes have been identified (RetNet), all of them leading to various forms of Retinitis Pigmentosa (RP) and RP-like retinopathies (Jones et al. 2012).

Degeneration of PRs initiates a long chain of events eventually leading to remodeling of the whole retina. Remodeling is usually a regressive phenomenon which begins in neurons postsynaptic to dying PRs and exhibiting (in first place) the consequences of neural deafferentation; this form of remodeling occurs in all forms of retinal degeneration sharing partial or complete PR loss. Remodeling progresses through three well defined phases of morphological and functional revision of the retinal cellular and connective network (Strettoi et al., 2003; Marc et al. 2007; Jones et al. 2011; Jones et al. 2012) (**Figure 1.8.**).

During phase 1, PR loss is partial, but initial signs of stress are detectable in form of opsin delocalization in surviving PRs (both rods and cones), as well as in alterations of glutamate receptor expression on BC dendrites (Strettoi and Pignatelli, 2000). In addition, as rod degeneration is

advancing, RBCs might make transient, ectopic synapses with cones (Puthussery et al., 2009). This is believed to cause a shift in BC function from ON to OFF response polarity (Marc et al. 2007; Jones et al. 2011; Jones et al. 2012).

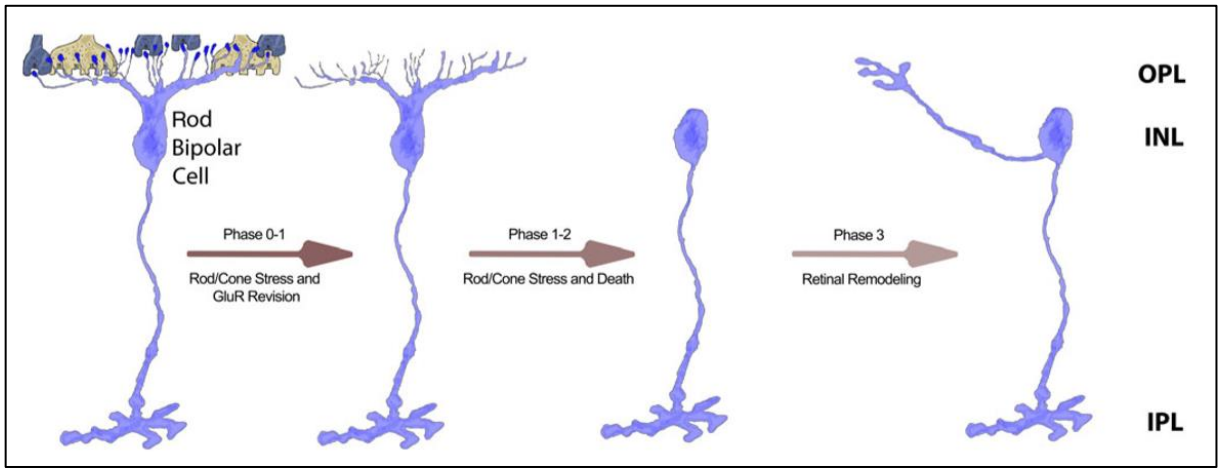

Figure 1.8. Schematic summary of the three phases of retinal remodeling according to the findings of Enrica Strettoi, Robert Marc and Brian Jones (Strettoi et al., 2003; Jones et al. 2012).

In phase 2, remodeling of the ONL becomes emphasized with advancing PR cell death and removal of dead cells by increased phagocytic activity of retinal microglia and invading macrophages. Müller cells turn hypertrophic with overexpression of glial fibrillary acidic protein (GFAP) and start to fill in the 'wounded' areas of the retina lacking PRs, subsequently sealing the neural retina from the retinal pigmented epithelium (RPE) and choroid. In the absence of PRs, BCs become deafferented: morphologically, by retracting and losing their dendritic trees, partially or completely, depending on whether the disease is cone-sparing or, as is the case of several forms of RP, cone-decimating; and functionally, due to the massive downregulation of glutamatergic receptors in the outer plexiform layer (OPL) (Strettoi and Pignatelli, 2000; Marc et al. 2007; Jones et al. 2011; Jones et al. 2012).

Phase 3 represents advanced stages of retinal degeneration and remodeling further altering the fundamental topology of the retina due to bidirectional, vertical migration of surviving, remnant neurons: BCs and ACs move into the ganglion cell layer (GCL); conversely, GCs relocate towards the INL (Jones et al., 2005). Evolution of new processes from the remaining cell types is also a characteristic feature of phase 3. Some new processes tend to form fascicles capable of stretching to great distances traveling in bundles within the neural retina; some others form tangles of neuropils termed micro-neuromas, typically extending outside the normal boundaries of the IPL. Pigmented granules of RPE origin, termed bone spicules, are a common finding in the neural retinal of patients

with RP therefore are responsible for the name of the disease. They are typical to animal models of the disease as well (Marc et al. 2003; Jones et al., 2005; Marc et al. 2007; Jones et al. 2011; Jones et al. 2012).

Functional remodeling goes hand in hand with morphologic abnormalities during retinal degeneration. Changes in metabotropic glutamate receptor expression patterns on BC dendritic tips, in parallel with advancing rod PR death, result in progressive alterations in the response kinetics of mGluR6-induced currents in RBCs based on whole-cell patch-clamp recordings. The fact that ON-CBCs retain close to normal response kinetics for a longer time than RBCs could be the net result of slower cone death progression, likewise the even longer preservation of ionotropic glutamate currents in OFF-CBCs (Puthussery et al., 2009). Calcium imaging of cones, RBCs and HCs revealed synchronized clusters of spontaneous oscillatory activity driven by these cells in the outer degenerated retina, seemingly driven by GABA-ergic inputs from HCs and/or feasibly interplexiform ACs also known as dopaminergic ACs. Deletion of gap junctions in cones reduced the observed rhythmic activity in the outer retina demonstrating that electrical coupling of cones plays a pivotal role in the generation of the aforementioned phenomenon (Haq et al., 2014). Similarly, in the inner degenerated retina, ectopic interactions between AII ACs and CBCs trigger aberrant spontaneous oscillatory spiking activity in GCs, however unlike in the outer retina, where voltage-gated Ca^{2+} channels were found to be responsible for this activity, in the inner retina, traces of the source of the mechanism lead to voltage-gated Na^{+} and K^{+} channels of AII ACs based (Stasheff, 2008; Sekirnjak et al., 2009; Stasheff et al., 2011; Borowska et al., 2011; Trenholm et al., 2012).

1.6. Retinitis Pigmentosa

The term, Retinitis Pigmentosa (RP) refers to a group of hereditary rod-cone dystrophies that are among the leading causes of inherited blindness around the world with an estimated prevalence of 1/4000 (Hamel 2006). First symptoms in patients usually arise during teenage years and comprise night blindness and tunnel vision, later advancing into central visual field loss and legal blindness (Heckenlively, Yoser, Friedman, & Oversier, 1988; Wong, 1997). Fundus examination (**Figure 1.9.**) may reveal pigmented bone spicules invading the neural retina from the adjacent RPE, thinning of the retinal tissue as a result of PR death, as well as attenuation of blood vessels and pallor of the optic nerve head (Marc et al., 2003).

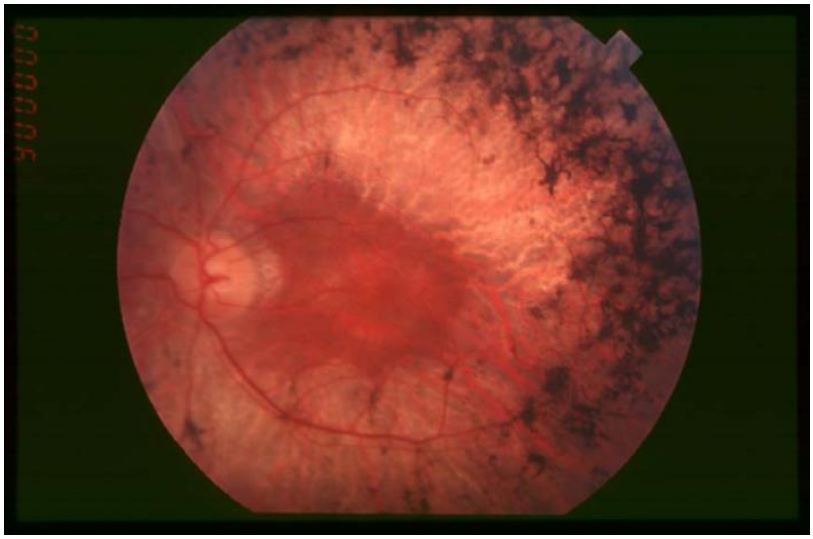

Figure 1.9. Fundus of a patient with Retinitis Pigmentosa, mid stage (Hamel 2006)

RP, like other inherent retinopathies, is caused by mutations usually in retinal specific genes, most commonly PR and RPE gene-mutations. The rhodopsin gene (*rho*) encoding for rhodopsin protein (RHO), expressed in rod PRs, was the first found to harbor RP-related mutations; at present, as many as 100 different mutations (many of them causing RP) are known for this gene alone (Dryja & Li, 1995; Gal, Apfelstedt-Sylla, Janecke, & Zrenner, 1997).

Inheritance of RP can be extremely versatile. Autosomal dominant (AD) RP is usually the mildest form, typically manifesting after the age of fifty, although severe disease cases can also belong here (Hamel 2006). AD RP caused by RHO mutations may be subdivided into two major types – A and B – according to disease progression. Type A patients are characterized by fast and aggressive disease development with early onset night blindness, while symptoms become severe more slowly in type B patients (Cideciyan et al., 1998; Gal et al., 1997). Type B RHO mutations can be further subdivided in B1, with focal phenotype, restricted to specific retinal areas, and B2, where the phenotype is pan-retinal. Although in general most RP-causing RHO mutations are characterized by light sensitivity in patients, this is especially true for B1 type patients, where in addition to hypersensitivity to brightness, strong light exposure has been associated with triggering and/or accelerating disease progression (Cideciyan et al., 1998).

Autosomal recessive forms of RP are known to be very severe and manifest already in the first decade of the patient's life, although in some cases mild disease progression has been reported. X-linked RP is known to cause severe forms of the disorder as well, frequently associated with myopia. In spite of the fact that theoretically, X-linked forms are transmitted recessively, and thus only male offspring should be affected, rare cases with dominant inheritance pattern and affected

female offspring have been registered as well. A very rare, digenic form of RP was also described, where a combination of heterozygous mutations in *ROM1* (encoding for rod outer segment membrane protein 1) and heterozygous mutations in *RDS* (the human retinal degeneration slow gene) caused digenic RP, inheritable in a pseudo-dominant way. Several syndromic forms of RP are also well known, among which the most frequent types are Usher syndrome, associated with neurosensory deafness; and Bardet Biedl syndrome (BBS), characterized by PR degeneration (sometimes in a cone-to-rod manner), obesity already in childhood, mild psychomotor delay or even mental retardation, post axial polydactyly, hypogonadism and functional renal abnormalities, eventually resulting in complete renal failure (Hamel 2006).

1.7. Common rodent models of Retinitis Pigmentosa

1.7.1. Retinal degeneration 1 (Pde6b^{rd1})

A well-studied and historically important model of autosomal recessive RP is the *rd1 mouse*. Mice homozygous for the *rd1* mutation develop early onset and rapidly proceeding, severe PR degeneration. This spontaneous mutant was originally bred on a C3H background, designed to study the influence of vision on mouse behavior. *rd1* mutants carry a nonsense mutation on exon 7 of the *Pde6b* gene encoding for the rod-specific, beta subunit of cGMP-phosphodiesterase. Major hallmarks of the phenotype are retarded growth of the outer and inner segments in PRs, late development of the OPL and subsequent death of PRs in a typical rod-to-cone order (Sanyal and Bal, 1973; Chang et al., 2002). In this mutant, PR degeneration, starting as early as 6 days after birth, is characteristically overlapping with late retinal development and by 4 weeks of age PR loss is practically complete. This stage is characterized by complete light-insensitivity and absence of recordable electroretinography (ERG) responses (Carter-Dawson et al., 1978; Jimenez et al., 1996; Strettoi et al., 2002).

1.7.2. Retinal degeneration 10 (*rd10*)

Mice homozygous for the *rd10* mutation show the signs of PR degeneration as early as 3 weeks of age – approximately being 25 days of age at the peak of rod death and 45 days of age at the peak of cone death (Gargini et al., 2007;). Sclerotic retinal vessels are detectable at around 4 weeks of age. The ERG of the *rd10* mouse is continuously declining from 3 weeks of age until extinction at 2 months of age. The underlying genetic cause of the disease lies in an autosomal recessive missense mutation mapped to mouse chromosome 5, on exon 13 of the beta subunit of the rod phosphodiesterase gene, due to which *rd10* mutants are also known as Pde6b^{rd10}. Because of a later onset of PR degeneration and milder disease progression compared to that of *rd1* mice, *rd10*

mutants (noticeably showing a different genetic defect in the same Pde6b gene affected in rd1 mice) provide a good model to study the pathogenesis of autosomal recessive RP and pharmacologically-based retinal repair strategies (Chang et al., 2002).

1.7.3. P23H rhodopsin transgenic rats

There are more than 80 RHO mutations associated with AD RP in humans identified to date. The one known as P23H, a missense mutation on the N-terminus of RHO, exchanges amino acid Proline to a Histidine. This was the first identified *rho*/RHO mutation and accounts for at least 12% of the AD RP cases in the United States. The P23H transgenic rat displays progressive rod outer segment (ROS) shortening and ONL cell death with primarily normal cone function, consistently with clinical results from P23H patients. ERG b-wave amplitude decreases with age, but the photopic b-wave remains constant over the time of degeneration, until the ONL thickness decreases to its half. Phototransduction sensitivity and dark adaptation recovery after RHO bleaching are normal in P23H rats, differently from what known for human traits (Machida et al., 2000). It is important to point out that the main limitation of using a transgenic model is the fact, that the overexpression of transgenic RHO (which sums up with wild type rhodopsin) can cause PR degeneration *per se* (Olsson et al., 1992).

1.8. Therapeutic strategies – focus on bipolar cells

At early stages of retinal degeneration, when surviving PRs can still be found, gene augmentation for loss of function mutations or drug-based neuroprotection to delay PR loss can be effective strategies to improve/preserve visual function. For these approaches, clinical trials are ongoing: valproic acid, a suppressor of microglia associated inflammatory response in RP (Clemson et al., 2011) has been approved for clinical trials (ClinicalTrials.gov, 2017), however it's efficacy has not yet been successfully proven; more importantly a phase III clinical trial of voretigene neparvovec (AAV2-hRPE65v2, Luxturna) recently demonstrated significant effectiveness for RPE65-mediated inherited retinopathies including Leber congenital amaurosis and RP (ClinicalTrials.gov, 2018) and has been approved by the U.S. Food and Drug Administration (FDA) and by the European Medicines Agency (EMA). In parallel, cellular therapy (based on embryonic derived and/or induced pluripotent stem cells) to restore lost PRs or support surviving cells is greatly advancing on experimental models (Lagali et al. 2008; Lakowski et al., 2015).

At later stages, when PRs are minimally functional, or no PRs are left alive, retinal prosthesis electrically stimulating inner retinal neurons or optogenetics based on the expression of optical

neuromodulators in inner retinal cell types to make them directly photosensitive are considered feasible solutions. Some electronic implants like ArgusII are already commercially available and implanted in several patients with no residual vision. Optogenetics has reached the stage of clinical trials as explained below. It appears that both available prosthesis and optogenetic strategies need further development and fine-tuning to avoid the non-selective stimulation of inner retinal cell populations, which may contribute to the production of inadequate visual signals (Lagali et al. 2008).

A promising subretinal prosthesis was reported in Nature Materials quite recently by an Italian research group, who achieved some vision restoration and increased basal metabolic activity in the primary visual cortex of Royal College of Surgeon (RCS) rats, a model of RP carrying a null mutation on the *Mertk* gene in the RPE possibly responsible for the defect in Gas6 mediated outer segment phagocytosis in these rats (Hall et al., 2001). Unlike previously described prosthesis – whose limitations include the mechanical composition of the electrode array, creating a mismatch with the soft retinal tissue – this is a completely organic, flexible and biocompatible device, and is nevertheless directly light-excitable. In vivo installation of this prosthesis improved light sensitivity and visual acuity of RCS rats as assessed by ERG recordings and behavioral tests, for up to 6-10 months after the surgery, demonstrating long-term efficacy (Maya-Vetencourt et al., 2017).

Optogenetic tools, developed to provide a spatiotemporal control over neurons through light stimulation for studying neuronal circuits, are presently promising approaches for vision restoration as well. Basically, we can distinguish between two major types of effectors used in optogenetic vision restoration: ion channels and G-protein coupled receptors (GPCRs) (**Figure 1.10.**). Strategies using light activated ion channels entail high intensity light which can be risky at lower wavelengths, therefore requiring optimization and red-shifting of the used excitation spectra. GPCRs on the other hand are far more sensitive to light, however both activation and inactivation kinetics tend to be much slower as well (Baker and Flannery, 2018).

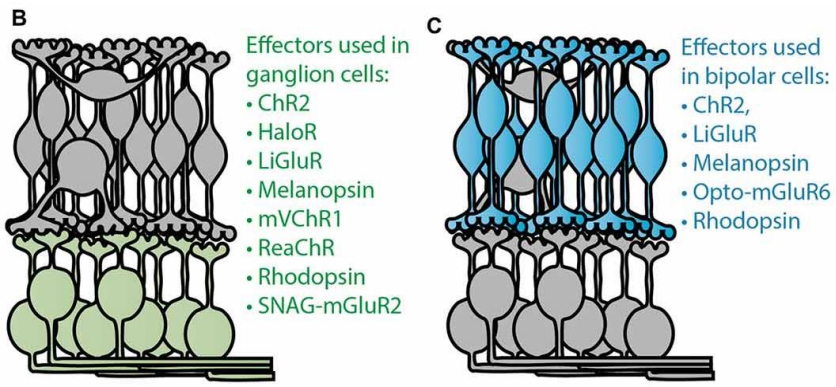

Figure 1.10. Panel (B) is depicting optogenetic effectors tested in retinal ganglion cells; panel (C) shows effectors tested in bipolar cells (modified figure from Baker and Flannery, 2018)

Recent refinements of the design strategy of cell-type specific promoters have conferred optogenetic stimulation of inner retinal neurons the potential to be cell-type specific as well. Expression of a light-activated protein in cells which in theory utilize a specific retinal circuit downstream the PRs supposedly evokes a biologically relevant activity pattern in RGCs. Researchers targeted channelrhodopsin-2 (ChR2) to ON BCs to test the aforementioned theory in the rd1 mouse model of PR degeneration. They found that optogenetically modified, light sensitive BCs triggered light evoked firing in RGCs and in the visual cortex, resulting in enhanced performance of treated rd1 mice in behavioral based visual acuity tests (Lagali et al. 2008). Also other research groups reported promising results based on the aforementioned strategy lately: restoration of ON and OFF responses via targeting ChR2 to ON-BCs in blind mice (Macé et al. 2015); restoration of visual responses using the MAG_{460} (Maleimide-Azobenzene-Glutamate activated at 460 nm) system in mice and dogs (Gaub et al. 2014); vision restoration using a ChR2 chimera, the ReaChR, in mice as well as macaque and human retinal explants (Sengupta et al., 2016); discovery of a new, red-shifted microbial ion channel, termed ChrimsonR, with faster deactivation kinetics than ReaChR (Klapoetke et al., 2014). Indeed, ChrimsonR is a very powerful optogenetic tool and is currently under clinical trial (ClinicalTrials.gov, 2015).

Altogether, prosthetic and optogenetic approaches are feasible only if targeted retinal circuits have not been corrupted as a consequence of PR death.

1.9. Rhodopsin – key molecule in phototransduction and photoreceptor degeneration

RHO is present in the outer segments of rod PRs and plays a crucial role as a photopigment molecule especially in dim light conditions making rods exquisitely tuned to night/scotopic vision. RHO is a G-protein coupled receptor composed of the apoprotein opsin and the chromophore 11-cis-retinal.

The high photon sensitivity of RHO allows the initiation of the phototransduction cascade (**Figure 1.11.**) during which 11-cis-retinal first undergoes photoisomerization transforming into all-trans-retinal. This then detaches from opsin hereby initiating its conformational change to metarhodopsin II. Active RHO (metarhodopsin II, or R*) interacts with the regulatory protein transducin, allowing it to dissociate from GDP and to bind GTP instead. This activates transducin, which triggers a photo-signaling pathway initiated by a cGMP-phosphodiesterase (PDE), leading to increased hydrolysis of cGMP. This in turn leads to the closure of cyclic nucleotide-gated cationic channels which allow Na^+ and Ca^{2+} influx, therefore suppressing a circulating current flowing in darkness, ultimately resulting in the hyperpolarization of rods. Reduction in Na^+ and Ca^{2+} mediated photocurrent leads to the decrement of glutamate neurotransmitter release from rod synaptic terminals, translating into modifications of transmission to the second order neurons – HCs and BCs (Pugh and Lamb 1993; Hofmann and Heck 1996).

The phototransduction cascade (and its connection with synaptic transmission at the PR terminal) is very similar in cones as well, except that the specific photo pigments present in the outer segments are known as cone opsins. Mice generally express two types of cone opsins throughout the retina resulting in the presence of two cone types: the “blue cones” and the “green cones”. Cone PRs co-express both opsin types, however there is a dorso-ventral gradient in the ratio of the expressed opsins within each cone cell, that is creating a spatial distribution between green and blue cones. Cones with a generally higher M opsin level (sensitive for mid-wavelengths light) are predominant in the dorsal retina, while cones with S opsin dominance (sensitive for short-wavelength and UV light) reside in the ventral part, whereas in the central part of the retina S and M opsins are coexpressed at similar levels it the cone PRs (Lyubarsky et al., 1999; Applebury et al., 2000; Nikonov et al., 2006).

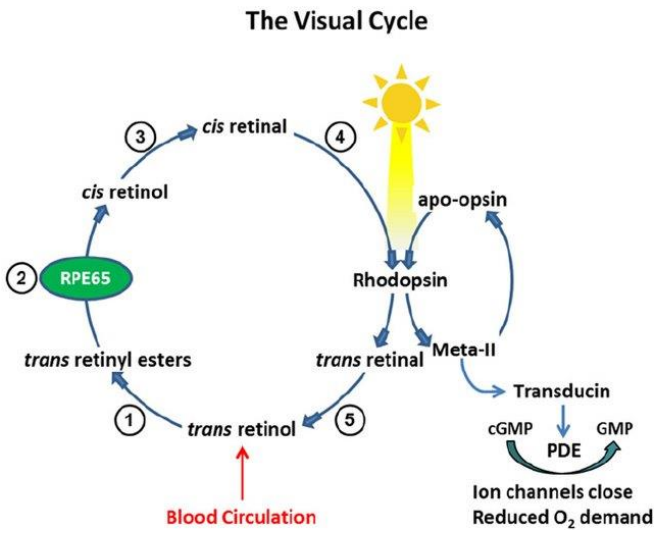

Figure 1.11. Schematic illustration and summary of the visual cycle (retrieved from Bavik et al., 2015)

The phototransduction cascade has to be interrupted since persistent activity saturates the PR, inhibiting signaling subsequent absorption of photons and thus affecting its sensitivity and temporal resolution. Moreover, failure in the deactivation of phototransduction has been reported to cause PR degeneration and RP *per se* (Chen et al. 1999; Fain 2006). To restore light responsiveness of the PR, the cGMP-gated channels must reopen. Hence, cGMP hydrolysis by PDE has to decrease whereas cGMP must be resynthesized by guanylate cyclase, the latter being activated by a drop in the intracellular calcium levels accompanying the photo-response. The process in which rhodopsin kinase (GRK1) phosphorylates R* allowing arrestin to bind it with high affinity and preventing it from further activation of additional transducin and thus PDE molecules consequently shuts down cGMP hydrolysis by PDE. Heteromeric G-proteins like transducin normally stay activated as long as the α subunit hydrolyses the bound GTP to GDP, which is catalized by RGS-9 (regulator of G-protein signaling 9). (He et al. 1998; Burns 2010).

1.10. Rhodopsin mutations

Rho mutations are among the most common causes of RP and at least 25% of AD RP cases are linked to this gene (Hartong, Berson, & Dryja, 2006). Referring the latest reviews, over 150 missense/nonsense RHO mutations were found to cause AD RP directly (Gal et al. 1997; Briscoe et al., 2004; Mendes et al. 2005; Rakoczy et al. 2011; Athanasiou et al., 2018). Long years of phenotypic characterizations demonstrated that phenotypes could vary anywhere between severe and asymptomatic (see **Figure 1.12.**). Also, a very recent characterization of 33 RHO mutations revealing molecular and cellular bases of AD RP and possible new therapeutic approaches was published by Behnen et al. in 2018.

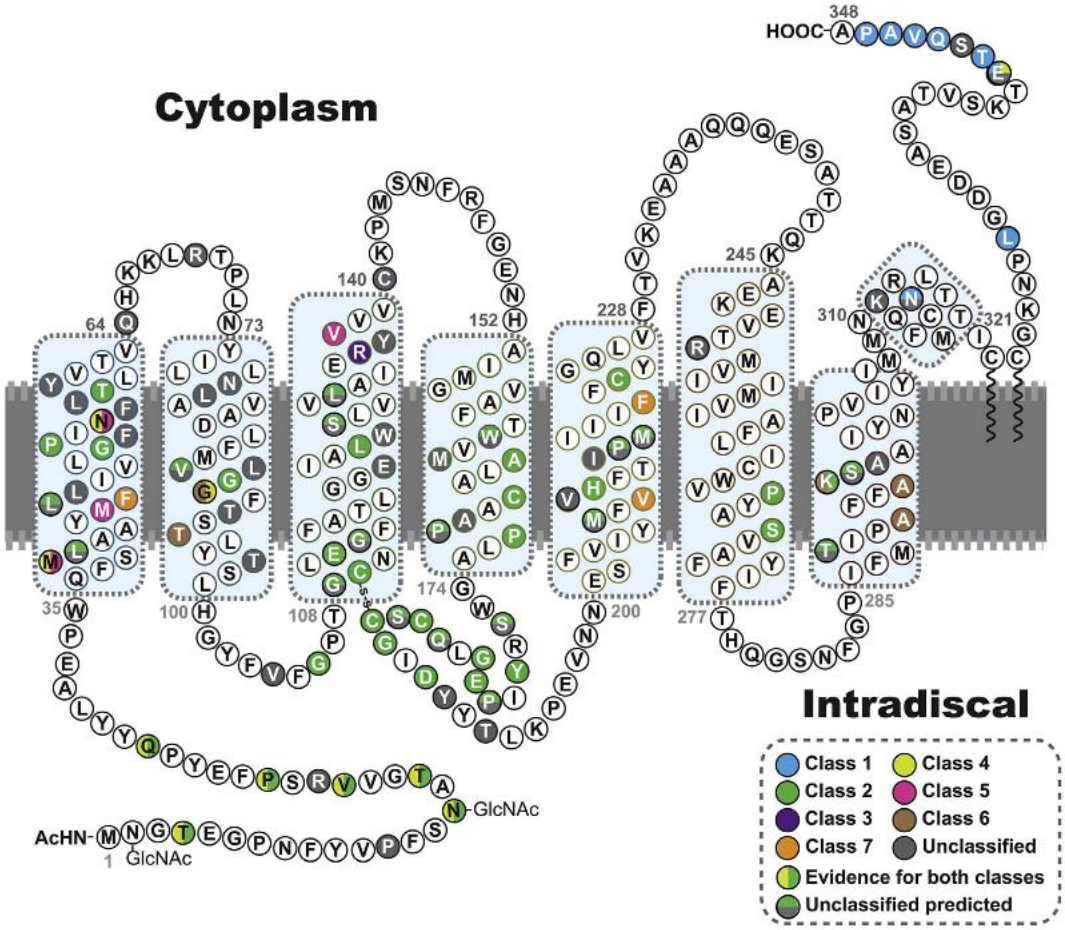

Figure 1.12. Schematic picture of RHO with a summary of the registered RP-linked mutations up to 2018 (Athanasiou et al., 2018)

The most updated classification of the aforementioned mutations can be seen on **Table 1.**, from Athanasiou et al., 2018. According to the classification system of this study, we can distinguish seven classes of RHO mutations (Gal et al., 1997; Mendes, Van Der Spuy, Chapple, & Cheetham, 2005; Rakoczy et al., 2011; Athanasiou et al., 2018), characterized as follows (Mendes et al., 2005; Rakoczy et al., 2011; Athanasiou et al., 2018):

Class I

RHO folding is normal, transportation to the ROS is blocked, mutation usually affects the cilia-binding motif.

Class II

RHO is misfolded, blocked in the endoplasmic reticulum (ER), no transportation to ROS, difficulties in reassembling with 11-cis-retinal. Class IIa – the mutation destabilizes the protein, more severe folding effects; Class IIb – the mutation affects folding by interfering with the retinal binding site; Class IIc – mutation affects RHO ''residues facing the lipid bilayer'' disturbing ''integration into the membrane and RHO stability when the mutant residues are polar or charged" (Rakoczy et al., 2011).

Class III

RHO mutation alters endocytosis.

Class IV

RHO is not inevitably misfolded, rod-opsin interaction and posttranslational modifications are involved.

Class V

''Mutations show increased activation rate for transducin.'' (Mendes et al., 2005). Rakoczy et al. deleted this class due to the fact that ''the constitutive activity is not the basis of their pathogenesis'' (Rakoczy et al., 2011).

Class VI

RHO mutants ''show constitutive activation of opsin in the absence of chromophore and in the dark'' (Mendes et al., 2005).

Class VII

RHO mutation alters binding capacity to partner proteins e.g. transducin (Rakoczy et al., 2011).

Classification	Key features	Mutations
1	Post Golgi trafficking and OS targeting	*L328P, T342M*, Q344R/P/ter, V345L/M, A346P, P347A/R/Q/L/S/T, ter349/Q/E
2	Misfolding, ER retention and instability	N15S[§], T17M[†], V20G[§], P23A/H/L[§], Q28H[§], G51R/V, P53R, T58R/*M*, V87D, G89D, G106*R*/W, C110F/R/S/Y, E113K, L125R, W161R, A164E/V, C167R/W, P171Q/L/S, Y178N/D/C, E181K, G182*S*/V, C185R, C187G/Y, G188R/E, D190N/G/Y, H211R/P, C222R, P267R/L, S270R, K296N/E/M
3	Disrupted vesicular traffic and endocytosis	R135G/L/P/W
4	Altered post-translational modifications and reduced stability	T4K[†], T17M[†], M39R, N55K, G90V
5	Altered transducin activation	M44T, V137M
6	Constitutive activation	G90D, T94I, A292E, A295V
7	Dimerization deficiency	*F45L, V209M, F220C*
Unclassified	No observed biochemical or cellular defect or not studied in detail	P12R, R21C, Q28H, L40R, L46R, L47R, F52Y, F56Y, L57R, Y60ter, Q64ter, *R69H*, N78I, L79P, V87L, L88P, T92I, T97I, V104F, G109R, G114D/V, E122G, W126L/ter, S127F, L131P, Y136ter, C140S, T160T, M163T, A169P, P170H/R, S176F, P180A/S, Q184P, S186P/W, Y191C, *T193M*, M207R/K, *V210F*, I214N, P215L/T, M216R/L/K, *R252P*, T289P, S297R, A298D, K311E, N315ter, E341K, S343C

Table 1. Classification of AD RP and AD Congenital Stationary Night Blindness-linked RHO mutations registered in clinical studies until 2018 (Athanasiou et al., 2018) (Mendes et al., 2005; Rakoczy et al., 2011)

Some RHO mutations are linked to type B1 RP (causing a phenotype similar to that of the mouse model used in this study) causing a corrupted deactivation response in the phototransduction cascade following bright light flashes (Cideciyan et al., 1998). Class B1 RHO mutations are the following: T17M, P23H, T58R, V87D, G106R, D190G (Cideciyan et al., 1998) and P180A (Iannaccone et al., 2006). All of these mutations belong to Class IIa except for T17M, which was categorized to Class IV (Rakoczy et al., 2011). Note that Q312ter RHO mutation, reported from one RP patient, was not included in **Table 1.,** but available data suggests that it belongs to the Class B1 RP-causing RHO mutations (Cideciyan et al., 1998).

1.11. The I307N RHO mutation

I307N RHO carrying mice were generated through chemical mutagenesis within the Translational Vision Research Models (TVRM) program at the Jackson Laboratory to annotate binding sites and functional domains within RHO and to further understand *rho* mutation-linked pathological conditions of the retina (Budzynski et al., 2010).

I307N RHO exhibits spectroscopic properties very similar to the wild type (WT) RHO with close to the same molar extinction coefficients, spectral $A_{280}/A_{\lambda max}$ ratios and an absorption maximum at 500 nm, exactly the same of the WT protein. These properties indicate physiological structure and stability of the mutant protein with no misfolding. In fact, I307N RHO localize to the ROS, excluding defects in protein transportation.

Western Blot and SDS-PAGE analysis of I307N RHO revealed two, low intensity bands below the main 40 kDa monomer opsin band (the lower around 27 kDa), which can contribute to truncated forms of RHO or non-glycosylated protein species.

Hydroxylamine, a chemical compound capable of entering the retinal binding site of RHO and breaking the SB linkage, is widely used in biochemical tests to determine whether a mutation is affecting the stability and structural compaction of RHO in the SB environment. I307N RHO, when treated with hydroxylamine in dark state, showed a remarkably stable structural compaction around the SB-linkage site, demonstrating traits quite similar to those of the WT protein.

In the thermal stability test monitored at 48^{o}C, dark state I307N RHO appeared unstable with a 23 minutes half-life indicating a four times faster degradation compared to WT RHO.

The meta II decay test measures stability of the active state RHO by means of spectroscopy, monitoring the tryptophan fluorescence increase upon illumination resulting from its release from the binding pocket. This test showed that I307N RHO had a meta II decay value of 7.9 minutes compared to 5.9 minutes of the WT RHO.

After photobleaching, chromophore regeneration was examined, surprisingly showing that I307N RHO had a slightly higher regeneration rate (97%) than the WT (Herrera Hernández, 2017).

Transducin activation was monitored with a radionucleotide filter binding assay, in which I307N RHO exhibited twice as slow activation kinetics to that of the WT protein. A possible explanation to this phenomenon may lay in recent studies, showing that Ile307 and Try306 play crucial roles in activating RHO. During photoisomerization of RHO, the β-ionone ring between transmembrane domains 3, 5 and 6 moves up creating a cavity. Then, the cytoplasmic side of transmembrane domain 6 is pushed away from the rest making previously inaccessible residues available. Many of these residues are known to participate in GDP release from G-proteins, like transducin. In the inactive state of RHO, V254 is known to maintain a contact with L131, Y306 with T58 and F313 with R314 and I307. Once activated, V254 breaks its contact with L131 to make a new bond with Y306 (**Figure 1.13.**). It is thus possible that the I307N mutation slows down the aforementioned process resulting in slower transducin activation (Tehan et al. 2014; Flock et al. 2015; Venkatakrishnan et al. 2016; Herrera Hernández, 2017).

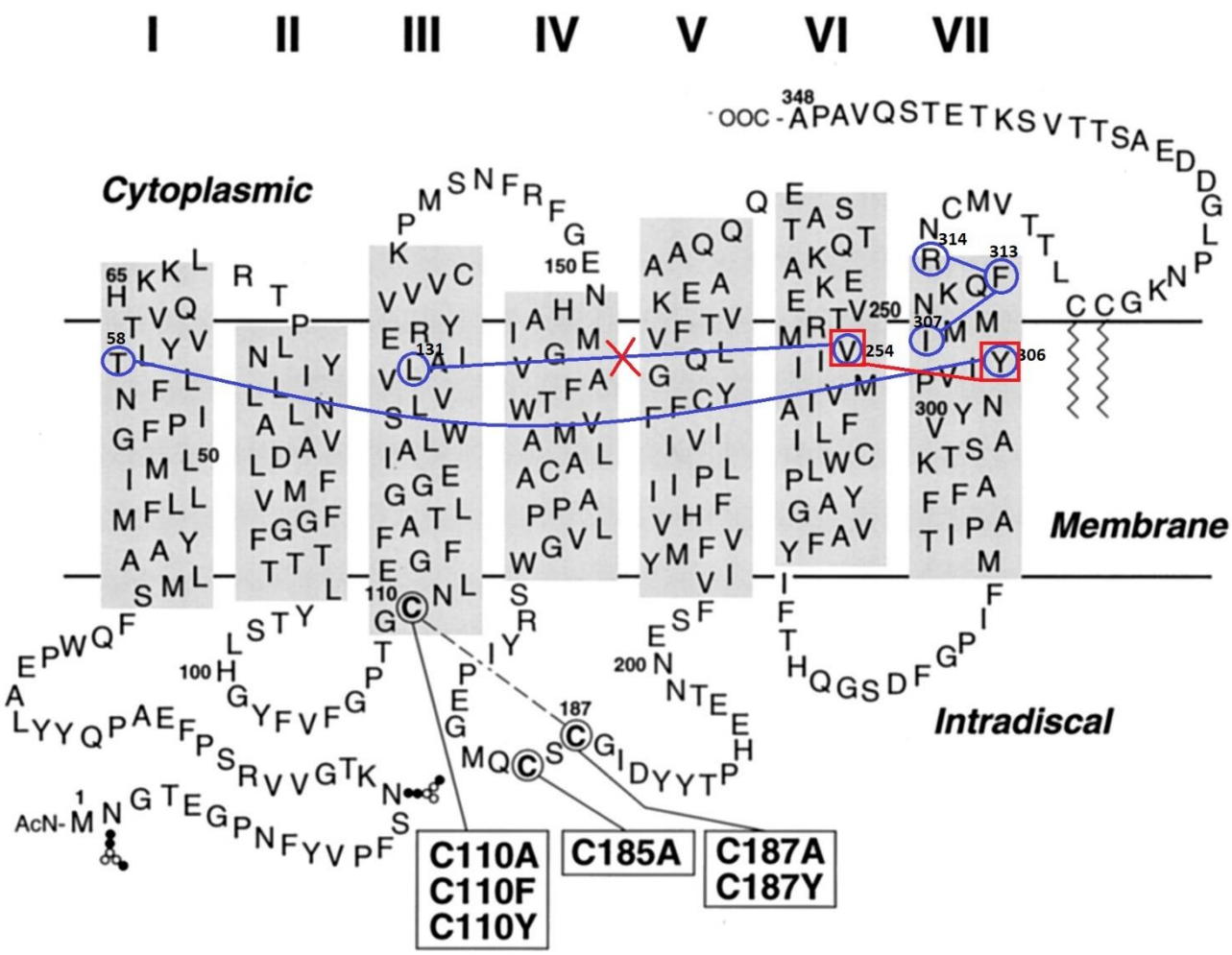

Figure 1.13. Schematic illustration of selected amino acid connections in dark state RHO circled and connected in blue (V254:L131, Y306:T58, F313:I307+R314) and in the active state RHO in red (V254:Y306). Adapted and modified from Hwa et al., 1999.

1.12. The Tvrm4 mouse model

The TVRM program sited in the Jackson Laboratory (Bar Harbor, Maine, USA) aims to create mouse lines with PR defects using chemically mutagenized embryonic stem cells to elucidate new functional regions of PR-specific proteins, including RHO. Mouse model number 4 (Tvrm4), a mutant but not a transgenic mouse, has normal levels of RHO and was found to carry a single nucleotide missense mutation replacing (ATC) isoleucine (I) 307 with (AAC) asparagine (N) in the 7th transmembrane domain of RHO, highly conserved among species including humans, macaques, mice, rats, cats and dogs (**Figure 1.14.**). The I307N mutation has a dominant inheritance pattern as confirmed by the F1 generation of an outcrossing of heterozygous Tvrm4 to WT B6 mice, where 50% of the offspring was affected.

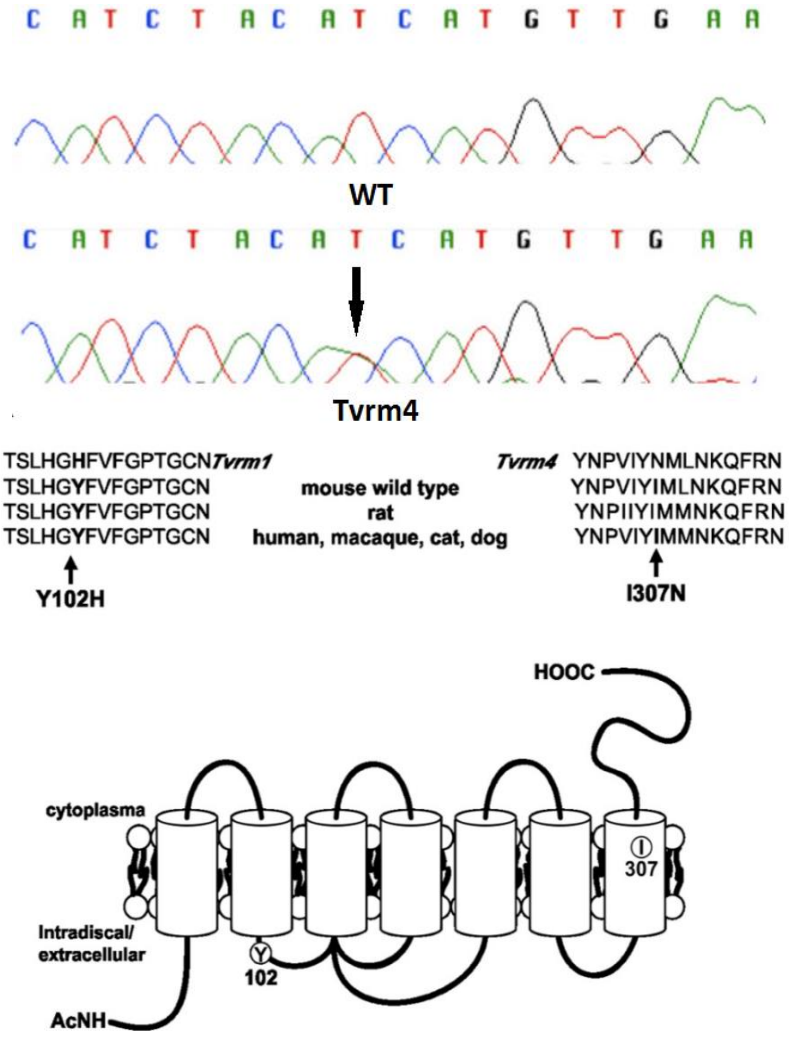

Figure 1.14. Schematic summary of the single nucleotide polymorphism carried by TVRM4 mice on the *rho* gene affecting the 307th amino acid in the 7th transmembrane domain of RHO protein (Budzynski et al., 2010).

As multiple ophthalmoscopy examinations were necessary to monitor the phenotype, an obvious link of cause and effect was recognized between fundus examinations and bleaching of the central, most exposed retinal area. Further experiments where Tvrm4 mice were exposed to light flashes of 12.000 lux light for 5 minutes confirmed the light-dependent manner of the I307N mutation, selectively triggering PR degeneration in the light-hit, central retinal regions. Moreover, the rate of degeneration was found to be dependent on the length of light exposure.

Western blot and immunohistochemical studies proved normal amounts of mutant RHO in 6 months old heterozygous Tvrm4 mice compared to WT controls; moreover, a proper localization of RHO to the rod outer segments was demonstrated (Budzynski et al., 2010).

Unlike other retinal degeneration models like rd1 or rd10 (phosphodiesterase mutants), Tvrm4 mice raised under ambient light conditions do not undergo PR loss even at 1-year of age. Furthermore, ERG recordings of light and dark-adapted animals at 4 and 12 months of age showed no reduction in the a- and b-wave amplitudes, demonstrating an overall normal retinal function compared to WT controls. Special ERG recordings and analysis were used to study deactivation of phototransduction and bleaching recovery. While a normal pattern of phototransduction deactivation was recorded, bleaching recovery was found to be impaired, both in time constant and in dark-state asymptote values compared to WT controls.

High-performance liquid chromatography (HPLC) with both fluorescence and multi-wavelength absorbance detection revealed no significant differences in the levels of major retinoid species in whole dark-adapted eyes of Tvrm4 or WT mice. Although significantly lower levels of all-trans-retinol were detected in Tvrm4 eyes immediately after photo-induction, the phenomenon was no longer detectable after 1 hour of recovery. Thus, the observed changes in retinoid levels in the mutants were transient and did not seem to significantly affect availability of 11-cis-retinal after bleaching (Budzynski et al., 2010).

To better understand the link between the disease phenotype and the nature of I307N mutation, Budzynski et al. expressed the mutant opsin in COS cells and first analyzed the effectiveness of receptor signaling. When 11-cis-retinal was added, I307N RHO formed pigments with WT characteristic visible absorbance spectra. The mutant receptor was proven to activate transducin in a light dependent manner, but the protein remained activated constitutively. As constitutive activation of opsins is toxic for PR cells, the time course of binding 11-cis-retinal to regenerate RHO had to be determined; the results indicated not only constitutive activation, but also slow regeneration kinetics. These results differ from recent data obtained by Herrera Hernández et al. in 2017, reporting surprisingly higher rate of RHO regeneration. As Budzynski et al. concluded: ”the threshold at

which degeneration is induced reflects the bleaching level at which the capacity of the visual cycle is surpassed, thereby allowing free opsin to remain in an active state for a damaging period of time." In addition to the time window in which the mutant opsins remain unbound, the toxic nature of this particular mutant opsin might be responsible for PR death, as demonstrated by 11-cis-retinal deprivation experiments, which confirmed a higher toxicity of the free I307N opsin molecule, compared to that of the WT (Budzynski et al., 2010).

Altogether, the retinal degeneration phenotype arising from photo-induction of Tvrm4 mutants recapitulates features of the RHO class B1 human RP, including focal PR degeneration and physiological PR function with delayed dark adaptation. In fact, the single nucleotide polymorphism present in Tvrm4 mice leading to I307N residue alteration in RHO closely resembles the Q312ter mutation that leads to Class B RP in humans, or the A295V mutation associated with stationary night blindness (Cideciyan et al. 1998; Mendes et al. 2005; Rakoczy et al. 2011). Protracted dark adaptation after bleaching as well as focal PR deterioration were also reported in the T4R English Mastiff dog model of AD RP, carrying a naturally occurring point mutation in the *rho* gene (Kijas et al., 2002).

A systematic secondary characterization of Tvrm4 mice and optimization of the photo-induction protocol for appropriate modeling of the RP phenotype was done by Gargini et al. in 2017. They confirmed normal retinal morphology in heterozygous Tvrm4 mice kept in normal light conditions (animal house standards) and reported no phenotype induction following 12.000 lux light exposure for various durations (1-5 minutes) without atropine eyedrops for pupil dilation. This protocol is extremely useful for internal controls: one eye treated with atropine would show the signs of PR degeneration, while the other (without atropine) might be used as control for 'WT' phenotype.

Photo-induction with 12.000 lux white-neon light after pupil dilation for 1-2 minutes caused a PR degeneration wave in the central retina, already detectable after 48 hours staining the retina with a simple nuclear marker like Ethidium homodimer (**Figure 1.15.**). This revealed significant numbers of brightly fluorescent, pycnotic nuclei in the outer nuclear layer (ONL). A transition zone with gradually less degenerating PRs and more rows of nuclei in the ONL towards the retinal periphery was obvious obtaining equatorial sections of frozen eye-cups as well as in retinal whole-mount preparations (Gargini et al. 2017).

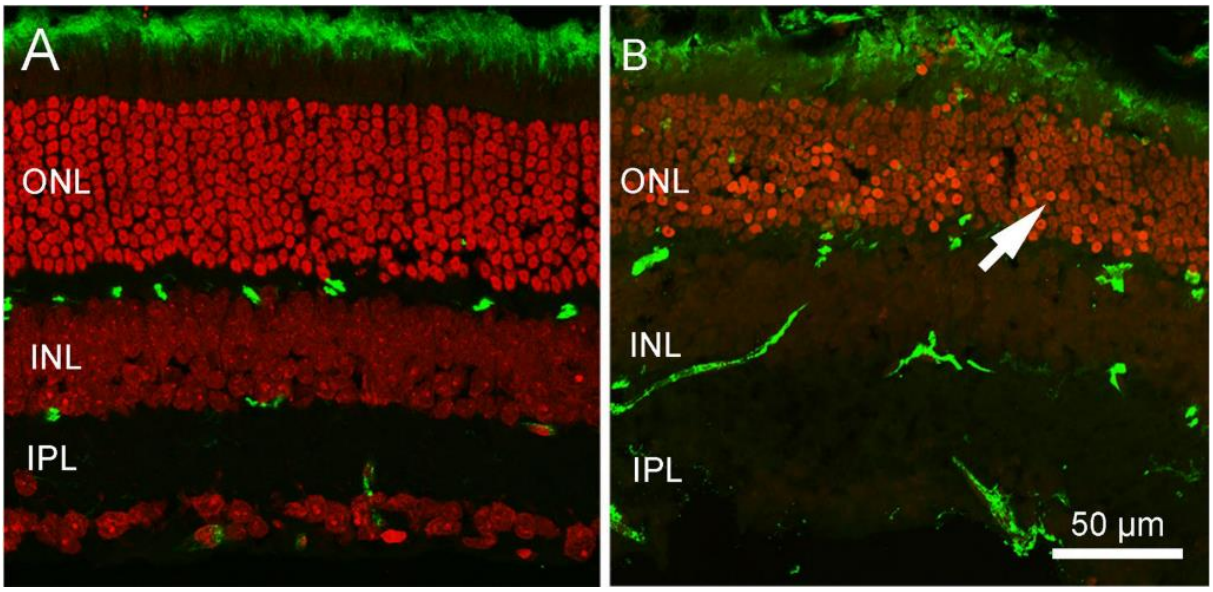

Figure 1.15. Adapted from Gargini et al. 2017. Ethidium and Rhodopsin staining in vertical retinal sections of adult, heterozygous Tvrm4 mice, (A) without light induction; (B) central retina 48 hours after a 1 minute, 12.000 lux exposure, showing with pycnotic PR nuclei in the ONL (white arrow).

The finding that PR degeneration is solely affecting the central retina is explained by the physical properties of the mouse eye (small size and high curvature), which limits the exposure to photo-inducing stimulus to the posterior pole of the eye, rather than by differences in expression levels of the mutant RHO, which is pan retinal. In other words, the central retina of Tvrm4 mice degenerates simply because it is the area hit by enough intense light for induction. The induced, irradiated retinal area was found to be approximately 5,3 mm^2 (roughly represented by a circle with a 1-1,3 mm radius) which makes up ~32-35% of the whole retinal area, which is on average 16 mm^2.

Normal retinal physiology was confirmed in non-induced animals by ERG recordings. However, a gradual and net reduction in both the scotopic and photopic a- and b-waves have been reported in Tvrm4 mice following a 12.000 lux, 1-minute exposure 2, 7 and 14 days post-induction (PI) with respect to WT controls (**Figure 1.16.**) (Gargini et al. 2017).

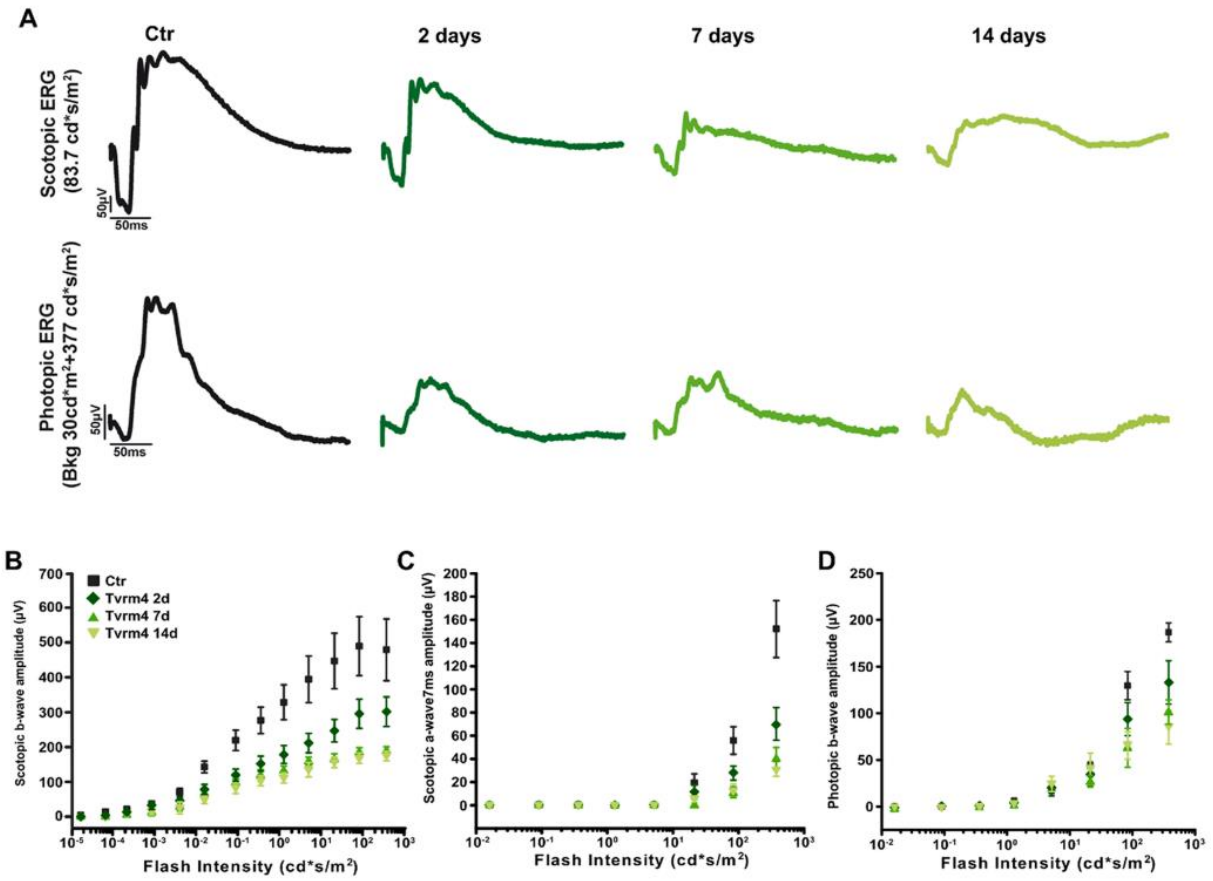

Figure 1.16. Adapted from Gargini et al. 2017. A: main properties of scotopic and photopic ERG traces in heterozygous Tvrm4 mice induced by 12.000 lux for the duration of 1 minute over 2, 7 or 14 days PI. B: scotopic b-wave amplitudes; C: t scotopic a-wave amplitudes at 7 ms; D: photopic b-wave amplitudes over the time frame of 2, 7 or 14 days PI.

The process of PR degeneration in Tvrm4 mice was accompanied by obvious micro- and macroglial activation like in other retinal degeneration models. After 1 minute of 12.000 lux irradiation, and as early as 48 hrs PI, the central retina was invaded by activated, amoeboid, microglia cells positive for IBA1 antibodies. Active microglia were observed entangling the dying cells while the retinal periphery hosted only passive, normally ramified microglia. At the same time, Müller glial cells showed expected signs of glial fibrillary acidic protein (GFAP) overexpression in the central, but not in the peripheral retinal areas.

PR degeneration was followed up to 30 days PI in animals induced for 1 minute at 12.000 lux. Strikingly, the irradiated, degenerating central area did not increase in size, but on the contrary, the area of PR death shrunk to occupy 21% of the total retinal area, instead of the 35% reported at earlier time points. Consequently, ERG properties of the induced mice examined 30 days PI demonstrating that the amplitude of the scotopic ERG recovered partially (**Figure 1.17.**), while the

amplitude of the photopic waves did not change significantly over time after the first major decrement. Gargini et al. explained the phenomenon assuming that PR cells in or close to the transition zone could escape death, probably due to less intense light reaching the mutant RHO molecules and could therefore regenerate partially damaged outer segments (Gargini et al. 2017).

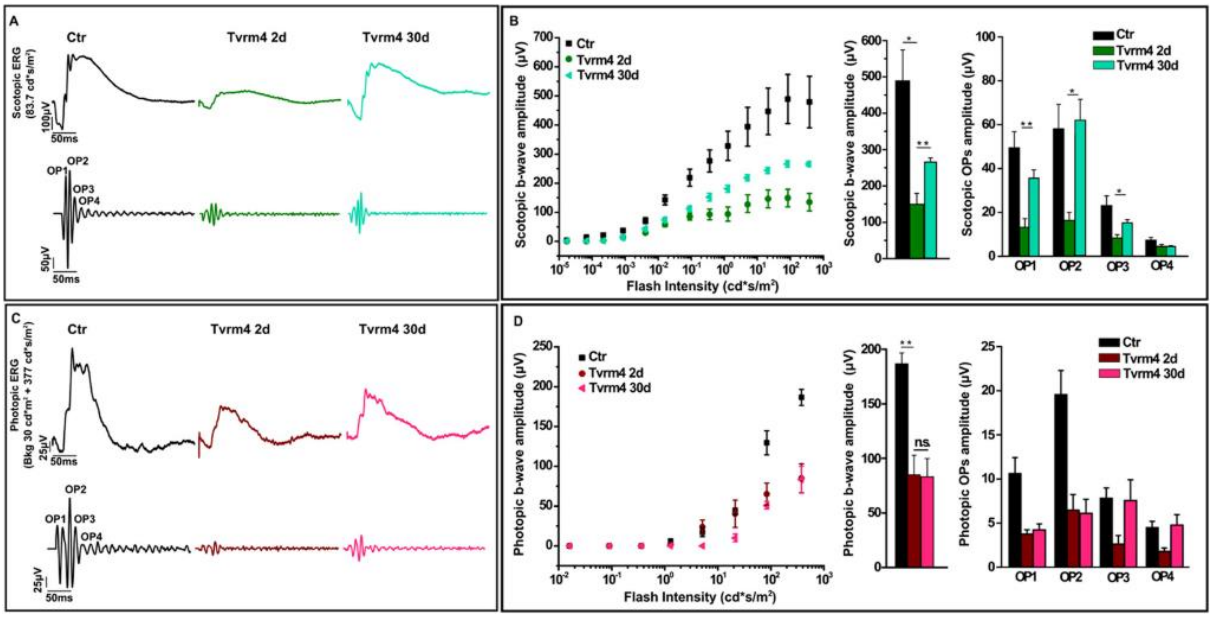

Figure 1.17. Regeneration of the scotopic ERG and maintenance of the photopic response in time. Comparison of non-induced control animals and Tvrm4 mice induced for 1 minute at 12.000 lux and recorded 2 days thereafter (Gargini et al. 2017).

2. PURPOSE OF THE STUDY

In common forms of Retinitis Pigmentosa (RP), primary degeneration of rods triggers a complex chain of events among other retinal cells, which remodel to various extents, typically in a regressive manner (Marc et al. 2003). Bipolar cells undergo gradual dendritic atrophy, loss of synaptic receptors, formation of ectopic synapses and secondary cell death (Gargini et al. 2007; Jones et al. 2012), with rod and cone BCs exhibiting different types and kinetics of reaction (Puthussery et al. 2009). Vision restoration through inner retinal intervention (i.e. optogenetics to endow BCs with intrinsic light sensitivity) is likely to be strongly affected and possibly impaired by adverse remodeling and synaptic circuitry corruption.

The majority of rodent models available to study the progression of the disease phenotype (e.g. rd1 and rd10) exhibit signs of retinal degeneration already before the completion of cellular and synaptic development in the tissue (Strettoi, Porciatti, Falsini, Pignatelli, & Rossi, 2002). This casts a shadow over the possibility of interpreting our results on human RP, where PR degeneration starts (in most of the cases) during early adulthood, way after the completion of retinal development (Hartong, Berson and Dryja 2006). Therefore, a mouse model inducible during adulthood is extremely useful to gain insight into similarities and differences between the progression of retinal remodeling in the developing and mature retina.

Knowledge of the nature and entity of cellular and synaptic rearrangements occurring in the retina as a function of the underlying causative mutation and of the influence of the retinal developmental stage at the time of phenotype manifestation onto severity of remodeling is still incomplete. The understanding of cellular remodeling and synaptic rewiring in the inner retina is particularly limited, especially for paradigms of rhodopsin mutations, which are common forms of RP, still incurable by gene therapy in the case of dominant mutations. The novel mutant mouse Tvrm4 presently under study in this laboratory, carries a light-inducible, dominant rhodopsin mutation. A typical rod-cone degeneration can be induced in 48 hours in this otherwise normal mouse by a brief exposure to very bright light (Budzynski et al. 2010).

We exploited the Tvrm4 mutant to study inner retinal remodeling in general and that of second order neurons in particular, with a main focus on BCs. We assessed the entity of BC survival and described their dendritic and axonal rearrangements, possible formation of aberrant connections and alteration of synaptic circuitry in the inner plexiform layer, for which only limited knowledge is available. We gained a broad picture of remodeling in this mouse model, hopefully extensible to homologous RP cases found in humans.

3. OBJECTIVES

Main objectives of the present thesis work are the following:

(**1**) To gain insight into the nature and time course of morphological remodeling and survival of second order neurons in the retina of the Tvrm4 mouse.

To this purpose, initial studies were conducted on adult, 3-5 months old animals and concentrated on RBCs and their connective network in the IPL. Observation of remodeling and changes in survival rates of RBCs was done by staining these neurons with specific antibodies in retinal whole mounts and frozen vertical sections, followed by confocal analysis and estimates of their total density at two different time points from phenotype induction. Studies were carried out 3 and 6 weeks past light exposure, respectively reflecting intermediate and advanced stages of retinal degeneration. On the same confocal specimens, we also examined the morphology of RBC dendritic trees, as well as the fine structure of their axonal arborizations, searching for signs of remodeling, such as re-lamination, sprouting, formation of ectopic contacts, atrophy etc. Both cell counting for population studies and single cell analysis was be performed with the aid of MetaMorph, a dedicated image analyzer software. A similar analysis was carried out for CBCs and HCs as well. Amacrine and ganglion cells were also studied.

(**2**) To reveal synaptic rearrangements in the inner retina of Tvrm4 mutants as a function of degeneration progression.

Morphological studies of RBCs were paired to an analysis of inner retinal synaptic architecture studied by a combination of confocal and Transmission Electron Microscopy (TEM). For confocal analysis of connections in the inner retina, retinal sections from Tvrm4 mice at the age points described above were stained with antibodies against Synaptotagmin2/RIBEYE to visualize synaptic ribbons, whose density was estimated as a function of retinal degeneration using an image recognition tool of MetaMorph. An antibody against Connexin 36, was also used to perform a similar quantitative analysis on gap junctions of the inner retina. These data provide information about the maintenance of glutamatergic (i.e. bipolar) synapses in the inner retina and gap junctions known to involve cone bipolar cells but also shared by the rod pathway. A similar quantitative analysis was done also using retinal EM sections in which conventional as well as ribbon synapses were counted across the entire depth of the IPL. Briefly, conventional synapses are established by ACs only. They are therefore GABA- or Glycinergic. Ribbon synapses are established by rod and cone BCs and are glutamatergic. Both have distinctive, well established ultrastructural features allowing their clear and univocal identification by EM observations (see material and methods).

(3) To understand the influence of the age at which the phenotype manifests on the outcome of BC remodeling.

To address this issue, phenotype onset was induced in young mice (aged 15-19 days, close to the time of eye opening) to unmask possible higher susceptibility of newly differentiated BCs to the loss of PR input. The morphological analysis described above for adult mice was repeated on these young, partially immature animals.

This approach provides data about a) preservation of synaptic contacts in the inner retina of adult Tvrm4 mutants; b) possible changes in the relative distribution of excitatory (ribbon) versus inhibitory (conventional) synapses in a model of retinal degeneration. The analysis also shows the potentially different effects of early-onset phenotype manifestation on the wiring diagram of immature retinas.

4. RISK MANAGEMENT STRATEGIES

A general risk with inducible mutants is the occurrence of intrinsic variations in geno- and/or phenotypic manifestation. In case of Tvrm4 mice, we can exclude any difference between homo- and heterozygous mice since they have never been reported (Budynsky et al., 2010; Gargini et al. 2017). Yet, we chose to work with heterozygous mice only because they mimic better the human disease, found as heterozygous genotype for most of the dominant mutations. Only genotyped animals were included in the experiments.

Phenotypical variability is a risk of Tvrm4 mutants, since this is an inducible rhodopsin mutation and light induction is incomplete and uneven over the retinal surface. We use a protocol for light induction in which animals are kept freely moving in a cage exposed to 12.000 lux and pupils dilated with atropine eye drops. We are aware of the fact that the animal's nose may project a variable shadow onto a part of the retina that is therefore shed from light and escape the phenotype induction. As explained before, the high curvature radius of the mouse eye prevents the illumination of the retina in the far periphery. Altogether, both the geometry and the extension of the illuminated retinal area vary from animal to animal, translating into a variability of the morphological observations. To overcome this limit, we immunostained each retina with antibodies against rhodopsin or cone specific opsins. Since PRs are the first cells to die as a consequence of the mutation onset, their absence/abnormal shape guided our observations inside the areas of true phenotype manifestation, in which remodeling was assessed.

Similarly, cell counting for assessment of survival was performed following strict topographical rules, identical for all the observed specimens, thus containing the risk of phenotypic variability. Increasing the number of mice used for each experiment also contributed to generate reproducible data.

At the beginning of our TEM studies, we realized that ultrastructural preservation of the tissue needed improvement. Protocols that usually work perfectly on intact or slightly degenerated retinal tissue, were inadequate for our fragile samples, which showed a number of mechanical and chemical artifacts, including micro-ruptures along retinal laminae and broken cell membranes in the central retina, particularly thin as it is almost completely devoid of PRs. An optimal fixation, dissection and embedding protocol for EM studies was therefore implemented, by combining multiple available bibliographic sources, as explained in materials and methods. As a result, excellent preservation of retinal ultrastructure was achieved.

Further troubleshooting was necessary in the second part of our project, aiming to photo-induce Tvrm4 mice at the age of eye-opening. In fact, in vivo photo-induction of P15 mice failed in all the animals on which it was attempted, for none of them showed a retinal degeneration phenotype. We hypothesize 3 different causes:

The first could be an insufficient amount of (mutant) rhodopsin present in immature rod outer segments (ROS). Although the expression of rhodopsin can be detected in the mouse retina as early as P6-7, the development of ROS and disc formation finishes only at P25 by reaching mature length (Carter-Dawson et. al. 1986).

The second reason could be insufficient intensity and/or amount of light reaching the retina during the induction protocol we used. At young ages, the mouse eye has even a higher curvature than the adult and a small diameter. Moreover, very young mice tend to create groups staying close to each other, hiding their heads, which may be the reason why light is unable to reach the retina during photo-induction.

A third, intriguing, possibility is the occurrence of still unknown, neuroprotective mechanisms acting during development and contributing to prevent PR degeneration.

To test these hypotheses, we implemented a suitable incubation chamber to photo-induce P15 eyecups ex vivo (see materials and methods), prior removing the cornea, iris and lens. This could maximize irradiance of the retina and also indicate whether immature PRs are intrinsically more resistant to degeneration.

5. MATERIALS AND METHODS

5.1. Mouse model and experimental design

Animal experimenting protocols were approved by the Italian Ministry of Health (Protocol #14/D-2014, CNR Neuroscience Institute) and by the Ethical Committee of the CNR Institution. Animals were treated in accordance with the Association for Research in Vision and Ophthalmology (ARVO) statement for the use of animals in research. Experiments were conducted using heterozygous (HT) Tvrm4 mice (RhoTvrm4/Rho+) carrying a photo-inducible, I307N (7^{th} transmembrane domain of rhodopsin protein) mutation on the *rho* gene, and where indicated, WT littermates. Genotyping protocols were carried out according to Jackson laboratories and the protocol published by (Budzynski et al. 2010). Tvrm4 mice have a C57Bl6/J background and exhibit WT retinal phenotype when raised in ambient light conditions. Exposure to bright light (i.e. 6000 lux and higher) for short times (minutes) induces PR degeneration provided pupils are dilated. Without pupil dilatation, PR degeneration is not induced (Gargini et al. 2017). This gives the unique opportunity to expose one eye only, using the opposite eye as internal control, reducing the number of necessary animals and individual variability. In our experiments, HT mice's right eyes are photo-induced (on figures referred as HT) and the left eyes serve as controls (on figures referred as CTRL). The notation WT reported on figures refers to C57Bl6/J mice. A total of 30 adult mice (aged 3-5 months) were used for immunohistochemistry and 6 mice were used for TEM. Retinal phenotype was examined 3, 6 and 9 weeks after photo-induction, where at least n=3 animals were used per experimental group. To compare vulnerability to light exposure of mature and developing retinas, additional mice (a minimum of n=3/experimental group) aged postnatal day 15 (P15) and P19 were also studied. Ten HT Tvrm4 mice were photo-induced in vivo at P15, 3 P15 mice were used for ex vivo photo-induction and 5 additional mice were photo-induced in vivo at P19.

5.2. Photo-induction protocol

Following 4 hours dark adaptation in a black cage, Tvrm4 mice (all aged 3-5 months) received unilateral (right eye-only) eye drops of 1 µl, 0.5% atropine (Allergan). After 10 mins, mice were placed in the photo induction chamber (**Figure 5.1.**): a black box (140 × 30 cm size; 30 cm height) lined with mirrors on the inner sides and closed with a lid holding 4 neon bulbs (Philips Master TL5 HE 28 W/840, length 115 cm; 16 cm in diameter; Cool White mercury lamps). Intensity of the light could be controlled by changing the number of light bulbs switched on (for 12.000 lux 2 neon bulbs were needed) and was monitored by an inbox light meter sensor (mod. LX103, Lutron, Digital

Instruments). Timing of photo-induction was controlled with the aid of a digital clock. During photo-induction animals were completely awake and freely moving. Temperature did not change significantly during light exposure (Gargini et al. 2017). Adult and P15 animals were exposed to 12.000 lux light for 2 mins, P19 animals for 4 mins. Light-intensity was monitored and registered every 30 seconds. Post-induction (PI) animals were kept in the chamber in the dark for an additional minute ('cooldown' time), then returned to the local animal facility where they were kept in ambient light conditions (below 60 lux) on a 12/12-hour light/dark cycle with water and food ad libitum until the time of retinal examination.

Figure 5.1. Light-induction chamber for freely moving and fully awake mice. Rod degeneration is induced upon a short, high intensity illumination.

Ex vivo photo-induction: P15 HT Tvrm4 mice were kept in complete darkness for 4 hours, euthanized and explanted in the dark using red light source. Eyecup preparation (removal of cornea, iris and lens) was performed in oxygenated artificial cerebro-spinal fluid (ACSF) under dim light. Subsequently, eyecups were placed in freshly oxygenated medium with PR side up and photo-induced in the same light induction chamber used for live animals for 2 minutes at 12.000 lux. After 1-minute cooldown, eyecups were placed into a special double floor incubator for 6 hours at 37 C^{o}, with continuous oxygenation and heating of ACSF of the lower floor. Evaporation of oxygenated ACSF ensures direct gas exchange between the atmosphere in the box and the eyecups positioned on the upper floor. Retinas were harvested after 6 hours incubation.

5.3. Tissue preparation, histology and immunocytochemistry

Retinal tissue was harvested 3, 6 or 9 weeks PI from adult animals; 2 days, 1-week or 3 weeks PI from P15 animals induced for 2 minutes in vivo; and 1-week PI from P19 animals induced for 4 minutes in vivo. Mice were anesthetized with intraperitoneal Avertin (3-bromo-ethanol in 1% tert-amyl alcohol) (0.1 ml/5 g body weight) and killed by quick cervical dislocation following explantation of eyeballs, which were previously labeled on the dorsal pole with a surgical skin marker (Secureline Surgical Skin Marker, Aspen Surgical – 616-698-7100). Eyecup preparation was performed in 0.1 M phosphate buffer (PB) by removing the anterior segments (cornea, iris, lens) of the eye followed by immediate fixation in 4% paraformaldehyde (PFA) in 0.1 M PB, pH 7.4, for 30 minutes or 1 hour at room temperature. Fixation was followed by repeated (5x5 minutes) washes in 0.1 M PB, infiltration in 30 w/w% sucrose dissolved in 0.1 M PB and infiltration in Tissue-Tek O.C.T. compound (4583, Sakura Olympus, Italy). Sample freezing in tissue molds was achieved using isopenthane cooled down with dry ice; samples were stored at −25 °C until use. Ex vivo induced P15 eyecups were fixed and processed for storage in the same way. Frozen eyecups were later processed for either whole mount preparation or cryo-sectioning.

Frozen, vertical sections were cut at a cryostat at 12 µm thickness and collected on Super Frost slides for immunocytochemistry (ICCH). For whole mount preparations, defrosted eyecups were extensively washed in phosphate buffered saline (PBS), the retina was gently detached from the sclera and flattened by making four radial cuts toward the optic nerve head maintaining a reference on the dorsal 'petal' of the retina.

For ICCH, both retinal whole mounts and sections were incubated in: blocking solution (0.03% Triton-X 100 + 5% serum from the species in which the secondary antibody was generated in 0.01 M PBS) for 2 hours at room temperature if sections and overnight at 4 C^o if whole mounts; primary antibody (Ab) solution (diluted in PBS + 0.01% Triton-X 100 + 1% serum) overnight at 4 C^o if sections and 3 days at 4 C^o if whole mounts; in fluorescent secondary Ab solution – diluted as the primary Ab – for 2 hours at room temperature if sections and 2 days at 4 C^o if whole mounts (Barone et al. 2012).

Mouse monoclonal primary Abs used on retinal sections were: Rhodopsin (O4886 Sigma-Aldrich, Italy; diluted 1:1000); Protein Kinase Cα (PKCα; P5704, Sigma-Aldrich, Italy; diluted 1:800); CD68 (KP1; sc-20060, Santa Cruz Biotechnology; diluted 1:250); C-Terminal Binding Protein-2 (CtBP2/RIBEYE; 612044; BD Biosciences; diluted 1:800); Glutamine Synthetase (GS; MAB302; Merck-Millipore, Italy; diluted 1:1000); non-Phosphorylated Neurofilament H (SMI32R,

Covance, CA, USA; diluted 1:800); Glutamic Acid Decarboxylase-67 (GAD67; MAB5406; Merck-Millipore, Italy; diluted 1:500).

Rabbit polyclonal primary Abs were: Cone Arrestin (AB15282, Merck-Millipore, Italy; diluted 1:5000); Calbindin D (CB38a, Swant Ltd., Switzerland, diluted 1:500); Connexin 36 (Cx36; 51-6200; Invitrogen, Carlsbad, CA; diluted 1:500); Protein Kinase Cα (PKCα; P4334, Sigma-Aldrich, Italy; diluted 1:800); Glial Fibrillary Acidic Protein (GFAP; G9269, Sigma-Aldrich, Italy; diluted 1:1000); Ionized Calcium Binding Adapter Molecule 1 (IBA1; 019-19741, Wako Chemicals GmbH, Germany; diluted 1:500); Disabled-1 (DAB1; diluted 1:200; a generous gift from Botond Roska, Friedrich Miescher Institute for Biomedical Research, Basel, Switzerland); RBPMS (1830-RBPMS; PhosphoSolutions, Colorado; diluted 1:500); Tyrosine Hydroxylase (TH, AB152; Merck-Millipore, Italy; diluted 1:1000).

A sheep polyclonal Secretagogin (SCGN, RD184120100; BioVendor GmbH, Germany; diluted 1:2000) antibody and a goat polyclonal Choline Acetyltransferase (ChAT, AB144P, Merck-Millipore, Italy; 1:500) were also used.

Antibodies against Cone Arrestin, Calbindin D, PKCα and TH were also used in whole mount preparations, at 10x the concentrations used for sections.

Secondary antibodies were: donkey anti-mouse Alexa Fluor 488 (715-547-003); donkey anti-rabbit Alexa Fluor 488 (711-546-152); donkey anti-goat Alexa Fluor 488 (705-546-147); donkey anti-sheep Alexa Fluor 488 (713-546-147); donkey anti-mouse Rhodamine Red X (715-295-151); and donkey anti-rabbit Rhodamine Red X (711-295-152) all from Jackson ImmunoResearch laboratories, Inc., USA; these were diluted 1:800 both for retinal sections and whole mount preparations.

For nuclear counterstaining, retinal sections were incubated in Hoechst (33342; Life technologies, Italy; diluted 1:1000) for 3 minutes at room temperature; retinal whole mounts were incubated over night at 4 C^{o}. After multiple washing steps in PBS, specimens were mounted in Vectashield Antifade Mounting Medium (H-1000; Vector Laboratories, Burlingame, CA) and cover slipped.

Mouse monoclonal primary antibodies	Source	Dilution rate
Rhodopsin	Sigma-Aldrich, Italy; O4886	1:1000
Protein Kinase Cα (PKCα)	Sigma-Aldrich, Italy; P5704	1:800
CD68 (KP1)	Santa Cruz Biotechnology; sc-20060	1:250
C-Terminal Binding Protein-2 (CtBP2/RIBEYE)	BD Biosciences; 612044	1:800
Glutamine Synthetase (GS)	Merck-Millipore, Italy; MAB302	1:1000
Non-Phosphorylated Neurofilaments (SMI32)	Covance, CA, USA; SMI-32R	1:800
Glutamic Acid Decarboxylase-67 (GAD67)	Merck-Millipore, Italy; MAB5406	1:500
Rabbit polyclonal primary antibodies		
Cone Arrestin	Merck-Millipore, Italy; AB15282	1:5000
Calbindin D	Swant Ltd., Switzerland; CB38a	1:500
Connexin36 (Cx36)	Invitrogen, Carlsbad, CA; 51-6200	1:500
Protein Kinase Cα (PKCα)	Sigma-Aldrich, Italy; P4334	1:800
Glial Fibrillary Acidic Protein (GFAP)	Sigma-Aldrich, Italy; G9269	1:1000
Ionized Calcium Binding Adapter Molecule 1 (IBA1)	Wako Chemicals GmbH, Germany; 019-19741	1:500
Disabled-1 (DAB1)	gift from Botond Roska, Basel, Switzerland	1:200
RBPMS	PhosphoSolutions, Colorado; 1830-RBPMS	1:500
Tyrosine Hydroxylase (TH)	Merck-Millipore, Italy; AB152	1:1000
Sheep polyclonal primary antibody		
Secretagogin (SCGN)	BioVendor GmbH, Germany; RD184120100	1:2000
Goat polyclonal primary antibody		
Choline Acetyltransferase (ChAT)	Merck-Millipore, Italy; AB144P	1:500
Secondary antibodies	**all from Jackson ImmunoResearch laboratories, Inc., USA;**	
donkey anti-mouse Alexa Fluor 488	715-547-003	1:800
donkey anti-rabbit Alexa Fluor 488	711-546-152	1:800
donkey anti-goat Alexa Fluor 488	705-546-147	1:800
donkey anti-sheep Alexa Fluor 488	713-546-147	1:800
donkey anti-mouse Rhodamine Red X	715-295-151	1:800
donkey anti-rabbit Rhodamine Red X	711-295-152	1:800

Table 2. Summary of primary and secondary antibodies used in this study.

5.4. Transmission Electron Microscopy (TEM)

To achieve optimal preservation of mouse retina ultrastructure and overcome several technical problems (including mechanical artifacts, presence of tissue swelling, poor contrast of the tissue, membrane rearrangements etc.) encountered when using published embedding methods, we implemented a protocol optimized for fragile, highly degenerated mouse retinal tissue (**Figure 5.2**), merging indications obtained from several laboratories, including ours (Morrow et al. 2005; Ghinia et al. 2016).

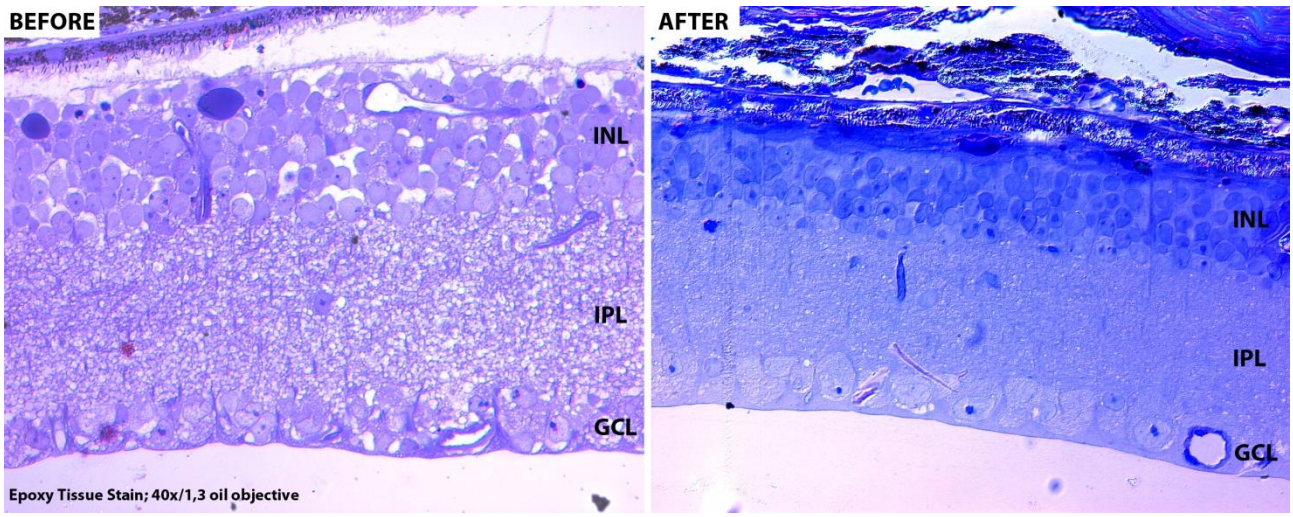

Figure 5.2. Semi-thin sections of the Tvrm4 retina 6 weeks after photo-induction before and after our tissue preservation protocol optimization. The tissue became obviously more compact with less mechanical and chemical induced micro damages (i.e. lower contrast, white areas around cell bodies in the image on the left).

Animals were deeply anesthetized with intraperitoneal 0.1 ml / 5 g body weight Avertin injections, the eyes quickly explanted, and mice killed by cervical dislocation. Enucleated eyes – with a blue mark on the dorsal pole – were immediately transferred in oxygenated ACSF where the cornea, iris and lens were removed, and the eyecups were immersed in primary fixative (1 %(w/v) Glutaraldehyde + 2 %(w/v) Formaldehyde in Sorenson's buffer M/30, pH 7.4 + 5 % (w/v) Sucrose) for 2 hours at 4 C^{o}. Following primary fixation, the eyecups were cut into 4 equal pieces corresponding to the retinal quadrants (dorsal, nasal, ventral and temporal) without detaching the retina from the sclera and transferred into secondary fixative (3 %(w/v) Glutaraldehyde in Sorenson's buffer M/30, pH 7.4 + 5 % (w/v) Sucrose) over night at 4 C^{o}. Afterwards, samples were extensively washed in buffer at room temperature (Sorenson's buffer M/30, pH 7.4 + 5 % (w/v) Sucrose - 10x5mins) and immersed for 2 hours in 3 %(w/v) Potassium Ferro-cyanide + 2%(w/v) OsO4 in H2O, at 4 C^{o}. Osmication was followed by washing steps (0.05 M Maleate buffer, pH 5.15

- 10x5minsand by staining an bloc with uranyl acetate (1 %(w/v) Uranyl Acetate in 0.05 M Maleate Buffer, pH 6) for 1 hour at 4 C^o. Blocks were than washed on room temperature (0.05 M Maleate buffer, pH 5.15 - 5x5mins), dehydrated with ethanol (70 %(v/v) Ethanol – 15mins; 80 %(v/v) Ethanol – 15 mins; 90 %(v/v) Ethanol – 15 mins; 100 % Ethanol – 4x15mins) and infiltrated first with propylene-oxide (Propylene-oxide – 2x15mins) then with a mixture of propylene-oxide and resin (50 %(v/v) Propylene-oxide 50 %(v/v) resin catalyzed with 2% DMP30) over the night on room temperature. The last step was embedding (100% resin catalyzed with 2% DMP30) followed by 24 hours heat treatment for proper polymerization of resin at 65 C^o. Sectioning was performed using a Leica Ultracut ultra-microtome and a diamond knife. Ultra-thin sections, 90 nm thick, were collected on single-hole copper grids (Formvar Support Film Slots, 2x1 mm Cu grids; FF2010-CU). No grid staining was necessary given the high contrast of the specimens and the sensitivity of the EM camera.

Step	Solution	Duration [min]	Temp. [˚C]
1st day			
Dissection	Oxygenated Artificial Cerebro-Spinal Fluid (ACSF)		RT
Fixation	1 %(w/v) Glutaraldehyde + 2 %(w/v) Formaldehyde in Sorenson's buffer M/30, pH 7.4 + 5 % (w/v) Sucrose	120	4
Fixation	3 %(w/v) Glutaraldehyde in Sorenson's buffer M/30, pH 7.4 + 5 % (w/v) Sucrose	over night	4
2nd day			
Extended Wash	Sorenson's buffer M/30, pH 7.4 + 5 % (w/v) Sucrose - 10x5mins	60	RT
Osmicating	3 %(w/v) Potassium Ferro-cyanide + 2%(w/v) OsO4 in H2O	120	4
Extended wash	0.05 M Maleate buffer, pH 5.15 - 10x5mins	60	RT
an bloc UA	1 %(w/v) Uranyl Acetate in 0.05 M Maleate Buffer, pH 6	60	4
Wash	0.05 M Maleate buffer, pH 5.15 - 5x5mins	30	RT
Dehydration	70 %(v/v) Ethanol	15	4
Dehydration	80 %(v/v) Ethanol	15	4
Dehydration	90 %(v/v) Ethanol	15	4
Dehydration	100 % Ethanol - (4x15mins)	60	4
Infiltration	Propylene-oxide - (2x15mins)	30	RT
Infiltration	50 %(v/v) Propylene-oxide 50 %(v/v) resin (catalyzed with 2% DMP30)	over night	RT
3rd day			
Embedding	100% resin (catalized with 2% DMP30) - cure in oven	1 day	65
4th day			
Sectioning			

Table 3. Summary of the enhanced tissue preservation protocol for TEM.

5.5. Imaging and analysis

5.5.1. Cell counts in retinal whole mounts.

Retinal whole mounts were imaged with a Zeiss Axioplan light microscope equipped with a Zeiss Axiocam color camera using a Plan Neofluar 1,25x/0,035 objective to measure retinal surface prior and post confocal microscopy. Image acquisition for cell number quantification was performed with a Leica TCS-SL confocal microscope equipped with 488 and 453 lasers, using a Plan Apochromat 40x/1.40 oil objective, employing identical laser and camera settings for all samples. Four fields (250 x 250 micrometers) were acquired at each eccentricity of the retina, as shown by the schematic figure below (**Figure 5.3.**), summed up representing 1/15 of the total area of the tissue. Images saved as TIFF files and transferred to a MetaMorph image analyzer, where cell counts were performed. Statistical comparison of experimental groups was executed in SigmaPlot applying one-way ANOVA test with Holm-Sidak post-hoc method. The one-way analysis of variance (ANOVA) is a powerful statistical test to determine whether the means of three or more independent groups are statistically significantly different or not. However, it is important to note, that ANOVA is an omnibus test, unable to identify those groups that were significantly different from one another, which is why a post-hoc test was applied. Post-hoc tests are able to determine which groups are statistically significantly different from each other and the Holm-Sidak method is specifically comparing the groups pairwise to elucidate this difference.

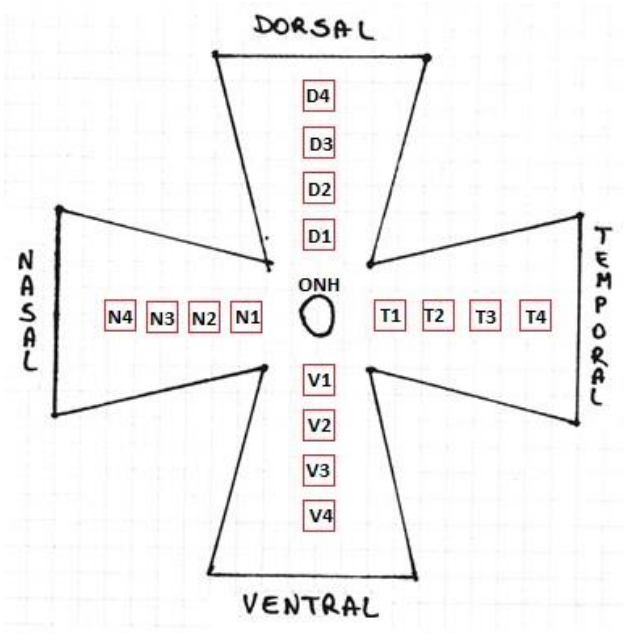

Figure 5.3. Scheme of image acquisition map for cell number quantification on retinal whole mounts.

5.5.2. Image thresholding analysis.

To estimate axonal ending complexity of bipolar cells in retinal whole mounts and vertical sections, or the area covered by immuno-positive puncta representing synapses in the inner plexiform layer, images were obtained with a Leica TCS-SL confocal microscope using a Plan Apochromat 40x/1.40 or 100x/1.30 oil objective. Micrographs were saved as tiff files; brightness and contrast were adjusted with the Zeiss software ZEN®PRO 2012 or with Adobe Photoshop. Images were homogeneously thresholded in the regions of interest, thresholded area was normalized to1 mm^2 and the average number of cells per retina averaged for each experimental group. Statistical evaluation was done in SigmaPlot using one-way ANOVA tests with Holm-Sidak post-hoc method.

5.5.3. Whole mount reconstruction.

Retinal whole mounts were imaged with an Imager.Z2 microscope using EC Plan-Neofluar 5x/0.16 M27, 10x/0.3 M27 and 20x/0.50 M27 objectives; images were tiled with ZEN module "Tiles & Positions" software to reconstruct the entire retinal surface. TH positive cells were counted on tile images of entire retinal images obtained with a 10x objective.
Additional images of vertical sections were obtained with a Zeiss Imager.Z2 microscope equipped with an Apotome2 device (Zeiss, Milan, Italy) using an EC Plan-Neofluar 20x/0.50 M27 objective.

5.5.4. TEM analysis.

Images were obtained using a Jeol 1200EX II electron microscope (Jeol, Milan, Italy) equipped with a charge-coupled device (CCD) Olympus Veleta Megaview (Olympus, Munster, Germany) camera at a magnification of 40.000x, covering systematically the entire width of the IPL. A total of 400 EM images/sample were obtained. Image files were saved as TIFF and transferred to MetaMorph image analysis workstation, where synapses were counted manually. Criteria applied to identify conventional synapses: the presence of synaptic vesicle clusters densely opposing the presynaptic membrane, the occurrence of synaptic densities, the clear identification of pre- and postsynaptic processes; and ribbon synapses: the presence of an osmiophilic ribbon, sheet or globular synaptic machinery at the active zone with the archiform density or freely floating in the cytoplasm but always undoubtedly tethering synaptic vesicles, the clear identification of pre- and postsynaptic processes. Counts were averaged per experimental group and statistically analyzed in SigmaPlot with one-way ANOVA tests with Holm-Sidak post-hoc method.

6. RESULTS

6.1. Retinal degeneration in adult Tvrm4 mice

Within 48 hours from light-induction, a typical rod-to-cone degeneration with the main features of RP becomes evident in the posterior pole of the eye of Tvrm4 adult mice. The ONL width is visibly reduced and numerous pyknotic nuclei of dying PRs appear at the transition zone between central and more peripheral retina, the latter having not been reached by the beam of inducing light. Giant, membrane-bound clusters of DNA, hallmarks of this model species, form at regions where PRs die out. These are presumed products of the fusion of multiple degenerating PR nuclei and can reach several microns in diameter, at times bulging into the INL. Photoreceptor death is accompanied by glial activation conforming to early RP symptoms: GFAP expression is upregulated in Müller glia at the central, degenerating retina, but this phenomenon is not spreading to peripheral retinal areas. Similarly, IBA1-positive microglial cells with highly activated, amoeboid forms, invade the central retina, while resident microglia maintain a normal state in the peripheral tissue. Retinal ERG recordings show a significant reduction in both a and b wave amplitudes demonstrating ongoing PR death. One week after induction, the central retina is devoid of PRs (**Figure 6.1**). Morphological remodeling of inner retina manifests the first sign, being represented by retraction of dendritic arbors from RBCs. Metabotropic glutamate receptor 6 (mGluR6) immunoreactivity in the OPL decreases dramatically in parallel to dendritic retraction, while residual mGluR6 positive puncta become misplaced in the inner nuclear layer (INL), where they appear on the axons of bipolar cells (**Figure 6.2.**)

The present study focuses on inner retinal remodeling after complete PR degeneration in the central retina, and in particular describes changes occurring 3, 6 and 9 weeks PI.

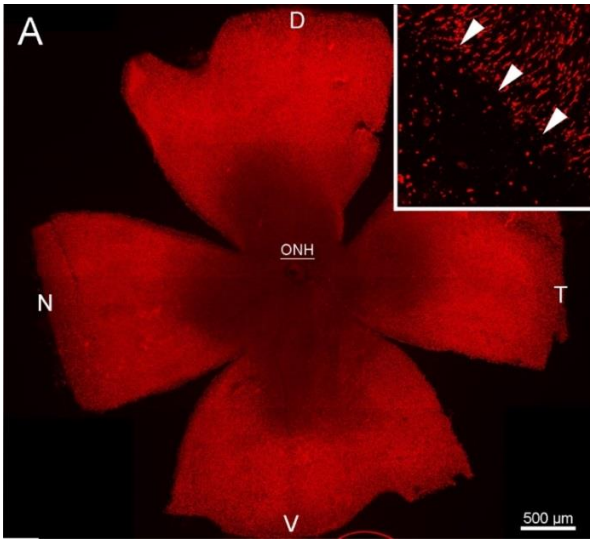

Figure 6.1. Tvrm4 retinal whole-mount stained for anti-Cone Arrestin, 1 week after 1 min 12.000 lux light-induction. The central retina shows reduced immunoreactivity indicating evident loss of cone PRs. The zoomed image is showing the border line between living and actively degenerating PRs, further referred as transition zone (arrow heads) (Gargini et al. 2017).

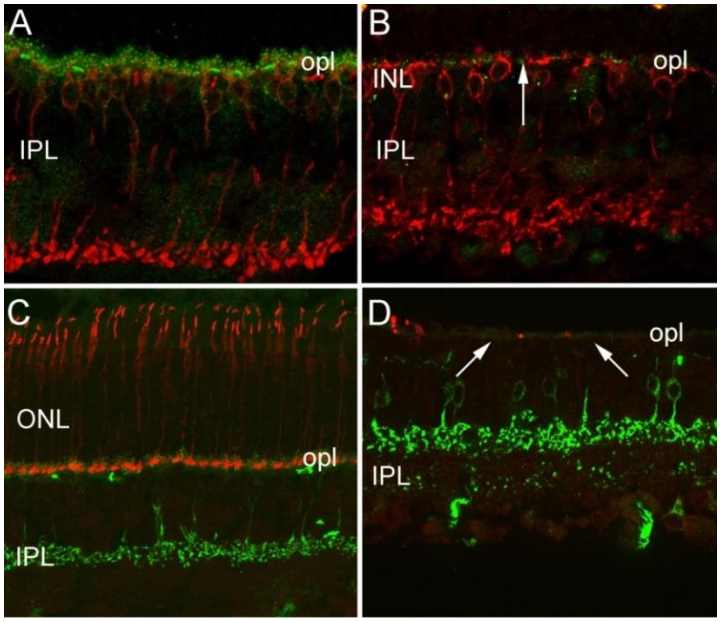

Figure 6.2. Tvrm4 retinal vertical sections obtained 1 week after 1-minute (12.000 lux) photo-induction. At this time PRs completely die out from the central, irradiated area. (A, B) Anti-PKCα (red) and anti-mGluR6 (green)staining, showing the WT and Tvrm4 induced retina, respectively. In the induced retina, RBCs start retracting dendrites and the large majority of mGluR6 signals disappear from the OPL leaving only a few residual receptors behind at the site of degenerating cone endings (white arrow on picture B) (C, D) Cone opsins (red) and ZNP1/synaptotagminII (green) staining, WT (C) and induced (D), respectively. One week after photo-induction, the central retina is lacking PRs; the complete loss of ZNP1 immunoreactivity in the OPL (white arrows on picture D) highlights dendritic retraction in type 2 CBCs (Gargini et al. 2017).

6.1.1. Retinal phenotype 3 to 6 weeks post-induction

By 3 weeks PI, PR degeneration and death in the central retina are terminated and surviving rods and cones can only be found in the far periphery. A similar phenotype is also visible in the retina 6 weeks PI (**Figure 6.3.**). Yet, at this stage DNA filled bodies are not completely cleared out by phagocytic cells and some of them persist in PR-lacking areas up to 9 weeks PI, the latest time point examined in this study (**Figure 6.11.**).

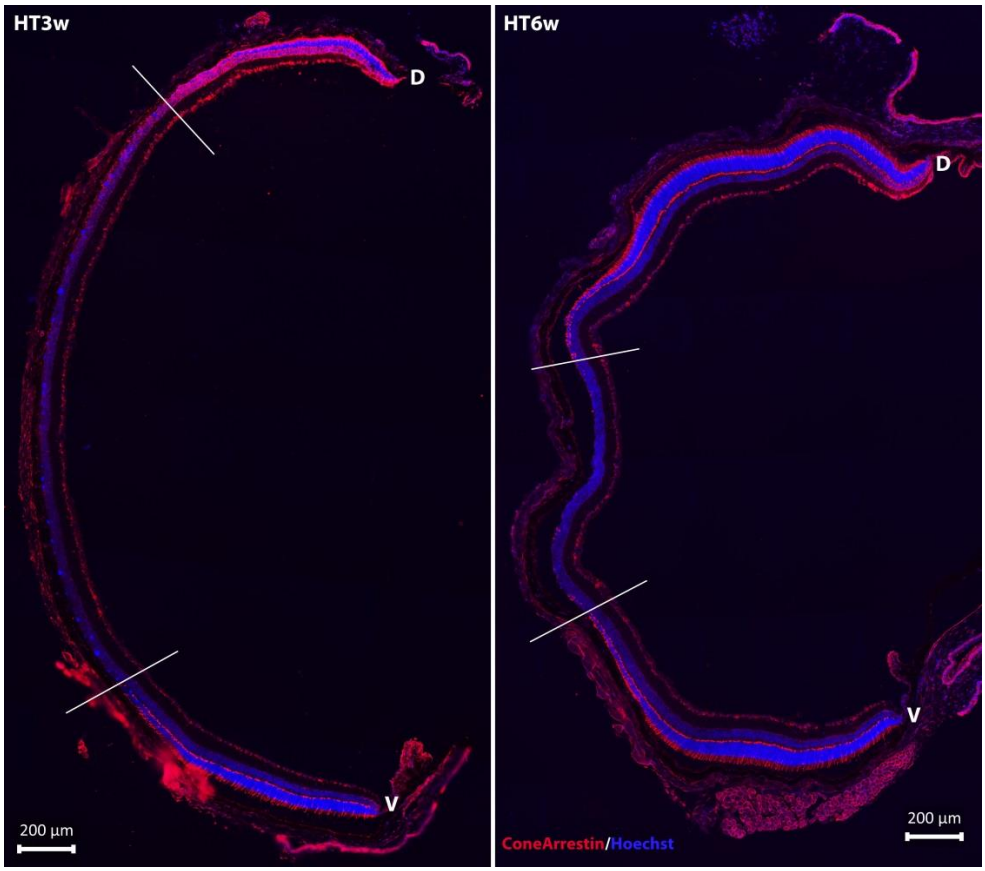

Figure 6.3. Dorso-ventral sections of the Tvrm4 retina 3 and 6 weeks PI, stained for anti-Cone Arrestin and Hoechst nuclear marker. Photoreceptor degeneration reaches advanced stages in the central retina 3 to 6 weeks PI: surviving rods and cones can only be found in the far periphery (white borderlines). (HT3or6w=heterozygous Tvrm4 mice 3or6 weeks PI; D=dorsal; V=ventral)

6.1.2. Rod Bipolar Cells

Dendritic atrophy and retraction in BCs is first observed around 7 days after photo-induction. By 3 weeks PI, RBC completely lost their dendrites in the central, degenerated retina, and this event is accompanied by a shrinkage of RBC axonal endings in the IPL. The same is generally true for the retina examined 6 weeks PI (**Figure 6.4.**).

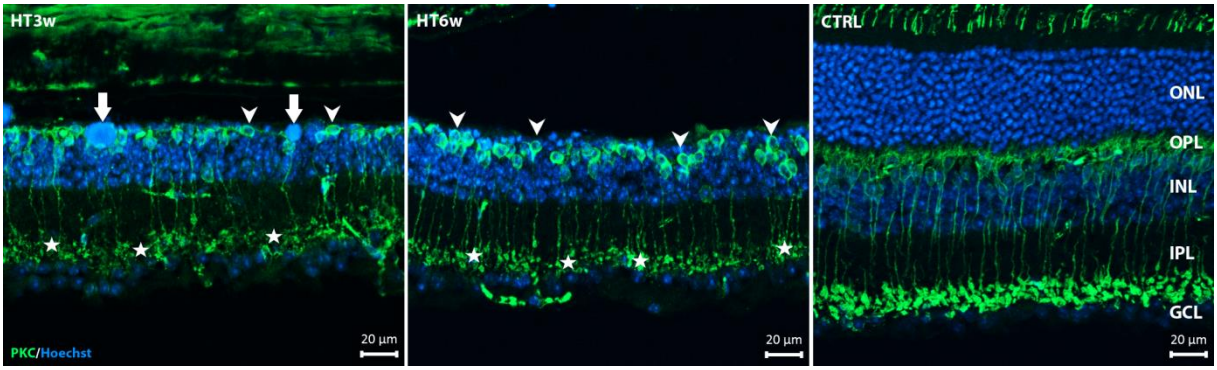

Figure 6.4. Vertical sections of the Tvrm4 retina 3 and 6 weeks PI stained for anti-PKCα and Hoechst nuclear marker. By 3 to 6 weeks PI, PRs die out from the central retinal completely, only giant DNA clusters (arrows) are observed in these regions corresponding to leftovers of PRs. In the same retinal areas, RBCs retracted their dendrites (arrowheads) and their axonal endings exhibited a shrinkage in surface and volume (stars).

The soma of RBCs were counted in retinal whole mounts stained against PKCα antibodies, respectively 3 (n=3 mice) and 6 weeks (n=4) following phenotype induction. RBCs did not undergo significant changes in the overall cell number (one-way ANOVA, p=0,295) demonstrating nearly 100% survival rate even 6 weeks PI (**Figure 6.5.**). Survival of RBCs was observed despite regression of dendritic trees and significant shrinkage of axonal endings found at the two identical time points. Axonal shrinkage was quantified in vertical retinal sections by analyzing the retinal surface covered by axonal arborizations in sublamina 5 of the IPL. A decrement larger than 50% was observed in the surface occupied by RBC axonal arbors and lying within the illuminated, PR devoid areas (one-way ANOVA, p≥0,0001, n=3 retinas) compared to controls. This confirms the regression of axonal arbors secondary to the degeneration of PRs.

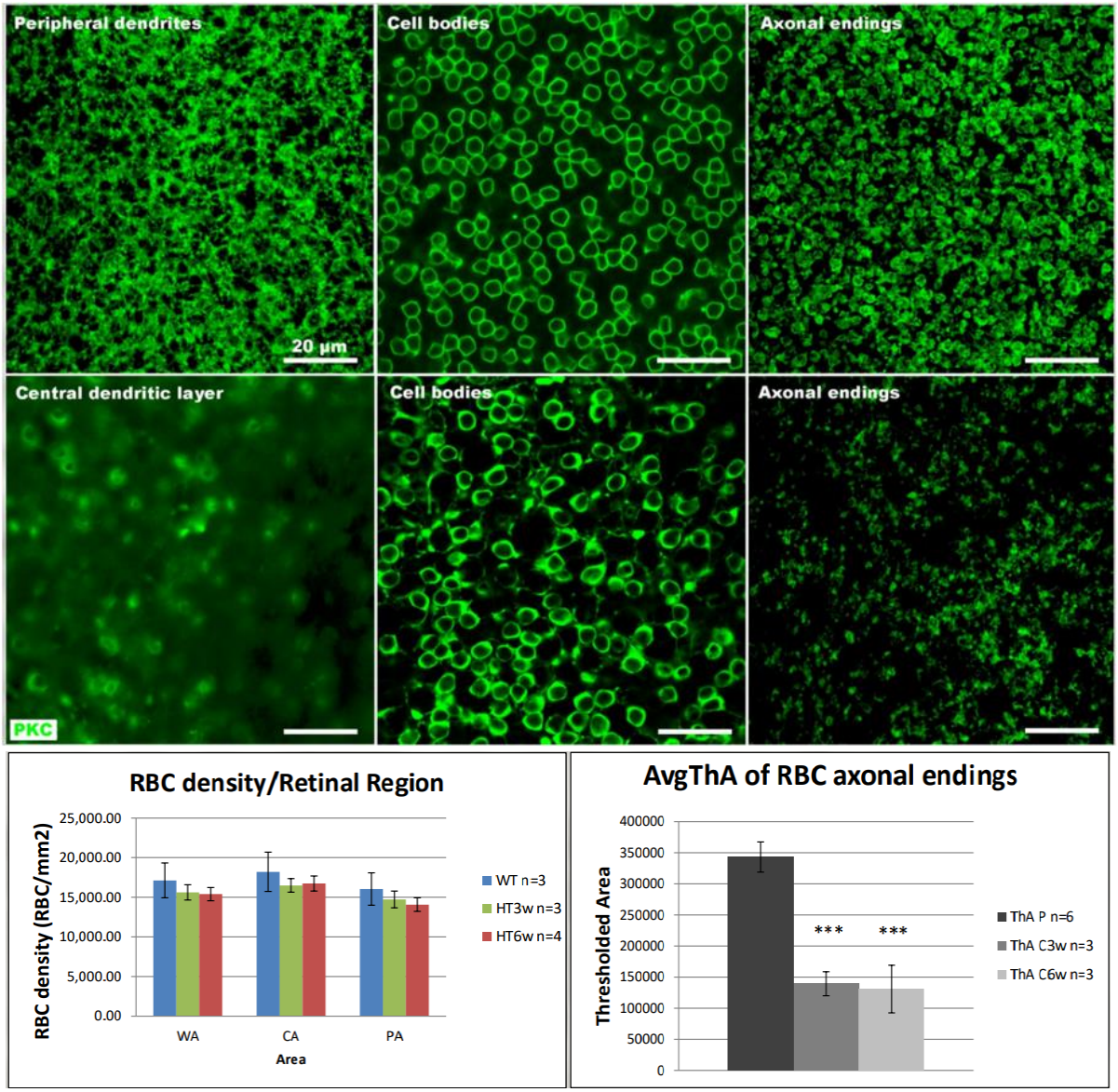

Figure 6.5. Retinal whole mount of a Tvrm4 mouse 3 weeks post-induction, stained for anti-PKCα. Rod bipolar cells positive for PKCα were analyzed in retinal whole mounts 3 and 6 weeks PI. Dendrites were fully retracted at both time points examined. No statistical difference was found in the number of cell bodies compared to WT controls (p=0,295) meaning that RBC survival rate was close to 100%. However, a significant shrinkage of axonal arborizations of these cells (***=p≤0,0001) was evident 3 and 6 weeks PI when comparing central retina to periphery. (WA=whole area; CA=central area; PA=peripheral area; WT=wild type; HT3w/HT6w=heterozygous mouse 3 or 6 weeks PI; ThA=thresholded area; P=periphery; C3w/C6w=central retina 3 or 6 weeks PI)

6.1.3. Horizontal Cells

The analysis of remodeling of second order neurons continued by counting HC bodies using retinal whole mounts stained for anti-Calbindin D. Retinal analysis 6 weeks PI demonstrated that HCs completely disappeared from islands of variable size and shape in the central retina, creating transition zones with extremely sharp edges between surviving and dead cells. Interestingly, these islands were not precisely overlapping with PR-lacking areas, as HC were typically missing in the transition zones of PR degeneration; moreover, numerous HCs with hypertrophic processes were preserved next to these islands albeit no PRs were left in the corresponding outer retina. HC body counts revealed a 28% decrease (one-way ANOVA, p≥0,01; n=3 retinas) over the whole retinal area with respect to WT controls (**Figure 6.6.**).

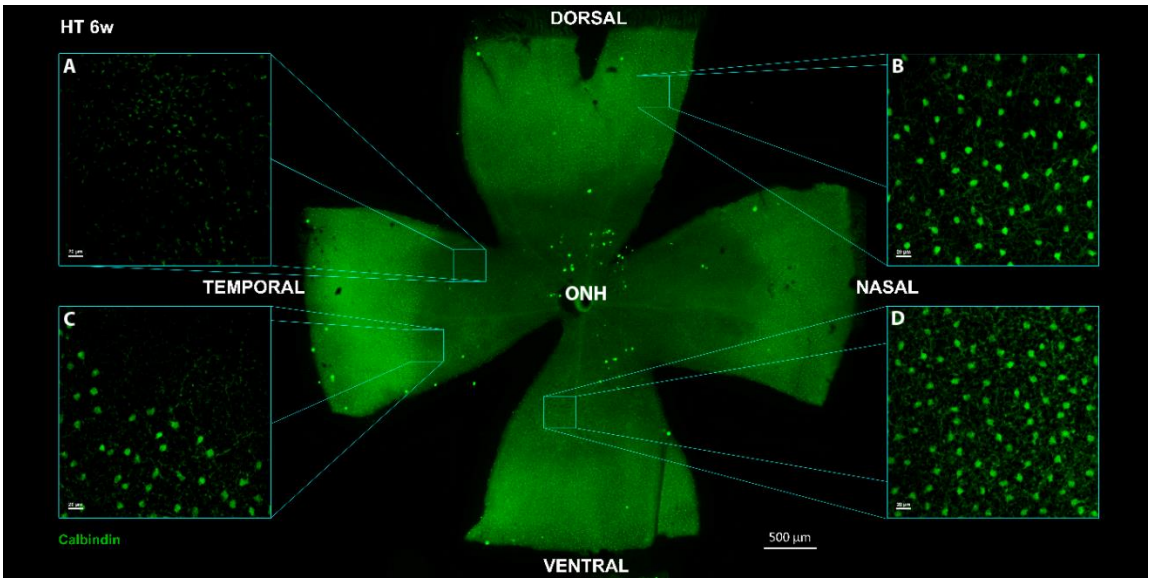

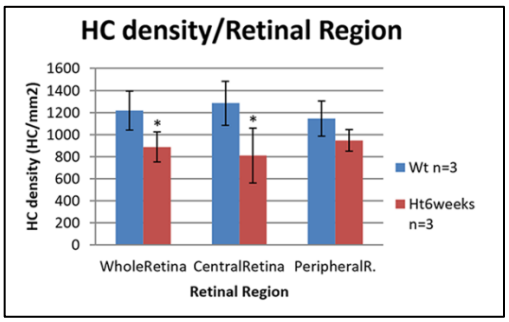

Figure 6.6. Retinal whole-mount of a Tvrm4 mouse 6 weeks PI stained for anti-Calbindin D antibody. Degeneration of HCs is visible even on low magnification micrographs and is represented by the faint central area, with reduced immunofluorescence. (A,D) Central retinal areas without HCs and with preserved HCs with hypertrophic processes respectively; (C) transition zone of HC degeneration; (B) peripheral retina with HCs of normal morphologic features. (ONH=optic nerve head; scale bar on images A,B,C and D represent 20 microns). The graph is summarizing quantification data of HCs 6 weeks PI compared to WT controls.

Frozen, vertical sections of the retina stained against Calbindin D and Neurofilament-200 (NF200) antibodies confirm the occurrence of preserved HCs bodies and dendrites in central retinal areas devoid of PR and of decreased HC density in transition zones. The fact that photoinduction affects first the axonal arbors of HCs (NF200 positive) postsynaptic to rods, while dendrites and cell bodies are maintained, confirms the primary degeneration of rods in this mutant (**Figure 6.7.**), albeit there is no obvious explanation for the higher severity of transition zones compared to the central retina observed for HC remodeling.

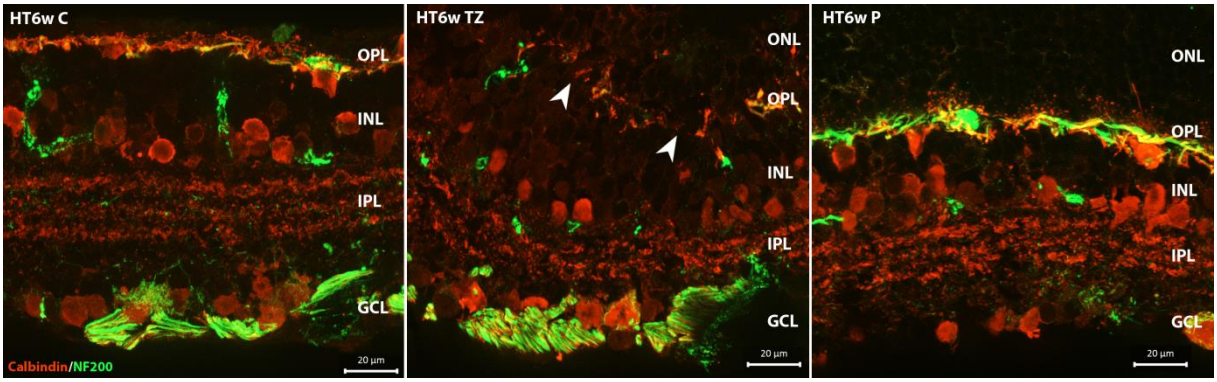

Figure 6.7. Retinal vertical section of the Tvrm4 retina 6 weeks PI stained for anti-Calbindin D and anti NF200 antibodies depicting the central (C) transition zone (TZ) and peripheral (P) areas. HC dendrites, cell bodies and intact HC with both dendritic and axonal compartments appear in the three pictures, respectively. Arrowheads indicate a transition zone completely missing HCs and their axons.

6.1.4. Cone Bipolar Cells

CBCs were studied on vertical sections stained for anti-secretagogin (SCGN), which reveals six different types of cone bipolar cells, stratifying at various depths in the outer and innermost tiers of the IPL. Observations were done 3 and 6 weeks PI. In the central, PR lacking retinal areas, CBC dendritic trees appeared to have lost ramifications and complexity, although retraction was not as severe as for RBCs. No statistical difference was revealed in the number of cell bodies in any of the studied experimental groups, returning a survival rate of 100% of CBCs. However, we found a gradual, significant decrease in the thickness of SCGN+ profiles in the IPL (one-way ANOVA, $p \geq 0{,}001$; n=3 retinas) becoming more and more prominent over time, despite preservation of the thickness of the whole IPL (**Figure 6.8.**).

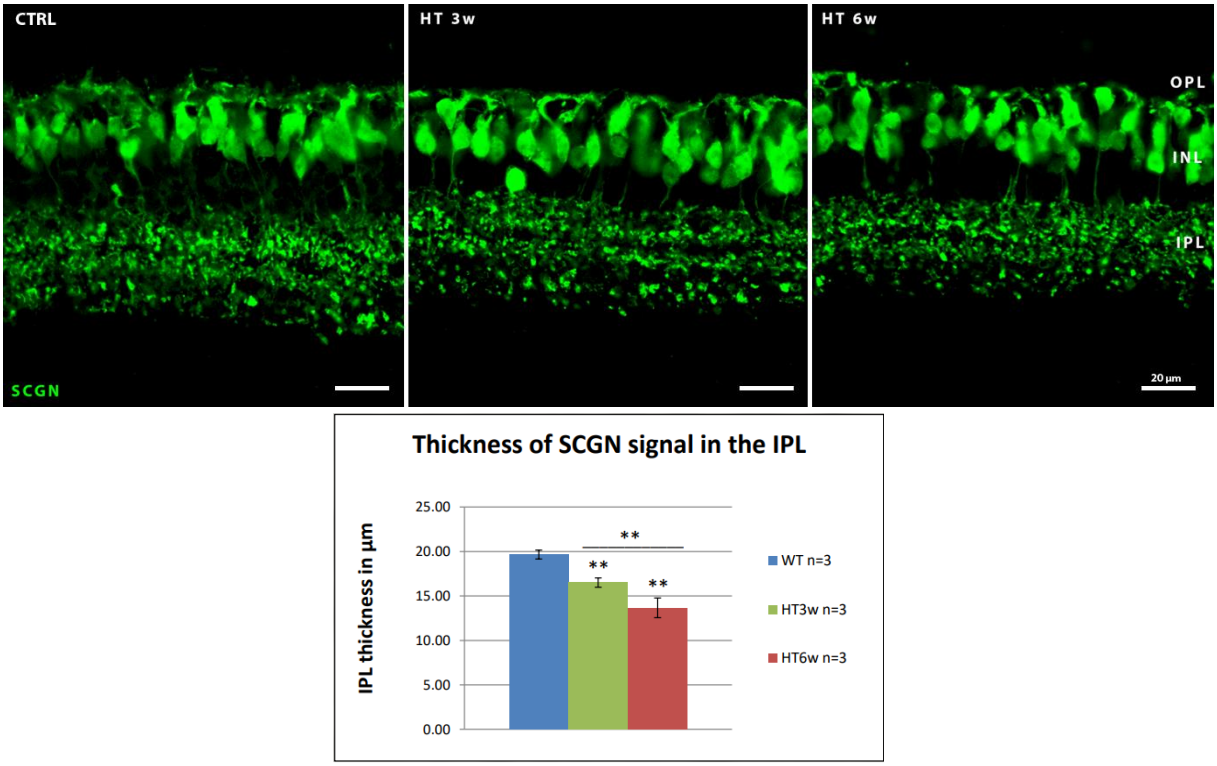

Figure 6.8. Cone bipolar cells were studied on vertical sections stained with anti-secretagogin (SCGN) 3 and 6 weeks PI. After quantification, no statistical difference appeared in the number of cell bodies. Yet, we found a gradual, significant decrease in the thickness of SCGN+ axonal arborization area (**=p≤0,001) over time, despite preservation of the thickness of the whole IPL.

6.1.5. Amacrine cells

Frozen, vertical retinal sections were stained against several AC specific antibodies to label cholinergic (ChAT), GABAergic (GAD67), dopaminergic (TH), AII ACs (DAB1) and Calbindin positive ACs. Immunohistochemistry confirmed the preservation of the aforementioned AC types and categories in the degenerated retina 3 and 6 weeks PI, with no obvious morphological modifications, as illustrated on **Figure 6.9.** It is to note that the AC chosen for staining comprise both large-size amacrines (i.e. dopaminergic and cholinergic cells) as well as small field, glycinergic amacrines, such as the AIIs.

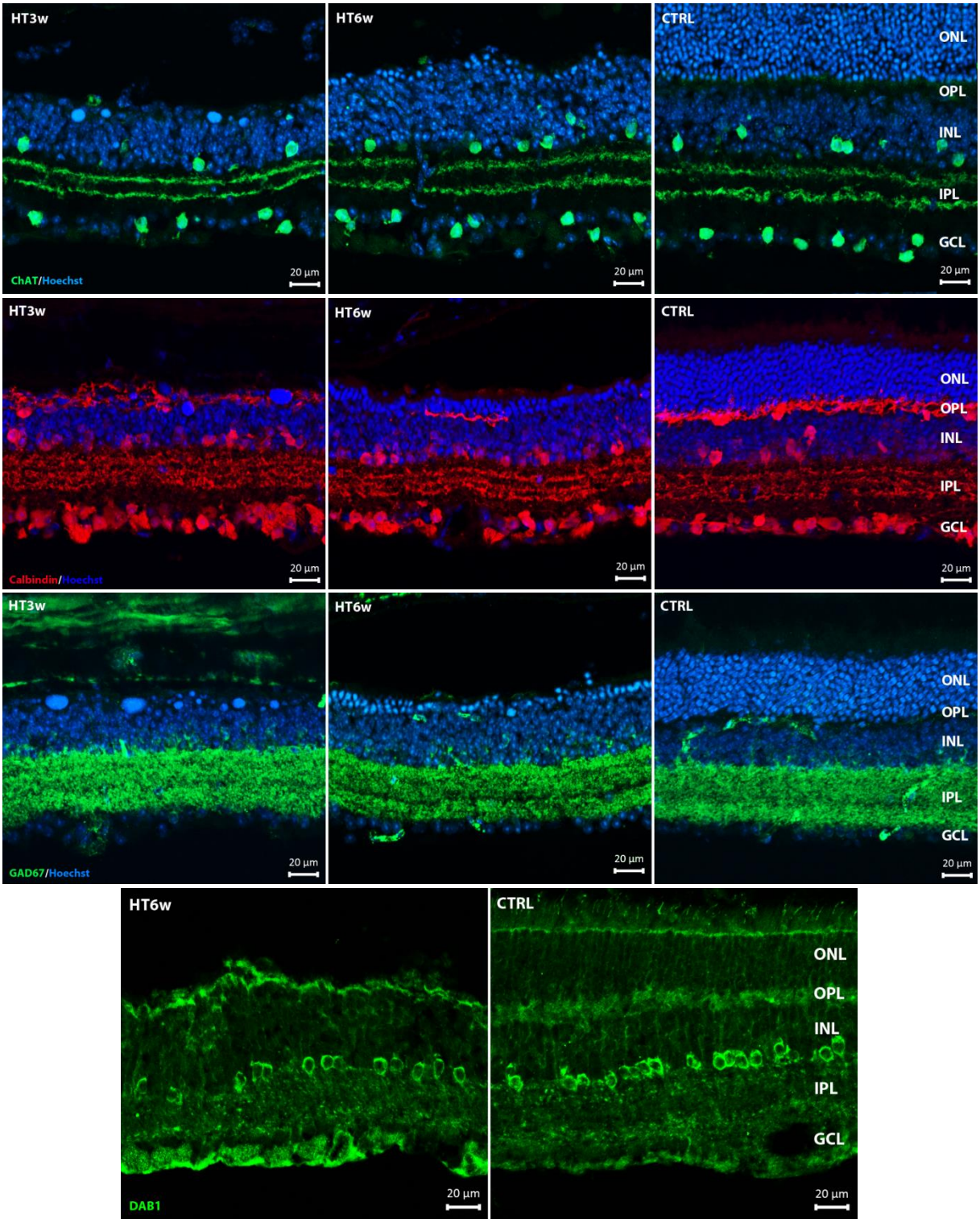

Figure 6.9. Frozen vertical sections of the Tvrm4 retina stained for AC markers: Calbindin, GAD67, ChAT and DAB1 respectively. All the aforementioned markers showed positive staining in the central retina 3 and 6 weeks PI compared to non-induced WT controls or far periphery of the HT induced eyes. No major changes were observed in the general morphology and laminar organization of these cells and their processes.

Noticeably, TH+ dopaminergic ACs (DAC) showed hypertrophic processes in the OPL, exclusively in the central retina and precisely co-localizing with the PR-lacking area. Furthermore, observations conducted 3, 6 and 9 weeks PI demonstrate that these hypertrophic processes target and entangle some but not all DNA filled bodies in the outer retina (**Figure 6.10 and 6.11.**).

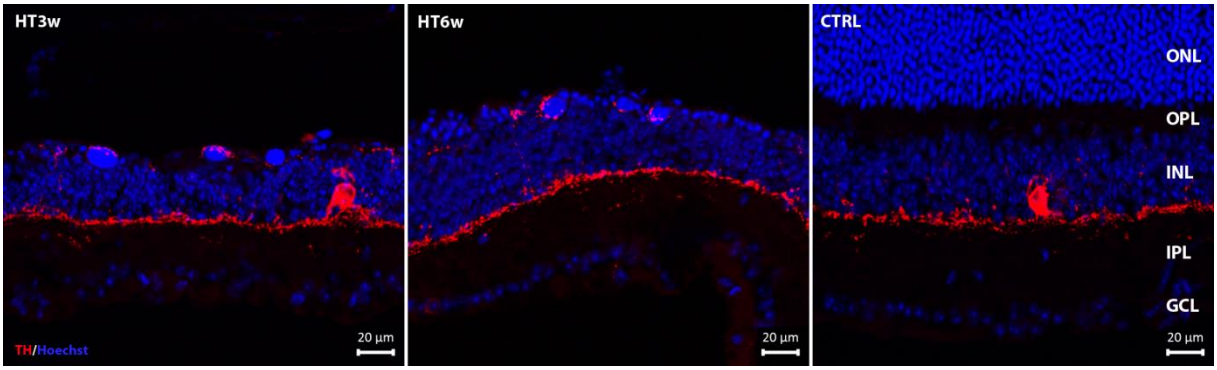

Figure 6.10. Vertical sections of the Tvrm4 retina 3 and 6 weeks PI versus non-induced controls stained for anti-TH. Normal morphology of DACs and their processes is visible throughout the INL and IPL, however hypertrophic OPL processes (arrowheads) reach out to entangle DNA filled bodies, leftovers of PR degeneration 3 and 6 weeks PI exclusively present in the central retina, completely devoid of PRs.

Cell counting of TH+ DACs demonstrated no significant change in the photo-induced retina of Tvrm4 mice 3 and 6 weeks PI (one-way ANOVA, n=3 for each group) compared to the published number of WT B6/J mice (Whitney et al. 2009), showing that the hypertrophic plexus in the OPL arises from sprouting of the pre-existing dendritic arborizations (**Figure 6.11.**).

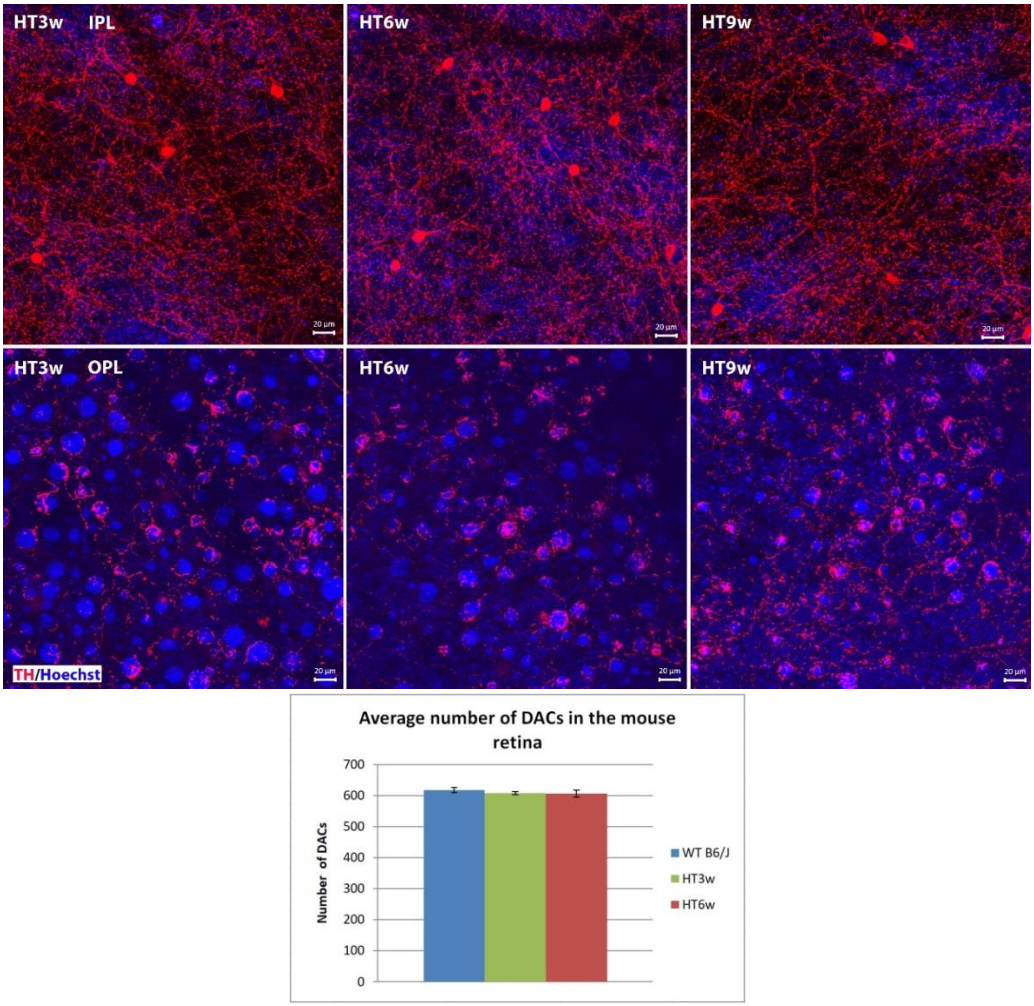

Figure 6.11. Whole-mount micrographs of the Tvrm4 retina stained against TH antibody 3, 6 and 9 weeks PI respectively, taken at the focal plane of the IPL (upper images) and the OPL (lower images). DACs and their processes show normal morphology in the INL/IPL in all experimental groups; cell counts revealed no significant change compared to the number of WT B6/J mice (Whitney et al. 2009). DAC processes in the OPL show obvious signs of hypertrophy exclusively in the central retina coinciding with the area devoid of PRs. Hypertrophic processes are observed entangling DNA bodies, originating from dead PRs. Note the increment in the density of the outer dendritic tiers at increasing PI times and restricted to the PR-devoid areas.

6.1.6. Ribbon Synapses and Gap Junctions in the IPL

To gain data about the distribution of connectivity markers in the IPL of Tvrm4 mice, we used RIBEYE/CtBP2 staining for ribbon contacts and examined vertical retinal sections 3, 6 and 9 weeks PI (n=3 for each group). Confocal micrographs were acquired and edited following identical settings; afterwards, immunoreactivity in the IPL was quantified to estimate the area covered by RIBEYE+ puncta using an image thresholding analysis in region of interest spanning the whole IPL width. A significantly increased threshold area (one-way ANOVA, p=0,010) attributable to RIBEYE+ puncta was revealed 3, but not 6 and 9 weeks after photo-induction with respect to controls (**Figure 6.12.**).

A similar method was used to estimate the density of Cx36+ puncta, revealing gap junctions expressing this particular isoform of Connexin. Thresholding analysis showed significantly higher threshold areas attributable to Cx36+ signals in the IPL (one-way ANOVA, p≥0,001) 3, 6 and 9 weeks after photo-induction with respect to WT controls (**Figure 6.12.**).

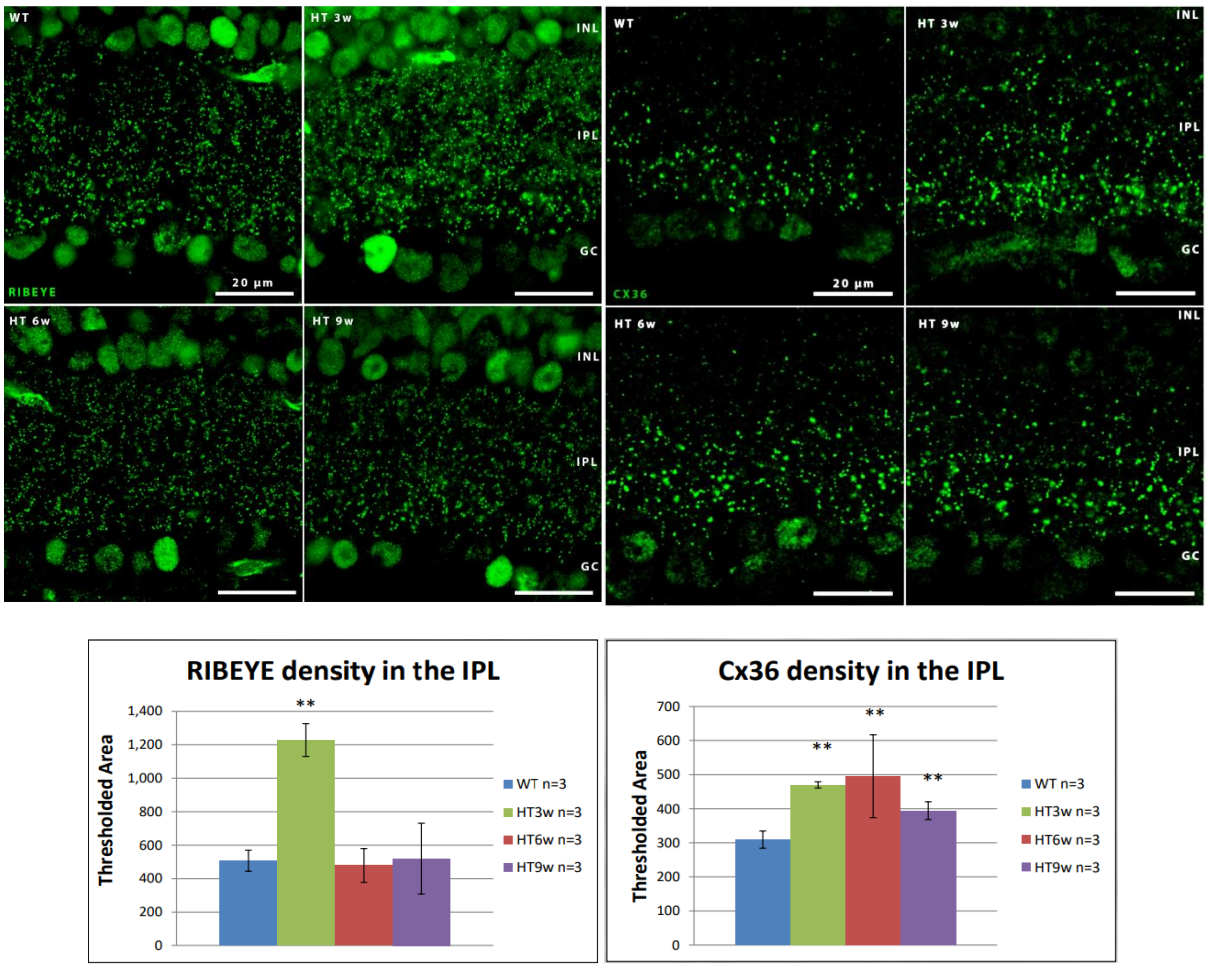

Figure 6.12. Anti-CtBP2/RIBEYE staining of ribbons in vertical sections 3, 6 and 9 weeks PI. A significant increase in the density of RIBEYE+ puncta in the IPL was revealed, 3 weeks PI (**=p=0,001). A similar analysis of IPL gap-junctions labelled with anti-Cx36 showed a significant increase of puncta density in all the experimental groups compared to WT controls (**=p≤0,001).

6.1.7. Transmission Electron Microscopy

To further investigate inner retinal connectivity after completion of PR degeneration, we performed Transmission Electron Microscopy (TEM) studies counting conventional and ribbon synapses across the whole width of the IPL 3 and 6 weeks PI (n=3 for each group).

Initial TEM observations revealed visibly smaller RBC axonal endings respect to CTRL specimens. The shrinkage of individual RBC axonal endings is clearly identifiable in virtue of their large size, position in sublamina 5 of the IPL, typical cytological features (presence of large number of vesicles, mitochondria, synaptic ribbons). Similarly, ultrastructural analysis demonstrated general preservation of number and appearance of conventional synaptic contacts in the IPL both 3 and 6 weeks PI compared to non-induced controls (n=3 for all experimental groups). For ribbon synapses,

a decreasing tendency in the overall number was observed from 3 weeks PI on, although their decrement became statistically significant only 6 weeks PI. Specifically, we found 9% less ribbons 3 weeks PI and 16% less ribbons (one-way ANOVA, p=0,034) 6 weeks PI compared to non-induced controls. More than a change in number, we found it interesting to note that in the photo-induced specimens the majority of ribbons appeared to have a globular, round-shape, totally different from the elongated appearance of normal ribbons. Quantitative analysis showed that as many as 72% of all ribbons were globular 3 weeks PI and 61% of them were similarly rounded 6 weeks PI, compared to 10% observed in our controls. Despite these ultrastructural changes, typical dyad synapses composed of RBC-AII-A17 AC synapses seemed well preserved in all experimental groups (**Figure 6.13.**).

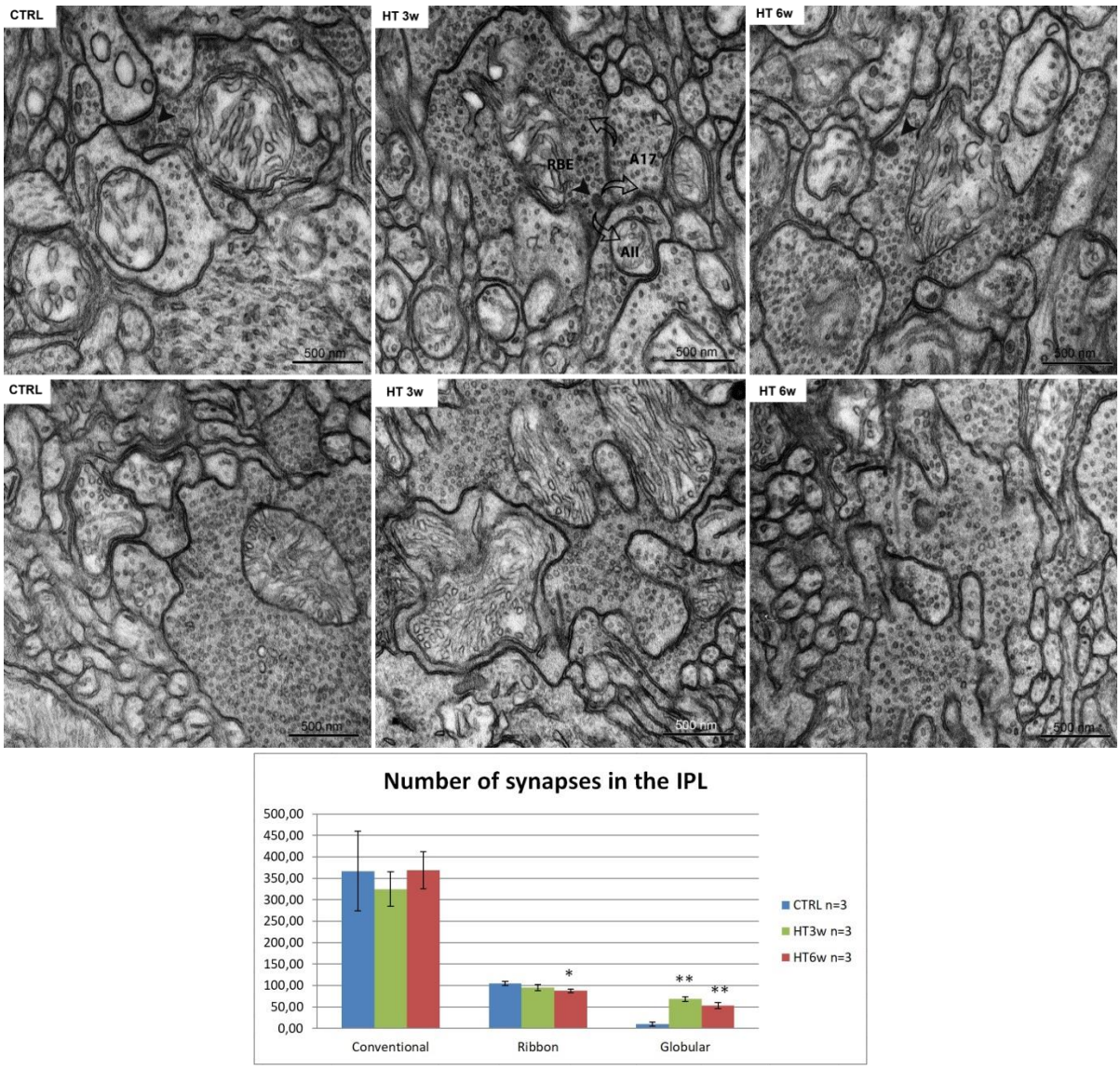

Figure 6.13. TEM micrographs illustrating ribbon synapses of (mainly) rod bipolar axonal endings (RBE). Significantly more ribbons appeared to be globular in shape (**=P<0,001) PI compared to non-induced controls. Globular ribbons (black arrowheads) represent 72% of all ribbons 3 weeks PI and 61% 6 weeks PI, in spite of the high preservation of the RBE-AII-A17 AC synaptic triad organization (2nd picture, upper row, arrows indicate the direction of neurotransmission). Total number of ribbons show a decreasing tendency, already significant 6 weeks PI.

6.1.8. Glial Cells

GFAP increased immunoreactivity in Müller glia and astrocytes was prominent at all the age points studied, although activation was limited to the central, degenerated tissue and did not spread to peripheral areas, indicating maintenance of tissue homeostasis outside the light-induced retinal region (**Figure 6.14.**).

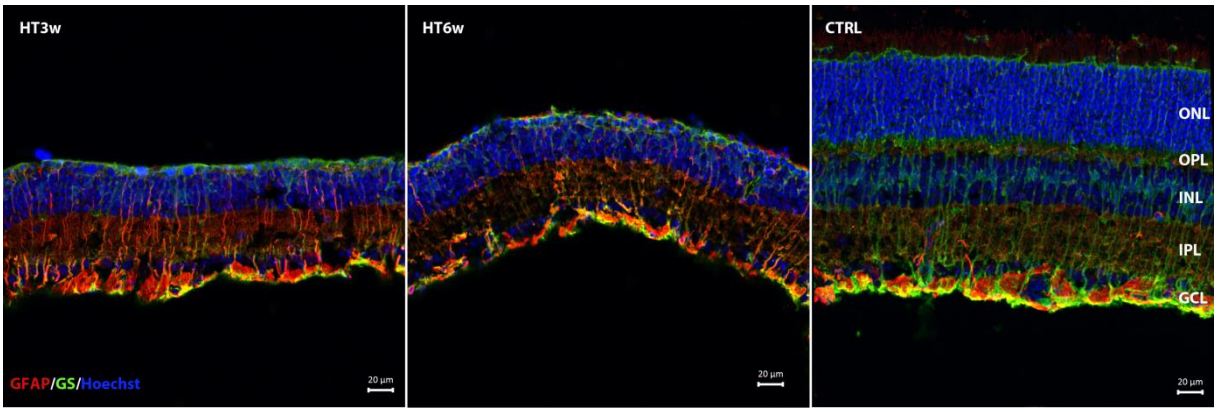

Figure 6.14. Tvrm4 vertical retinal sections stained for anti-GFAP, anti-GS and Hoechst nuclear marker 3 weeks PI, 6 weeks PI and not induced respectively. Radial GFAP hypertrophy is visible both 3 and 6 weeks following photo-induction but is not present in the non-induced or induced peripheral tissues serving as controls with WT phenotype.

It has been shown that activation of local microglia in Tvrm4 mice peaks around 1-week PI (Gargini et al. 2017). Here, we observed that when PR degeneration reaches more advanced stages (3 to 6 weeks PI), microglial activity is reduced, as demonstrated by the presence of quiescent, ramified microglia in the outer and inner plexa and virtual absence of IBA1 positive cellular profiles at the interface between retina and pigment epithelium (**Figure 6.15.**).

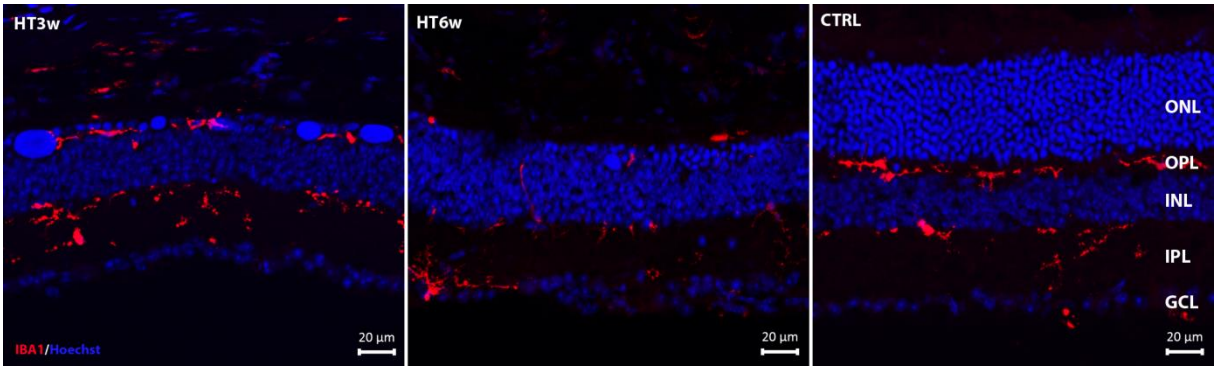

Figure 6.15. Vertical sections of the Tvrm4 retina 3 and 6 weeks PI stained for IBA1 antibody and Hoechst nuclear marker. Although microglial activation is reported in the Tvrm4 retina shortly after photo-induction (Gargini et al. 2017), by 3 to 6 weeks PI, with no or few PRs left in the central retina, microglial morphology turns back to the inactive, ramified state both in the OPL and IPL of the central and peripheral retina of photo-induced animals.

6.1.9. Ganglion Cells

Previous studies on ganglion cells in retinal degeneration rodents predict that no morphological alterations should be expected in these cells in relatively early stages of the retinal phenotype (Mazzoni et al. 2008, Damiani et al. 2012). Indeed, we did not observe alterations of the fundamental anatomical features of GCs. RBPMS and SMI32 staining showed normal organization of cell bodies, dendrites and axonal bundles of these cells in vertical sections at all the time points studied both 3 and 6 weeks PI (**Figure 6.16.**).

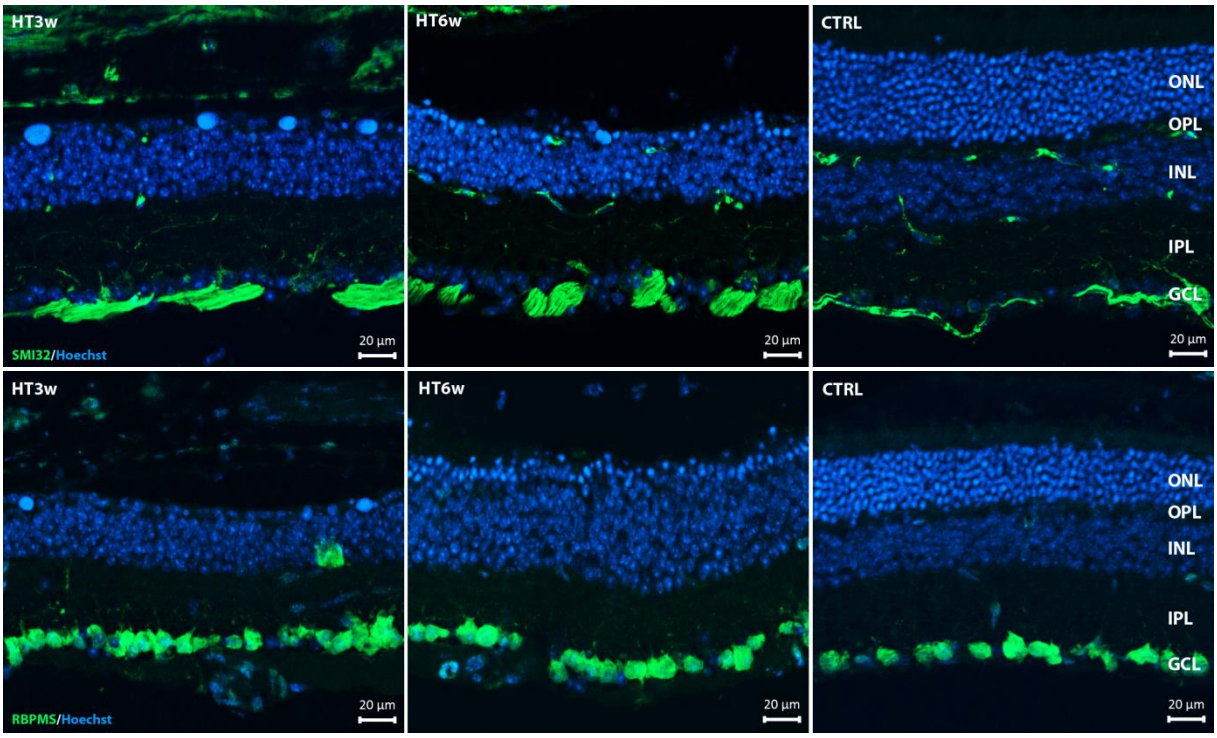

Figure 6.16. Tvrm4 retinal vertical sections stained for anti-SMI32 (upper images) and anti-RBPMS (lower images) along with Hoechst nuclear marker 3 and 6 weeks PI. Processes and cell bodies of ganglion cells show normal morphologic features in both experimental groups comparing the central, damaged retina to the healthy-looking periphery of the induced retina or to WT non-induced samples.

Altogether, the inner retina of adult Tvrm4 mice demonstrated considerably high levels of cellular and synaptic preservation weeks after PR death was terminated. A 100% survival rate was found among bipolar, amacrine and ganglion cells, in spite of the cell death observed among horizontal cells. Chemical and electrical synaptic structures in the inner plexiform layer were found to be present in large numbers and/or density, however ribbon synapse numbers showed a decreasing tendency (summarized in **Table 4.**).

	HT3w	HT6w	WT	
RBCs (avg num/retina)	223.383 ± 12.290	221.659 ± 12.000	246.416 ± 31.593	
CBCs (avg num/mm^2)	110.322 ± 4.538	106.822 ± 6.358	109.478 ± 5.607	
HCs (avg num/retina)	ND	13.078 ± 1.835	18.104 ± 2.624	
DACs (avg num/retina)	608 ± 5	606 ± 11	617 ± 8,3 (Whitney et al. 2009)	
	HT3w	**HT6w**	**HT9w**	**WT**
RIBEYE/CtBP2 (avg ThA (in pixels)/100 µm^2)	1.227 ± 169	478 ± 175	519 ± 366	507 ± 109
Connexin36 (avg ThA (in pixels)/100 µm^2)	469 ± 15	495 ± 210	394 ± 45	309 ± 43
Conventional synapses (avg num/0,005 mm^2)	324 ± 40	369 ± 42	ND	367 ± 92
Ribbon synapse (avg num/0,005 mm^2)	95 ± 7	87 ± 4	ND	104 ± 5
Globular ribbons (avg num/0,005 mm^2)	68 ± 5	53 ± 6	ND	10 ± 5

Table 4. Summary of quantified data. (ND=non-determined)

6.2. Phenotype induction in young Tvrm4 animals

To gain insight into the influence of the age of onset of PR degeneration upon the entity of inner retinal morpho-functional alterations, we found it relevant to inquire the occurrence of similar or more severe forms of remodeling of the inner retina by studying the same Tvrm4 mutant mice at a developmental stage, more precisely at the time of eye-opening (postnatal day 14-15). One litter (N=6) of Tvrm4 mice, heterozygous for the mutation, was induced at P15 for 2 minutes at 12.000 lux (using the same protocol applied on adult mice) and harvested 2 days, 1 week or 3 weeks thereafter. Frozen, vertical retinal sections were stained with Hoechst, a nuclear dye, and with antibodies against Cone Arrestin and Rhodopsin to visualize cone and rod PRs respectively. However, we failed to find any phenotype in all the eyes examined, where staining methods revealed that PRs were fully preserved.

To rule out the possibility that the light used for the induction did not reach efficiently the retina of very young animals, due to the high curvature radius of the eye or to very small lid fissure at this age, the experiment was repeated ex vivo. Mice of an additional litter (n=3) were harvested at P15, their eyes enucleated to produce eyecups upon removal of outer segments comprising cornea, iris and lens. Eye cups were placed into an oxygenated and heated incubation chamber and photo-induced using the same parameters employed for live mice. Six hours after ex vivo photo-induction,

visible signs of PR degeneration could be detected by Cone Arrestin staining in 2 of the illuminated eyecups (**Figure 6.17.**), although the irradiated areas were uneven in location and size. We concluded that immature PRs of Tvrm4 mice can be irradiated and undergo light-induced degeneration if the radiation can reach the back of the eye at adequate intensity, although this process is in general more difficult to achieve.

The reasons of inability to induce the phenotype in P15 old mice in vivo is not known. One reason could be an insufficient amount of (mutant) RHO present in immature rod outer segments (ROS). Although the expression of RHO can be detected in the mouse retina as early as P6-7, the development of ROS and disc growth is completed only at P25 by reaching a mature length (*Carter-Dawson et. al. 1986*). Another likely possibility is the difficulty to illuminate the back of the eye with adequate amounts of light, given the reduced size of the eye ball and unfavorable optics. A third, intriguing possibility is the occurrence of still unknown, neuroprotective mechanisms acting during development, which could contribute to prevent PR degeneration.

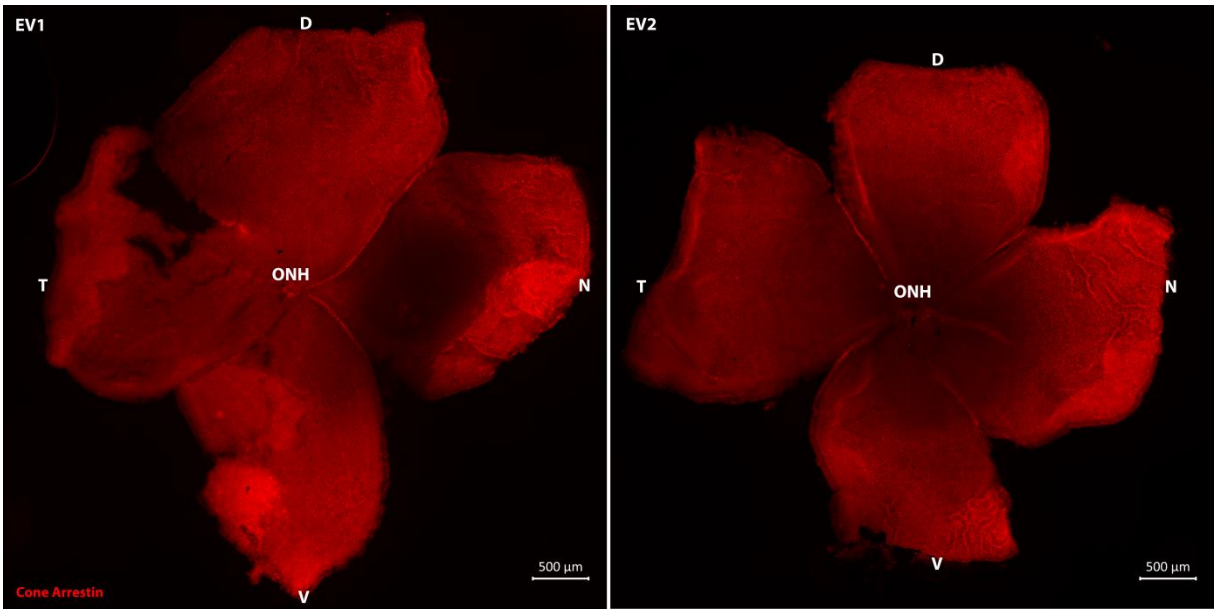

Figure 6.17. Whole mounts of P15 Tvrm4 retinas photo-induced for 2 minutes at 12.000 lux ex-vivo and harvested 6 hours later, immune labeled with anti-Cone Arrestin. Dark areas with low immunoreactivity in the central retina are reflecting obvious signs of PR degeneration. (EV=ex vivo, used as sample name here; ONH= optic nerve head; D=dorsal; V=ventral; N=nasal; T=temporal)

To overcome age-limits, we chose to photo-induce a third litter of mice (n=5), this time at P19 using an extended, 4 minutes light exposure at 12.000 lux, in vivo. A longer exposure maximizes the possibility of trigger the retinal phenotype in this mutant. Animals were harvested 1-week PI. As

a result, 2 eyecups showed severe phenotype, 2 eyecups showed mild PR degeneration and 1 eyecup was not induced. Results described below are based on one retina with a mild phenotype and on two preparations with more severe degeneration.

6.2.1. Photoreceptors

As a result of 4 minutes, 12.000 lux photo-induction at P19, PR degeneration could be clearly detected 1-week PI with the aid of anti-Cone Arrestin, anti-Rhodopsin antibodies combined with Hoechst nuclear staining. In the central retina a considerable population of PRs had died out (**Figure 6.18.**), although the affected area was definitely smaller than that of the adult animals 1-week after 2 minutes photo-induction, covering less than 30% of the total area of the retina. Yet, albeit restricted to a small retinal region an indication of phenotype severity was found in retinal preparations from very young mice: PR rosettes were observed in the peripheral retina of the two P19 mice with severe central retinal degeneration. These circular arrangements of PRs, often arising when these cells have lost contiguity with the retinal pigment epithelium, were surrounded by highly activated anti-IBA1 and anti-CD68 positive microglia, indicating retinal inflammation (**Figure 6.19.**) and appeared only indirectly related to the primary site of PR loss. Rather, rosettes are known to reflect altered metabolic state at retinal level and abnormal geometric interaction between the retina and the surrounding layers. They have been reported in other rd mutant mice, such as the rd7/rd7 mouse model of PR degeneration (Chang et al. 2002), but never observed in adult degenerating Tvrm4 mice, suggesting that the young, P19 Tvrm4 mutants are more vulnerable to light damage in that respect.

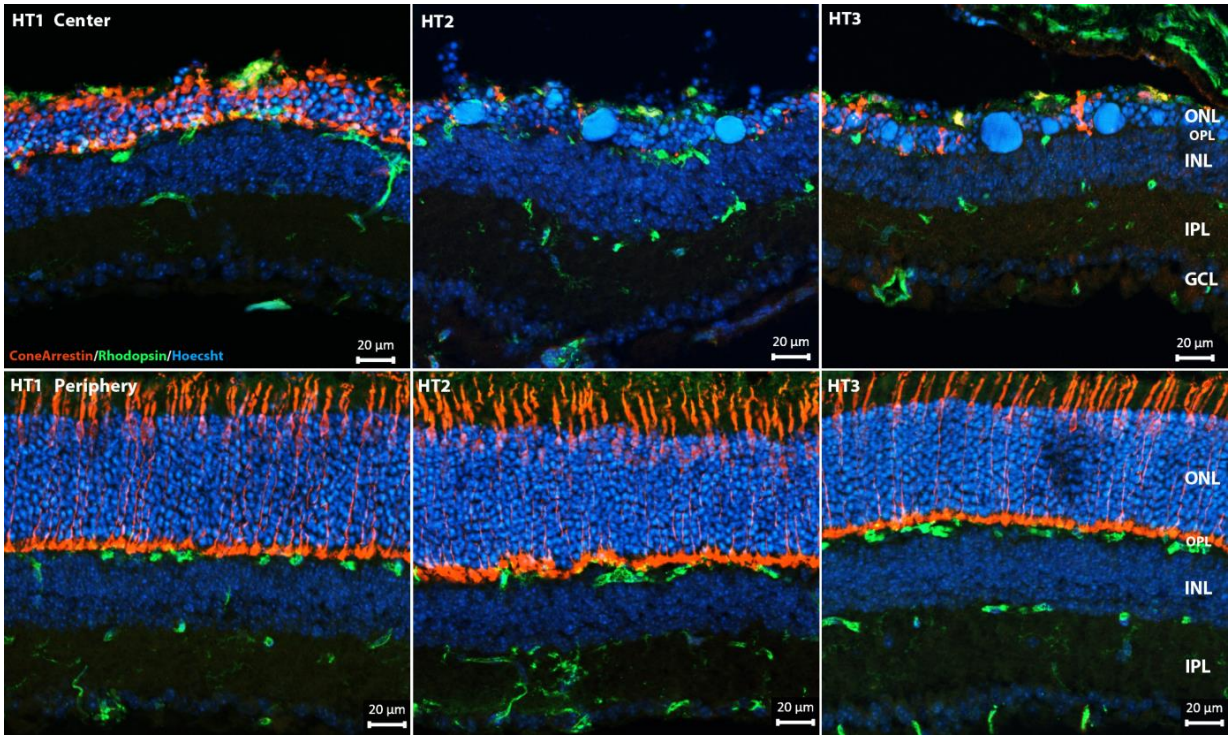

Figure 6.18. Vertical retinal sections of P19 heterozygous Tvrm4 mice 1-week after 4 minutes, 12.000 lux photo-induction stained against Cone Arrestin and Rhodopsin along with Hoechst nuclear marker. Micrographs show mild and severe central and peripheral phenotypes respectively. HT1 animal showed mild, HT2 and HT3 showed severe PR degeneration phenotype in central retina.

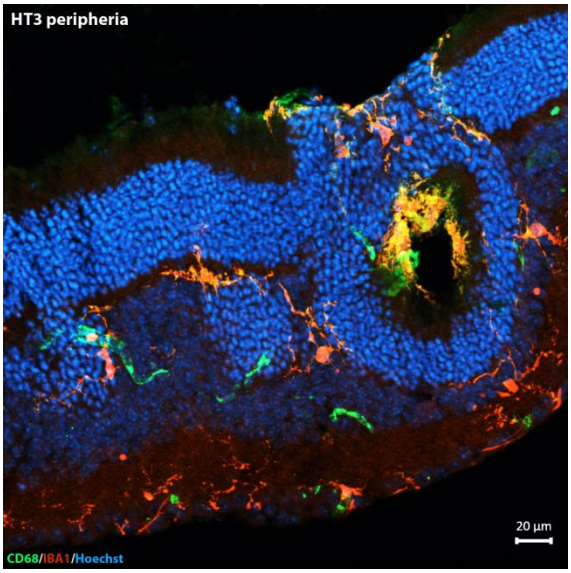

Figure 6.19. Vertical section of the peripheral retina of the HT3 animal, with severe PR degeneration in the central retina, shows PR rosettes surrounded by retinal inflammation as indicated by activated microglia positive for IBA1 and CD68 immuno-labels.

6.2.2. Microglia

Prominent microglial activation could only be observed in the central retina of animals with more severe phenotypes, while a mild PR degeneration resulted in a correspondingly milder microglial activation. As for adult animals, microglial increased reactivity did not reach the retinal periphery (**Figure 6.20.**), albeit PR rosette formations invariably showed high levels of microglial activation (**Figure 6.19.**).

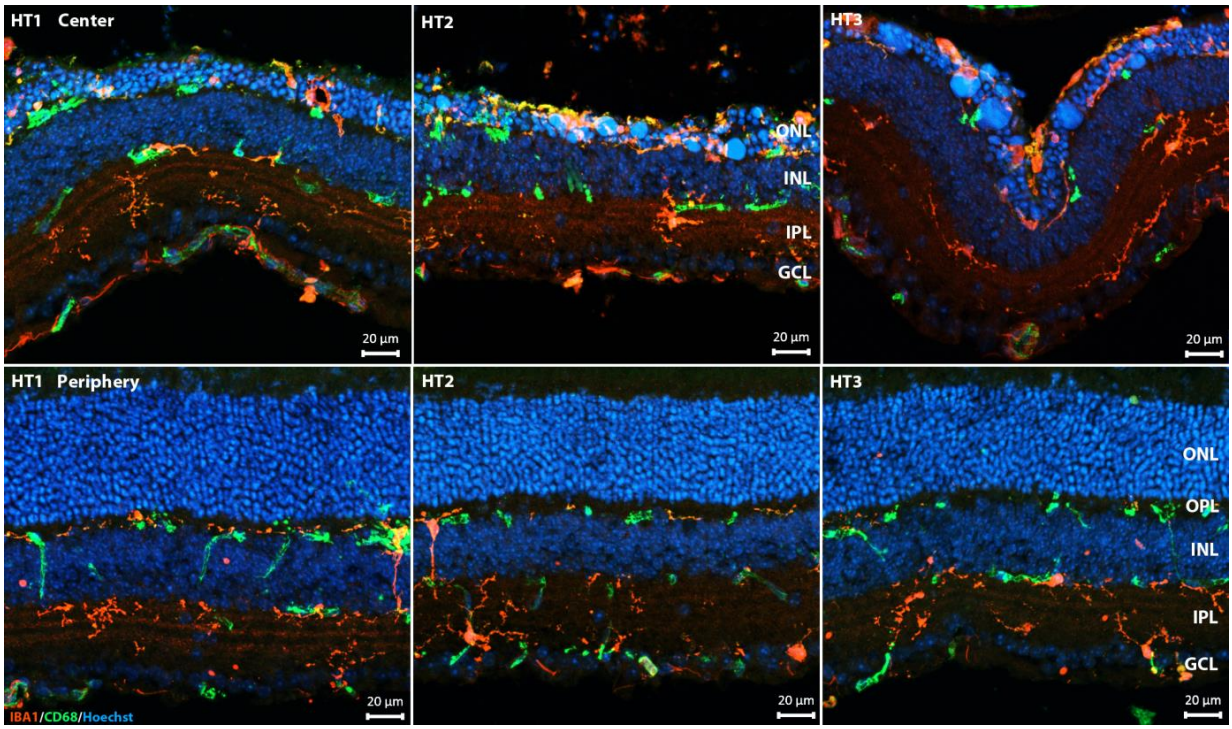

Figure 6.20. Vertical retinal sections of P19 heterozygous Tvrm4 mice 1-week after 4 minutes, 12.000 lux photo-induction stained for IBA1 and CD68 antibodies with Hoechst nuclear marker, showing mild and severe, central and peripheral degeneration phenotypes respectively. As indicated by microglial activation rates, HT1 with a mild phenotype shows mild microglial activation, unlike in HT2 and HT3 samples, where severe PR loss is accompanied with higher levels of inflammation, which is not affecting the peripheral, intact retinal areas.

6.2.3. Second order neurons

As for retinas of adult animals, we used cell type specific antibodies to visualize cells of all the retinal classes (rod and cone bipolar cells, horizontal cells, amacrine and ganglion cells) comparing remodeling in young and adult Tvrm4 mice. Similarly to what we reported for adult animals (**Figure 6.6.**), we found that Calbindin immunoreactivity disappeared from the central retina of animals showing severe PR degeneration. Likewise to what we found in adult mutants, RBCs and CBCs

showed dendritic retraction in severe degeneration mice (**Figure 6.21.**); however, the axonal endings of RBCs showed no signs of shrinkage 1-week PI (**Figure 6.22.**).

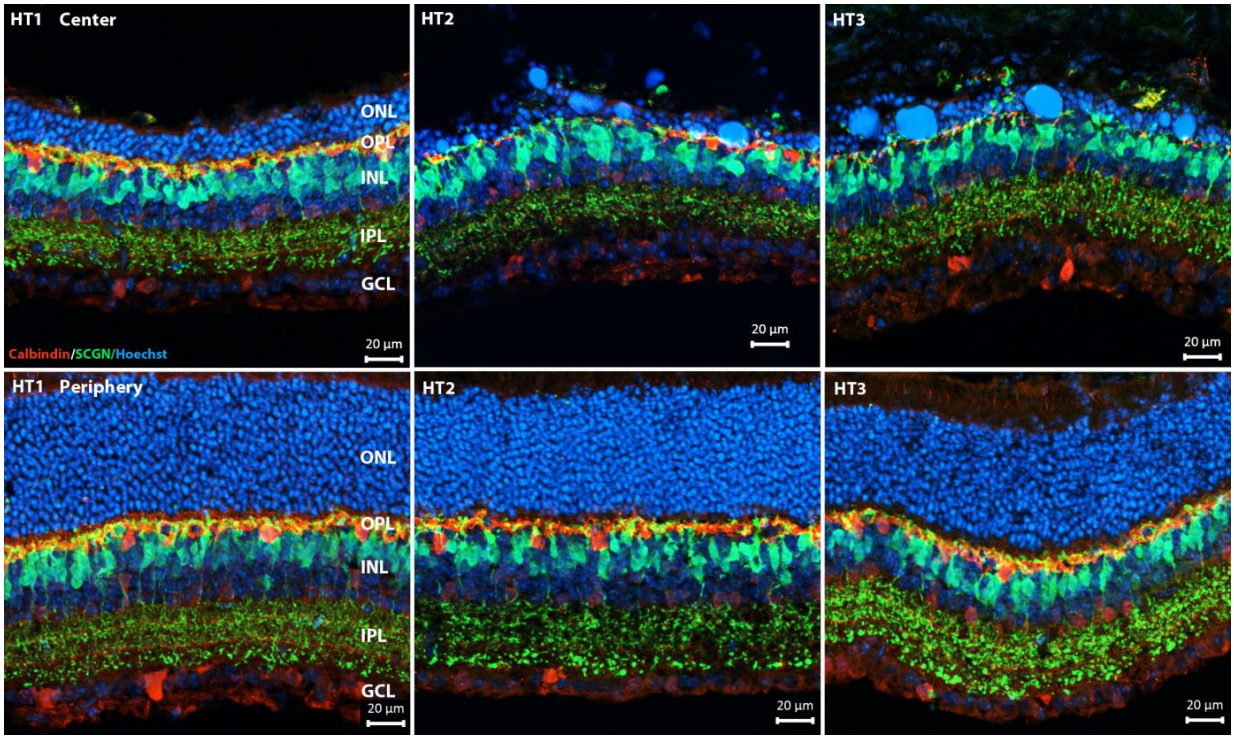

Figure 6.21. Vertical retinal sections of P19 heterozygous Tvrm4 mice 1-week after 4 minutes, 12.000 lux photo-induction stained for Calbindin and SCGN antibodies with Hoechst nuclear marker, showing mild and severe, central and peripheral degeneration phenotypes respectively. Calbindin immunoreactivity is gradually disappearing from the central retina of HT2 and HT3 showing severe phenotypes, at the same areas, SCGN positive CBCs show dendritic retraction comparing the central retina to the periphery.

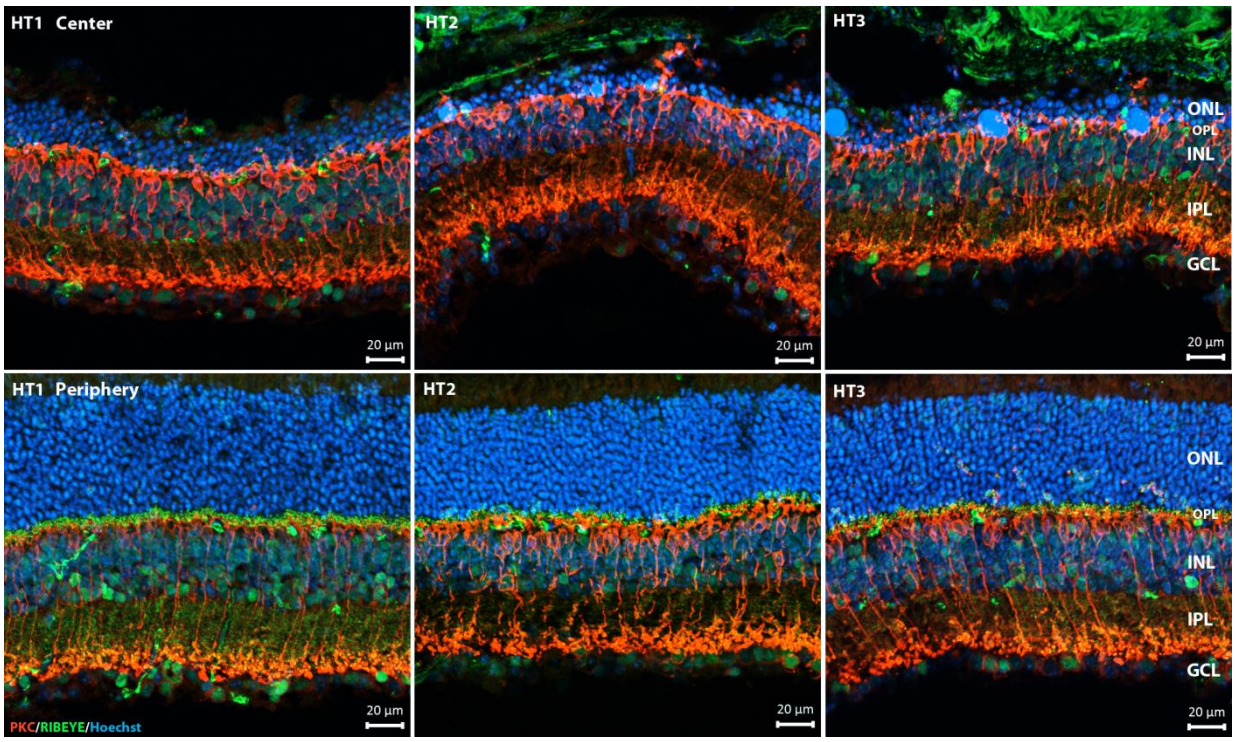

Figure 6.22. Vertical retinal sections of P19 heterozygous Tvrm4 mice 1-week after 4 minutes, 12.000 lux photo-induction stained for PKCα and RIBEYE antibodies with Hoechst nuclear marker, showing mild and severe, central and peripheral degeneration phenotypes respectively. RIBEYE immunoreactivity is gradually disappearing from the OPL of the central retina of all induced animals, at the same areas, PKCα positive RBCs show dendritic retraction, but no signs of axonal ending shrinkage comparing the central retina to the periphery.

Altogether, P19 mice show an overall lower vulnerability against light-induced PR degeneration than their adult counterparts, insofar surviving PRs persist in the central retina 1-week PI, in turn keeping the level of inner retinal remodeling milder. However, rosette formation in the retinal periphery suggest sensitivity of PRs to alterations of local interactions with the RPE, an issue that deserves a separate set of studies.

7. DISCUSSION

7.1. Remodeling in adult Tvrm4 mice

7.1.1. Bipolar cells

High survival rates of rod and cone BCs demonstrate that induced PR degeneration in the mature retina of Tvrm4 mice is by no means more severe than in the developing retina of (for example) rd1 or rd10 mice. Moreover, 6 weeks PI, rod and cone BC number was still close to 100%, unlike in rd10 mice, where RBC number dropped significantly following complete PR degeneration at around 3 months of age (Gargini et al. 2007), an age which is roughly corresponding to the retinal phenotype exibited 6 weeks PI by Tvrm4 mice.

These results suggest that the mature retina has a capacity to maintain viability of second order neurons higher than the developing retina, even at advancing stages of retinal degeneration and complete PR loss.

Denritic retraction of rod and cone BCs has been shown in rd1 and rd10 mice previously (Strettoi and Pignatelli 2000; Strettoi et al. 2002 and 2003; Pang et al. 2011) and it was speculated that this phenomenon might be a result of, or worsened by the fact, that the denritic trees of BCs are still incomplete in development at the beginning of PR degeneration in these mice. However, RBCs of adult Tvrm4 mice fully retract dendrites by 3 weeks PI in central, PR lacking retinal areas similarly to rd1 and rd10 mutants. SCGN positive CBCs also show signs of dendritic retraction, however only to a limited extent, confirming that not all CBCs lose dendrites following PR death. A previous study in Tvrm4 mice (Gargini et al. 2017) showed that, Synaptotagmin II/ZNP1 positive CBC dendrites disappear from the OPL when PR s have died out completely, meaning that at least type 2 CBCs remodel similarly to RBCs, albeit with a delay.

These findings indicate that dendritic remodeling following PR death is not depending on the age of phenotype onset or the underlying genetic mutation and is therefore a true hallmark of RP.

Conclusions referring to the remodeling of RBC axonal endings in rd10 mice have always been quite contradictory as Gargini and colleagues did not report any changes in RBC axon terminals, while Barhoum et al. reported clear atrophy in RBC axonal endings (Gargini et al. 2007; Barhoum et al. 2008). Recent data indicate that RBC axon terminals do remodel, gradually loosing complexity and reducing their surface as retinal degeneration proceeds (Phillips et al. 2010). In fact, Tvrm4 mice show the same traits as early as 3 weeks PI in the central, degenerated retina, where the surface of RBC axonal endings shrinks significantly. SCGN positive axonal endings in the IPL shrink

gradually as well but only in the ON sublaminae of the IPL, as indicated by a thinning in the width of SCGN positive profiles in the plexiform layer.

Altogether, these results suggest that rod-to-cone PR degeneration not only effects RBCs primarily but also, as it proceeds, other members of the ON pathway of retinal signaling, which can be considered as the first targets of inner retinal remodeling.

7.1.2. Horizontal cells

Quantitative analysis of HCs 6 weeks PI revealed an overall 28% reduction in the number of cells throughout the retina of Tvrm4 mice. This finding is in line with what was reported in rd10 mice at around 3 months of age (Gargini et al. 2007). Surprisingly however, unlike in rd10 mice, where HC death overlaps with PR loss, HCs of Tvrm4 mice die out in small islands of the mid-central and mid-peripheral retina, not necessarily overlapping with the retinal area totally devoid of PRs. Moreover, in some cases, the transition zone of PR death is the most severely affected. Furthermore, these HC-free islands show no transition zone whatsoever, instead exhibiting extremely sharp edges between the spots of surviving and dead cells. Counterintuitively, surviving HCs are still present in the central, most damaged retina, although with decreased intensity of fluorescence and hypertrophic processes.

According to these results, HC death is not necessarily coinciding with photo-induced PR death in this mouse model. The fact that the central retina maintains surviving HCs without PRs and other areas with reduced PR rows (generally 2-4 rows) lack HCs completely raises questions concerning cell death triggering factors in this retinal cell types. In vivo or ex vivo monitoring of genetically labeled HCs could help in understanding the precise time-course and locations of cell death following photo-induction in Tvrm4 mice; in addition, biochemical profiling of the mid-peripheral retinal area alongside HC transcriptome analysis might be able to answer these open questions.

7.1.3. Conventional and ribbon synapses

Immunohistochemical analysis of the IPL stained for anti-CtBP2/RIBEYE revealed excellent preservation of synaptic ribbons up to 9 weeks PI in adult Tvrm4 mice with respect to non-induced controls, with significantly higher thresholded area for RIBEYE positive puncta 3 weeks PI.

The latter finding is possibly indicating a peak in synaptic remodeling in the plexiform layer at this time point, which might be driven by the peripheral, PR preserving retinal areas in the attempt to save the flow of remnant visual signals despite extensive PR death in the central retina. In order to prove true retinal plasticity, a complete PR wipe-out experiment would be necessary to check

whether a similar synaptic preservation rate would still be observed in the retina or not. Our laboratory optimized the photo-induction protocol to extend the photo-induced area of the retina by elongating the exposure time and decreasing light intensity at the same time. Based on our observations, a 5 minutes and 6000 lux photo-induction can affect up to 70% of the retinal area, whereas a 10 minutes and 2500 lux induction triggers PR death on up to 90% of the retinal area (data not shown).

In line with the previous hypothesis, a recovery phase in the Tvrm4 retina has been reported 4 weeks after photo-induction based on ERG recordings and histological results. This was speculated to be the result of the presence of a 'halo zone' of the photo-induced retinal area, where PRs managed to survive probably due to insufficient amount of light reaching them. Partially damaged outer segments, still retaining a cilium, could eventually regenerate in 3-4 weeks PI (Gargini et al. 2017). Another possible mechanism to explain the increased density of synapses in the IPL might be the net result of PR migration attempting to fill in the lesioned area as reported by us and by other research groups in cases of focal photoreceptor death (Bush et al. 1999; Paulus et al. 2008; Lin, Masland an Strettoi, 2009).

To assess ultrastructural changes in the IPL of the central retina totally devoid of PRs, Tvrm4 retinas 3 and 6 weeks PI were studied with the aid of TEM imaging. Rod bipolar endings were visibly smaller, however the typical RBC – AII amacrine – A17 amacrine synaptic arrangement at rod bipolar axonal endings seemed to be well preserved in both time points examined. Quantitative analysis of synaptic contacts uncovered no significant changes in the number of conventional, inhibitory synapses in the overall width of the IPL; however, the total number of ribbon synapses displayed a decreasing tendency over time, with significantly less synaptic ribbons 6 weeks PI compared to non-induced control retinas. Moreover, approximately 70 % of all ribbons exhibited and abnormally globular or even amorphous shape 3 weeks PI. Yet, this percentage decresed to 60 % 6 weeks PI, with respect to 10% found in the controls.

Significantly higher thresholded area for RIBEYE positive puncta in the IPL 3 weeks PI shown with the aid of confocal microscopy can indicate two things: either a higher number and density of ribbons, or a larger area occupied by the same number of ribbons, implicating a growth in their area and/or volume. TEM results confirm the latter hypothesis, given the finding that 70 % of the ribbons were found to be globular at 3 weeks PI. This likely results in larger fluorescent profiles in the IPL, causing an increase in the thresholded area. The significantly lower number of ribbons and decrease in the number of globular synapses 6 weeks PI seems to balance immunofluorescence findings, indicating normal levels of signal, similar to what could be observed in control samples. Based on

our ultrasctructural observations, we believe that the number of ribbons might not decrease further at later stages of the disease, and remodeling of the IPL connectivity is tought to stabilize despite regressive changes in the outer retina.

7.1.4. Gap junctions

Immunohistochemical analysis of gap junctions revealed significantly higher thresholded areas for Cx36 positive structures in the IPL at all the time point studied, compared to non-induced controls. This possibly indicates a higher density of gap junctions following PR degeneration. A visible difference is the higher spread of Cx36 positive puncta into the OFF layers of the IPL compared to the control samples (see **Figure 6.12.**).

Gap junctions were proven to contribute to the spontaneous electrophysiological oscillations recorded from animal models of RP (including rd10 mice) and human RP patients. Pharmachological blockade of gap junctions was proven to decrease this spontaneous, aberrant oscillatory activity and restore light responses in the degenerating rd10 retina (Toychiev, Ivanova, Yee, & Sagdullaev, 2013). The increased expression level of Cx36 positive gap junctions obseved in induced Tvrm4 mice could reflect the occurrence of oscillatory activity in this mutant as well. Since nobody has ever attempted to test whether these spontaneous oscillations are indeed present in photo-induced Tvrm4 mice so far, the design of an experiment based on multi-electrode array (MEA) recordings from GCs throughout the timeframe of phenotype progression in this mutant would be of great importance in the future.

Since cell-to-cell coupling and the conductance of gap junctions are known to be highly dependent on and regulated by dopamine levels in the vertebrate retina (Witkovsky, 2004), we decided to study the dopaminergic AC network in Tvrm4 mice, in the attempt to explain the underlying cause of the increased density in Cx36 immunofluorescence.

7.1.5. Dopaminergic amacrine cells

TH labeled dopaminergic amacrine cells showed normal appearance in the IPL, with normal general architecture, process networks and number of cell bodies in the retina of Tvrm4 mice 3, 6 and 9 weeks PI. However, processes reaching out to the OPL were found to be markedly hypertrophic in the central retina, but not in the periphery. These outer directed dendrites were observed entangling the leftovers of dead PRs, represented by DNA filled, membrane bounded bodies, typical side products of photo lesion. Furthermore, the area of hypertrophic processes precisely and exclusively colocalizes with the area of PR loss. This observation and the fact that

DACs are highly reactive to photo-induced PR degeneration could suggest that DACs are electrically coupled to PRs, although there is no evidence either for anatomically defined chemical or electrical synaptic contacts between DACs, BCs and PRs in the outer retina (Witkovsky, 2004; Bloomfield and Völgyi, 2009).

It is also known, that dopamine is released when the retina is lit by light and regulates the gain of retinal neurons to adapt to bright light conditions (Witkovsky, 2004). Since Tvrm4 is a photo-inducible model, it seems logic that dopamine releasing processes get a boost by this extreme light intensity. However, the reason why the hypertrophy of DAC processes persists up to 9 weeks PI is not clear, but one could correlate the phenomenon with the DNA filled bodies, that are also permanent in Tvrm4 mice. Perhaps, dopaminergic processes are still attempting to restore light adaptability in the central retina by boosting whatever is left from PRs.

7.1.6. Other amacrine cell types

Calbindin D, ChAT, GAD67 and DAB1 antibodies were used to reveal GABAergic, cholinergic and glycinergic ACs in the retina of Tvrm4 mice 3 and 6 weeks PI. These markers revealed good preservation of all AC types based on basic anatomical observations on confocal micrographs of vertical sections of the retina. In particular, laminar organization of AC processes and cell body layering appeared absolutely normal.

These results are matching previous reports about long-term AC survival rate in rd10 mice, where all AC types were found in normal physiological and morphological organization, except for AII amacrine cells, which were recently reported to be reduced in number and disorganized in distribution in rd10 mice aged P40 (Barhoum et al. 2008). Tvrm4 mice observed 6 weeks PI, a stage corresponding to the phenotype of P40 rd10 mice, showed considerable preservation of AII ACs in the central retina, despite complete loss of PRs. This might indicate, once again, a higher capacity in maintaining the normal structural organization of the retina, when disease phenotype is activated in the mature tissue. Since AII ACs are key members of the rod signaling pathway, shared by CBCs as well, their long-term survival holds promising opportunities for therapeutic strategies in RP.

7.1.7. Ganglion cells

Previous studies on GCs in retinal degeneration rodent models predict no morphological alterations in these cells at relatively early stages of the retinal degeneration (Mazzoni et al. 2008; Damiani et al., 2012). Indeed, we did not observe alterations of the fundamental anatomical features

of GCs. RBPMS and SMI32 staining showed normal organization of cell bodies, dendrites and axonal bundles of these cells in vertical sections both 3 and 6 weeks PI.

Besides normal anatomical traits, there are multiple previous reports about the presence of a spontaneous, aberrant, oscillatory rhythm in the local field potentials (LFP) of GCs in both rd1 and rd10 retinas based on MEA recordings (Goo et al. 2011; Stasheff et al. 2011). We designed an experiment in close collaboration with Meng-Jung Lee, early stage researcher in the switchBoard project from the lab of Günther Zeck at the Natural and Medical Sciences Institute (NMI), University of Tübingen, to investigate the aforementioned phenomenon in Tvrm4 mice. Due to limited time availability and technical issues, we only managed to successfully record from one single mouse with the desired phenotype in the central retina (photo-induced for 2 mins with 12.000 lux, examined 1 weeks PI). Our preliminary data showed no aberrant spiking activity in the peripheral retina, though vigorous light evoked response activity when stimulated with 500 milliseconds green photopic light; some spontaneous oscillation in the LFP at the transition zone, with obvious light responses for the same light stimulation; and similar spontaneous oscillatory activity without detectable light responses in the central, degenerated retina (**Figure 7.1.**). This confirms previous findings in rd mutant mice and once again proves the potential of Tvrm4 mice in RP research, pointing out to another functional abnormality, the occurrence of spontaneous, oscillatory activity, likely to be a hallmark of most rod-cone retinopathies.

Results from this pilot study strongly encourage to continue and expand the electrophysiological characterization of the Tvrm4 retina, with the aid of either MEA recordings and/or patch-clamping approaches. Specifically, we believe it is important to identify the exact cellular origin of the spontaneous oscillatory activity and to map the changes in the electrical properties of GCs over the time course of PR degeneration exploiting this unique mouse model.

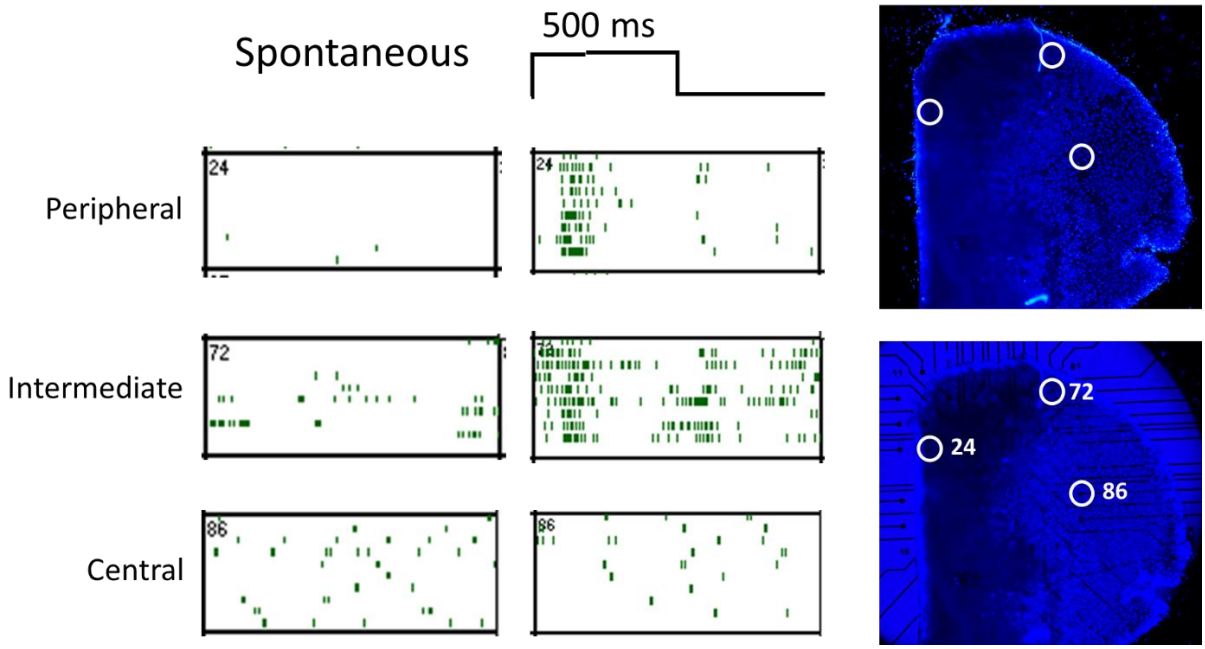

Figure 7.1. The raster plots summarize spontaneous and light evoked activity of GCs on a 60 MEA setup. Electrode number 24 represents the retinal periphery, number 72 is covered by the intermediate/transition zone, while electrode number 86 was covered by the central, most degenerated retinal piece. Placement of the retina related to the positions of the individual electrodes was confirmed with Hoechst nuclear staining post-recording. We recorded no aberrant spiking activity in the peripheral retina, though vigorous light evoked response activity when stimulated with 500 milliseconds green photopic light; some spontaneous oscillation in the LFP at the transition zone, with obvious light responses for the same light stimulation; and similar spontaneous oscillatory activity without detectable light responses in the central, degenerated retina.

7.1.8. Glia

Based on previous results produced in our laboratory, activation of micro- and macroglia are typical features associated with PR death in Tvrm4 mice, coherently with what was reported in general for rd mutants. Active, amoeboid (IBA-1 positive) microglial cells are recruited in the outer retina and seen to phagocyte the nuclei of dying rods and cones from the very initial phases of PR degeneration and up to 1-week PI, the last time point examined. However, microglia in the inner retina typically maintain the inactive, quiescent form. Also, microglia are inactive and ramified in the peripheral, PR preserving areas of the retina (Gargini et al. 2017). Long after photo-induction (3 and 6 weeks PI) microglia are only found in ramified forms both in the outer and inner retina as well as the central and peripheral retina, indicating that PR degeneration as a process is complete and finished in the tissue. Indeed, morphological data confirms no extensions of the central, degenerated retinal area over time (Gargini et al. 2017).

Müller cells activate in parallel with PR demise. As early as 48 hours PI, these cells show the predicted upregulation of GFAP immunoreactivity and increased radial process thickness, which become more evident over time. These features are present throughout the photo lesioned area, corresponding to the central retina, but do not spread to the periphery, as seen on frozen, vertical sections (Gargini et al. 2017). Unlike microglia, 3 to 6 weeks PI Müller cells still show upregulation of GFAP, as shown for other models (Marc et al. 2003); however, in Tvrm4 mutants this state is definitely restricted to the central retinal area.

These results match perfectly previous reports on rd1 and rd10 mice, where retinal inflammation and activation of microglia precede or coincides with the peaks of PR death but attenuates thereafter (Roque et al., 1996; Gupta et al., 2003; Zeiss and Johnson, 2004; Zeng et al., 2005; Gehrig et al., 2007), with persisting Müller gliosis (Marc et al. 2003).

7.1.9. Future perspectives

Based on remodeling data obtained from adult Tvrm4 mice in the present study – confirming and expanding previous ones regarding other animal models of RP – we can now state with high certainty that rod-to-cone degeneration triggers morphological remodeling of inner retinal neurons first acting on components of the ON signaling pathway, as proven by dendritic retraction from RBC in the OPL and ON BC axonal ending shrinkage in the ON sublaminae of the IPL. In spite of that, electrical and chemical synaptic contacts in the IPL are highly preserved, although synaptic ribbons show some ultrastructural abnormalities. However, preliminary data from our TEM analysis show ultrastructural signs typical of autophagy and/or paraptosis (Wei et al., 2015), including the presence of swollen mitochondria with broken or diminished inner membrane system with clear signs of invaginations, numerous empty vacuoles as well as concentric multi-membrane compartments in the IPL of Tvrm4 mice 3 and 6 weeks PI.

Experimental evidence of autophagy in the IPL would suggest resistance of inner retinal neurons following PR death and loss of input from the outer retina, consequently indicating the possibility of reversing inner retinal remodeling e.g. by replacing dead PRs. Existing TEM data and specimens grant the possibility of further analysis; quantification of e.g. degenerating mitochondria by itself could provide indications about autophagy in the IPL. At the same time, a combined IHCH and Western Blot analysis of LC3-II and other autophagy related antibodies would be highly informative as well. Furthermore, engineering Tvrm4 mice expressing fluorescent marker proteins like GFP under the promoter of ON BC specific genes would allow single cell transcriptome analysis looking for autophagy-related expression patterns.

Tvrm4 mice also hold promising opportunities to test on adult animals the most up-to-date optogenetic tools targeting ON BCs, like ChR2 (Lagali et al., 2008; Macè et al., 2015), MAG_{460} (Gaub et al., 2014), ReaChR (Sengupta et al., 2016) or ChrimsonR (Klapoetke et al., 2014) to restore intrinsic photo sensibility of the tissue.

A recent study published in Nature by Jorstad et al., achieved for the first time Müller glia driven neuronal regeneration in adult mice by overexpressing Ascl1 (proneural transcription factor naturally upregulated in the Müller glia of zebrafish) together with a histone deacetylase, to block epigenetic inhibition of Müller glial neurogenic capacity probably taking place in adult mammals. Newly generated neurons only expressed markers of inner retinal cells but it is likely that further improvement of the technique will eventually allow to regenerate PRs by activating Müller cells (Jorstad et al., 2017). Tvrm4 mice, likely representing the best existing mouse model of RHO AD RP type B1, will be an ideal platform to test this regenerating approach.

7.2. P15 Tvrm4 mice

To investigate the impact of the age of phenotype onset on the severity of retinal remodeling, we chose to study Tvrm4 mice at the time of eye-opening (postnatal day 14-15). We aimed at comparing PR degeneration phenotype in three different cases:

1. Adult Tvrm4 mice: missense mutation in the rhodopsin gene with dominant inheritance pattern produced on a C57BL/6 (B6) mouse line background and activated in adult animals.
2. Rd10 and rd1 mice: missense and nonsense mutation respectively on the phosphodiesterase gene (*Pde6b*) with recessive inheritance pattern produced on a C57Bl/6 and C3H mouse lines backgrounds, respectively, and active from the beginning of retinal development.
3. Young Tvrm4 mice: activation of the mutation at a certain developmental stage, close to the time of eye-opening.

We designed our experiments in hope for finding common traits and symptoms of RP in mice with different ages of onset and different genetic backgrounds, which eventually would allow us to translate our results to human cases of RP with higher relevance.

First, one litter of Tvrm4 mice (N=6), heterozygous for the mutation, was induced at the age of P15, for 2 minutes at 12.000 lux (using the same protocol applied on adult mice). However, we failed to find any phenotype in all the eyes examined where PRs appeared fully preserved (data not shown).

The reasons why photo-induction in P15 old mice in vivo was not successful is not known. One reason could be an insufficient amount of (mutant) RHO present in immature ROS. Although the expression of RHO can be detected in the mouse retina as early as P6-7, the development of ROS and disc growth is completed only at P25 by reaching a mature length (*Carter-Dawson et. al. 1986*). Another, likely possibility is the difficulty to illuminate the back of the eye with adequate amounts of light, given the reduced size of the eye ball and unfavorable optics. A third, intriguing possibility is the occurrence of still unknown, neuroprotective mechanisms acting during development, which could contribute to prevent photoreceptor degeneration.

To rule out the possibility that the light used for the induction did not reach efficiently the retina of very young animals, due to the eye geometry, the experiment was repeated using an oxygenated and heated incubation chamber to photo-induce P15 eyecups ex vivo, upon removal of outer segments comprising cornea, iris and lens. Six hours after ex vivo photo-induction, visible signs of photoreceptor degeneration could be detected. We concluded that immature photoreceptors of Tvrm4 mice can be successfully irradiated and undergo light-induced degeneration if the radiation can reach the back of the eye at adequate intensity.

7.3. P19 Tvrm4 mice

To overcome age-limits, we chose to photo-induce mice aged P19 using an extended, 4 minutes light exposure at 12.000 lux, in vivo. A longer exposure maximizes the possibility of triggering the retinal phenotype in this mutant. As a result, 2 eyecups showed severe phenotype, 2 eyecups showed mild PR degeneration and 1 eyecup was not induced 1-week PI, which means, that unlike in the adults, the induced phenotype was far from being uniform in Tvrm4 youngsters. Another confusing phenotypical feature found in the peripheral retina of P19 animals, were abnormal PR rosettes surrounded by highly activated microglia.

These observations suggest a controversial evidence for susceptibility and sensitivity to light-damage in P19 Tvrm4 mice: heterogeneity in the rate of PR degeneration proposes that these animals are less vulnerable to photo-lesion, however, inflammation and rosettes in the retinal periphery, never seen in the adult mice, suggest opposite different type of vulnerability.

Non-uniform rate of PR degeneration may be a result of multiple developmental factors, like body mass, size and nutrition levels, as well as gender of the animals. Variability in the body indexes in a big litter of small rodents is a normal phenomenon, as maternal care depends on litter size (smaller litters get more maternal care) as well as the success in the competition for breastfeeding obviously depends on the fitness of the pups (Draper, 1968; Grota and Ader, 1969;

Grota, 1973). Since the 5 heterozygous mice used in this experiment were raised in a litter of 12 (the remaining 6 animals were either wild types or homozygous for the mutation and thus excluded from the experiment), they might have had variable body indexes. Hence, repeating the experiment while registering body indexes and genders of the pups would be necessary to test this hypothesis. Only a limited rate of second order neuron remodeling, like death of HCs, dendritic retraction of BCs and synaptic rearrangements in the OPL could be seen in P19 Tvrm4 mice, most probably due to incomplete PR degeneration in all cases examined. Whether this phenomenon is the result of yet unidentified, protective mechanisms in the healthy, developing retina jeopardizing successful photo-induction is subject of further research in our laboratory.

Photoreceptor rosette formation in the peripheral retina is not a commonly reported phenomenon in RP patients or rodent models. Rosettes in the central retina of RP patients with advanced retinal degeneration have been characterized in only three case reports, the latest of which was referring to a patient with autosomal dominant RP (Milam and Jacobson, 1990; To et al., 1996; Tulvatana et al. 1999). Spectral-domain optical coherence tomography (SD-OCT) has revolutionized our potentials in imaging and examining structural alterations in the retina driven by disease progression. Outer retinal tubulation (ORT) as a term was first used to define a SD-OCT observation of "circular or ovoid structures with hyper-reflective borders", seen predominantly in patients with neovascular age-related macular degeneration (AMD). The hyper-reflectivity is believed to be represented by malformed PR outer segments in ORT patches. Importantly, in this study ORT patches were recognized in areas of normal retinal thickness and were not observed in end-stage RP (Zweifel et al., 2009). However, based on former histopathologic research, ORT has been anticipated to assemble into rosette-like structures from degenerating PR cells due to a misguided reparative procedure, in which outward folding of the PR layer enables the formation of new lateral connections eventually reconstituting the inner segment – outer segment (IS/OS) junction (Curcio et al., 1996; Zweifel et al., 2009). Histopathologically, rosettes seen in mouse models with retinal degeneration correspond to ORTs seen with OCT (Fischer et al., 2009). Induced PR degeneration with RPE sparing in adult rats resulted in IS/OS malformation and migration of PR nuclei in a circular pattern producing rosette-like structures (Pittler et al., 1995). Yet, as reported by other studies, rosette formation was also observed in murine eyes and shown to promote PR survival in the absence of viable RPE (Ma and Streilein, 1998). Although based on these studies it is quite controversial whether rosette formation is primarily triggered by RPE or PR lesions, it is feasible to hypothesize that acute damage to either one could eliminate proper adhesion between photoreceptor outer segments and the RPE, which may then allow subsequent invagination of the ONL to occur.

Likewise, although we are currently uncertain about the fine details of the pathogenic mechanisms prominent in rosette or ORT patch formation, ORTs seem to represent a common pathway in numerous retinal disorders of variable etiologies (Goldberg et al., 2013).

8. CONCLUSIONS

High rate of BC survival despite regressive dendritic and axonal remodeling, considerable percentage of HC death, ultrastructural remodeling of ribbon synapses and preservation of higher order neurons found in Tvrm4 mutants coincide with previously described characteristics of RP rodent models. Hence, we conclude that these remodeling features are independent of the age of disease onset and the underlying genetic mutation and are true hallmarks of rod-cone dystrophies and as well as RP.

Increased density of RIBEYE and Cx36 positive puncta in the IPL suggests alterations of inner retinal circuitry. TEM analysis revealed abnormally globular synaptic ribbons in BC axonal endings, which might account for a denser staining of RIBEYE positive puncta. The fact that most of the ribbons were deformed and detached from the active zones, freely floating in the cytoplasm, suggests abnormalities of BC signaling caused by PR degeneration. On the other hand, an overall denser Cx36 staining in the IPL suggests an attempt of saving the flow of remnant visual information possibly driven by peripheral, PR preserving retinal areas.

The presence of highly hypertrophic DAC processes in the OPL at the site of PR death is probably in close correlations with gap-junction remodeling and the possible result of photo-triggered rod-cone dystrophy, whereas the entangled DNA filled bodies (possible leftovers of dead PRs) might be indicating direct contact of these cells to PRs.

In vivo photo-induction of Tvrm4 mice around the time of eye opening (P15 and P19) was possibly jeopardized by so far unidentified factors rescuing PRs from light induced degeneration, possibly repressing oxidative stress and inflammation. And yet, when PR degeneration was successfully initiated, albeit at reduced rate, in young animals, the fundamental features of the disease phenotype were similar to what found in the adults or in other RP mouse models. The reason of PR rosette formation surrounded by activated microglia in the retinal periphery is subject to further investigation.

Altogether, cell survival, fundamental architecture of the retina and synaptic circuitry in the IPL are well preserved in Tvrm4 mutants, even in retinal regions totally devoid of PRs. The finding that remodeling in adult Tvrm4 mice is by no means more severe than in developmental models of the disease provides encouraging support for implementing retinal repair strategies for human RP. Furthermore, the inducible phenotype in Tvrm4 mice is faithfully mimicking type B1 human RP with focal PR senescence and moderate speed of disease progression. Therefore, we conclude, that the Tvrm4 mouse, a novel rhodopsin mutant with autosomal dominant inheritance pattern, is a

valuable and representative model of human RP encouraging vision restoration through inner retinal intervention.

9. REFERENCES

Athanasiou, D., Aguila, M., Bellingham, J., Li, W., McCulley, C., Reeves, P. J., & Cheetham, M. E. (2018). The molecular and cellular basis of rhodopsin retinitis pigmentosa reveals potential strategies for therapy. Progress in Retinal and Eye Research, 62(July 2017), 1–23.

Applebury, M. L., Antoch, M.P., Baxter, L.C., Chun. L.L.Y., Falk, J.D., Farhangfar, F., Kage, K., Krzystolik, M.G., Lyass, L.A. and Robbins, J.T. (2000) The murine cone photoreceptor: a single cone type expresses both S and M opsins with retinal spatial patterning. Neuron 27, 513–523.

Awatramani, G.B., and Slaughter, M.M. (2000). Origin of transient and sustained responses in ganglion cells of the retina. J. Neurosci. 20, 7087–7095.

Barhoum R, Martınez-Navarrete G, Corrochano S, Germain F, Fernandez-Sanchez L, de la Rosa EJ, de la Villa P, Cuenca N. (2008) Functional and structural modifications during retinal degeneration in the rd10 mouse. Neuroscience155:698–713.

Barone, I., Novelli, E., Piano, I., Gargini, C. & Strettoi, E. (2012) Environmental Enrichment Extends Photoreceptor Survival and Visual Function in a Mouse Model of Retinitis Pigmentosa. Plos One 7.

Bavik, C., Henry, S. H., Zhang, Y., Mitts, K., McGinn, T., Budzynski, E., … Kubota, R. (2015). Visual cycle modulation as an approach toward preservation of retinal integrity. PLoS ONE, 10(5). https://doi.org/10.1371/journal.pone.0124940

Behnen, P., Felline, A., Comitato, A., Di Salvo, M. T., Raimondi, F., Gulati, S., … Fanelli, F. (2018). A Small Chaperone Improves Folding and Routing of Rhodopsin Mutants Linked to Inherited Blindness. IScience, 4, 1–19.

Bloomfield, S. A., & Völgyi, B. (2009). The diverse functional roles and regulation of neuronal gap junctions in the retina. Nature Reviews Neuroscience, 10(7), 495–506. https://doi.org/10.1038/nrn2636

Bloomfield, S. A., Xin, D. & Osborne, T. Light-induced modulation of coupling between AII amacrine cells in the rabbit retina. Vis. Neurosci. 14, 565–576 (1997).

Borowska, J., Trenholm, S., and Awatramani, G. B. (2011). An intrinsic neural oscillator in the degenerating mouse retina. J. Neurosci. 31, 5000–5012. doi: 10.1523/JNEUROSCI.5800-10.2011

Briscoe, A. D., Gaur, C., & Kumar, S. (2004). The spectrum of human rhodopsin disease mutations through the lens of interspecific variation. Gene, 332(1–2), 107–118.

Budzynski, E., Gross, A. K., McAlear, S. D., Peachey, N. S., Shukla, M., He, F., … Nishina, P. M. (2010). Mutations of the opsin gene (Y102H and I307N) lead to light-induced degeneration of photoreceptors and constitutive activation of phototransduction in mice. *Journal of Biological Chemistry*, *285*(19), 14521–14533. https://doi.org/10.1074/jbc.M110.112409

Burns ME. Deactivation Mechanisms of Rod Phototransduction: The Cogan Lecture. Investigative Ophthalmology & Visual Science. 2010;51(3):1283-1288. doi:10.1167/iovs.09-4366.

Busch, Eelco-M., Theo G.M.F. Gorgels, and Dirk Van Norren. 1999. “Filling-in after Focal Loss of Photoreceptors in Rat Retina.” Experimental Eye Research 68(4): 485–92. https://www.sciencedirect.com/science/article/pii/S0014483598906285.

Cao, Y., Pahlberg, J., Sarria, I., Kamasawa, N., Sampath, A.P., and Martemya- nov, K.A. (2012). Regulators of G protein signaling RGS7 and RGS11 deter- mine the onset of the light response in ON bipolar neurons. Proc. Natl. Acad. Sci. USA 109, 7905–7910.

Carter-Dawson LD, LaVail MM, Sidman RL (1978) Differential effect of the rd mutation on rods and cones in the mouse retina. Invest Ophthalmol Vis Sci 17:489–498.

Carter-Dawson, L., Alvarez, R.A., Shao-Ling Fong, Liou, G.I., Sperling, H.G. and Bridges, C.D.B. (1986) Rhodopsin, 11-cis Vitamin A and Interstitial Retinol-Binding Protein (IRBP) during Retinal Development in Normal and rd Mutant Mice. Developmental Biology 116,431-438

Chang, B., Hawes, N.L., Hurd, R.E., Davisson, M.T., Nusinowitz, S. and Heckenlively, J.R. (2002) Retinal Degeneration Mutants in the Mouse. *Volume 42, Issue 4, February 2002, Pages 517-525*

Chen, C. K., Burns, M. E., Spencer, M., Niemi, G. A., Chen, J., Hurley, J. B., … Simon, M. I. (1999). Abnormal photoresponses and light-induced apoptosis in rods lacking rhodopsin kinase. Proceedings of the National Academy of Sciences of the United States of America, 96(7), 3718–22. http://doi.org/10.1073/PNAS.96.7.3718

Cideciyan, A. V, Hood, D. C., Huang, Y., Banin, E., Li, Z. Y., Stone, E. M., … Jacobson, S. G. (1998). Disease sequence from mutant rhodopsin allele to rod and cone photoreceptor degeneration in man. *Proceedings of the National Academy of Sciences of the United States of America*, *95*(12), 7103–7108. https://doi.org/10.1073/pnas.95.12.7103

Clemson CM, Tzekov R, Krebs M, et al Therapeutic potential of valproic acid for retinitis pigmentosa British Journal of Ophthalmology 2011;95:89-93.

ClinicalTrials.gov. (2018). Long-term Follow-up Study in Subjects Who Received Voretigene Neparvovec-rzyl (AAV2-hRPE65v2). Available online at: https://clinicaltrials.gov/ct2/show/study/NCT03602820.

ClinicalTrials.gov. (2017). Trial of Oral Valproic Acid for Retinitis Pigmentosa (VPA). Available online at: https://clinicaltrials.gov/ct2/show/study/NCT01233609.

ClinicalTrials.gov. (2015). RST-001 phase I/II trial for advanced retinitis pigmentosa. Available online at: https://clinicaltrials.gov/ct2/show/study/NCT02556736.

Curcio C.A., Medeiros N.E., Millican C.L. Photoreceptor loss in age-related macular degeneration. Invest Ophthalmol Vis Sci. 1996;37(7):1236–49.

Damiani, D., Novelli, E., Mazzoni, F. and Strettoi, E. (2012), Undersized dendritic arborizations in retinal ganglion cells of the rd1 mutant mouse: A paradigm of early onset photoreceptor degeneration. J. Comp. Neurol., 520: 1406-1423. doi:10.1002/cne.22802

Demb, J. B., & Pugh, E. N. (2002). Connexin36 Forms Synapses Essential for Night Vision. Neuron, 36(4), 551–553. https://doi.org/10.1016/S0896-6273(02)01062-0

DeVries, S.H. (2000). Bipolar cells use kainate and AMPA receptors to filter visual information into separate channels. Neuron 28, 847–856.

Draper, D. D. 1968. Litter size, maternal behaviour and pup development in the rat. Ph.D. thesis, University of Tennessee

Dryja, T. P., & Li, T. (1995). Molecular genetics of retinitis pigmentosa. *Human Molecular Genetics*, *4* (suppl_1), 1739–1743. Retrieved from http://dx.doi.org/10.1093/hmg/4.suppl_1.1739

Eggers, E.D., and Lukasiewicz, P.D. (2011). Multiple pathways of inhibition shape bipolar cell responses in the retina. Vis. Neurosci. 28, 95–108.

Euler, T., Haverkamp, S., Schubert, T., & Baden, T. (2014). Retinal bipolar cells: Elementary building blocks of vision. *Nature Reviews Neuroscience*, *15*(8), 507–519. https://doi.org/10.1038/nrn3783

Fain, G. L. (2006). Why photoreceptors die (and why they don't). BioEssays, 28(4), 344–354. http://doi.org/10.1002/bies.20382

Fischer M.D., Huber G., Beck S.C., et al. Noninvasive, in vivo assessment of mouse retinal structure using optical coherence tomography. PLoS One. 2009;4(10):e7507.

Flock, T., Ravarani, C. N. J., Sun, D., Venkatakrishnan, A. J., Kayikci, M., Tate, C. G., … Babu, M. M. (2015). Universal allosteric mechanism for Gα activation by GPCRs. Nature, 524(7564), 173–179. https://doi.org/10.1038/nature14663

Gal, A., Apfelstedt-Sylla, E., Janecke, A. R., & Zrenner, E. (1997). Rhodopsin mutations in inherited retinal dystrophies and dysfunctions. *Progress in Retinal and Eye Research*, *16*(1), 51–79. https://doi.org/10.1016/S1350-9462(96)00021-3

Gargini, C. , Terzibasi, E. , Mazzoni, F. and Strettoi, E. (2007), Retinal organization in the retinal degeneration 10 (rd10) mutant mouse: A morphological and ERG study. J. Comp. Neurol., 500: 222-238. doi:10.1002/cne.21144

Gargini, C., Novelli, E., Piano, I., Biagioni, M., & Strettoi, E. (2017). Pattern of retinal morphological and functional decay in a light-inducible, rhodopsin mutant mouse. Scientific Reports, 7(1), 1–14. https://doi.org/10.1038/s41598-017-06045-x

Gaub, B. M., Berry, M. H., Holt, A. E., Reiner, A., Kienzler, M. A., Dolgova, N., … Isacoff, E. Y. (2014). Restoration of visual function by expression of a light-gated mammalian ion channel in retinal ganglion cells or ON-bipolar cells. *Proceedings of the National Academy of Sciences*, *111*(51), E5574 LP-E5583. Retrieved from http://www.pnas.org/content/111/51/E5574.abstract

Gehrig A, Langmann T, Horling F, Janssen A, Bonin M, Walter M, Poths S, Weber BH (2007) Genome-wide expression profiling of the retinoschisin-deficient retina in early postnatal mouse development. Invest Ophthalmol Vis Sci 48:891–900.

Ghinia MG., Novelli E., Sajgo S., Badea TC., Strettoi E. (2016) Brn3a and Brn3b knockout mice display unvaried retinal fine structure despite major morphological and numerical alterations of ganglion cells. J Comp Neurol. 2016 Jul 8. doi: 10.1002/cne.24072.

Ghosh KK, Bujan S, Haverkamp S, Feigenspan A, Wa¨ssle H. 2004. Types of bipolar cells in the mouse retina. J Comp Neurol 469:70–82. Erratum in: J Comp Neurol 476:202–203.

González, D. et al. Regulation of neuronal connexin-36 channels by pH. Proc. Natl Acad. Sci. USA 105, 17169–17174 (2008).

Goldberg NR, Greenberg JP, Laud K, Tsang S, Freund KB. Outer Retinal Tubulation in Degenerative Retinal Disorders. Retina (Philadelphia, Pa). 2013;33(9):1871-1876. doi:10.1097/IAE.0b013e318296b12f.

Goo YS, Ahn KN, Song YJ, Ahn SH, Han SK, Ryu SB, Kim KH. Spontaneous Oscillatory Rhythm in Retinal Activities of Two Retinal Degeneration (rd1 and rd10) Mice. Korean J Physiol Pharmacol. 2011 Dec;15(6):415-422. https://doi.org/10.4196/kjpp.2011.15.6.415

Grimes, W.N., Zhang, J., Graydon, C.W., Kachar, B., and Diamond, J.S. (2010). Retinal parallel processors: more than 100 independent microcircuits operate within a single interneuron. Neuron 65, 873–885.

Grota, L. J. 1973. Effects of litter size, age of young and parity on foster mother behaviour in Rattus norvegicus. Anim. Behav., 21, 78-82.

Grota, L. J. & Ader, R. 1969. Continuous recording of maternal behaviour in female rats. Anim. Behav., 17, 723-729.

Gupta N, Brown KE, Milam AH (2003) Activated microglia in human retinitis pigmentosa, late-onset retinal degeneration, and age-related macular degeneration. Exp Eye Res 76:463–471.

Hall M.O., Prieto, A.L., Obin, M.S., Abrams, T.A., Burgess, B.L., Heeb, M.J. and Agnew, B.J. Outer segment phagocytosis by cultured retinal pigment epithelial cells requires Gas6. Exp Eye Res 2001; 73: 509–520.

Hamel, C. (2006). Retinitis pigmentosa. *Orphanet Journal of Rare Diseases*, *1*(1), 1–12. https://doi.org/10.1186/1750-1172-1-40

Haq, W., Arango-Gonzalez, B., Zrenner, E., Euler, T. and Schubert, T. Synaptic remodeling generates synchronous oscillations in the degenerated outer mouse retina. Front. Neural Circuits, 05 September 2014 | https://doi.org/10.3389/fncir.2014.00108.

Hartong, D. T., Berson, E. L., & Dryja, T. P. (2006). Retinitis pigmentosa. *The Lancet*, *368*(9549), 1795–1809. https://doi.org/10.1016/S0140-6736(06)69740-7

Haverkamp S, Wa¨ssle H, Du¨bel J, Kuner T, Augustine GJ, Feng G, Euler T. (2005) The primordial, blue cone color system of the mouse retina. J Neurosci 25:5438–5445.

Haverkamp, S., Specht, D., Majumdar, S., Zaidi, N.F., Brandstätter, J.H., Wasco, W., Wässle, H. and tom Dieck, S. (2008) Type 4 OFF cone bipolar cells of the mouse retina express calsenilin and contact cones as well as rods. The Journal of Comparative Neurology 507:1087–1101.

He W, Cowan CW, Wensel TG. (1998) RGS9, a GTPase accelerator for phototransduction. Neuron. 1998; 20:95–102.

Heckenlively, J. R., Yoser, S. L., Friedman, L. H., & Oversier, J. J. (1988). Clinical findings and common symptoms in retinitis pigmentosa. *American Journal of Ophthalmology*, *105*(5), 504–511. https://doi.org/10.1016/0002-9394(88)90242-5

Herrera Hernández, M. G. (2017). Structural and functional effects of natural phenolic compounds on rhodopsin mutants associated with retinitis pigmentosa. *TDX (Tesis Doctorals En Xarxa)*

Herrmann, R., Heflin, S.J., Hammond, T., Lee, B., Wang, J., Gainetdinov, R.R., Caron, M.G., Eggers, E.D., Frishman, L.J., McCall, M.A., and Arshavsky, V.Y. (2011). Rod vision is controlled by dopamine-dependent sensitization of rod bipolar cells by GABA. Neuron 72, 101–110.

Hofmann, P. K., & Heck, M. (1996). Light-induced protein-protein interactions on the rod photoreceptor disc membrane. Biomembranes: A Multi-Volume Treatise, 2, 141–198. https://doi.org/10.1016/S1874-5342(07)80006-7

Huang L, Max M, Margolskee RF, Su H, Masland RH, Euler T. 2003. G protein subunit G gamma 13 is coexpressed with G alpha o, G beta 3, and G beta 4 in retinal ON bipolar cells. J Comp Neurol 455:1–10.

Hwa, J., Reeves, R.J., Klein-Seetharaman, J., Davidson, F. and Gobind Khorana, H. Structure and function in rhodopsin: Further elucidation of the role of the intradiscal cysteines, Cys-110, -185, and -187, in rhodopsin folding and function. PNAS March 2, 1999 96 (5) 1932-1935; https://doi.org/10.1073/pnas.96.5.1932.

Iannaccone, A., Man, D., Waseem, N., Jennings, B. J., Ganapathiraju, M., Gallaher, K., … Klein-Seetharaman, J. (2006). Retinitis pigmentosa associated with rhodopsin mutations: Correlation between phenotypic variability and molecular effects. *Vision Research*, *46*(27), 4556–4567. https://doi.org/10.1016/j.visres.2006.08.018

Jimenez AJ, Garcia-Fernandez JM, Gonzalez B, Foster RG (1996) The spatio-temporal pattern of photoreceptor degeneration in the aged rd /rd mouse retina. Cell Tissue Res 284:193–202.

Jones B.W., Kondo M., Terasaki H., Watt C.B., Rapp K., Anderson J., et al. Retinal remodeling in the Tg p3471 rabbit, a large-eye model of retinal degeneration. J Comp Neurol. 2011; 519:2713–33. [PubMed: 21681749]

Jones, B. W., Kondo, M., Terasaki, H., Lin, Y., McCall, M., & Marc, R. E. (2012). Retinal remodeling. *Japanese Journal of Ophthalmology*, *56*(4), 289–306.

Jones, B. W., Watt, C. B. and Marc, R. E. (2005), Retinal remodelling. Clinical and Experimental Optometry, 88: 282-291. doi:10.1111/j.1444-0938.2005.tb06712.x

Jorstad, N. L., Wilken, M. S., Grimes, W. N., Wohl, S. G., Vandenbosch, L. S., Yoshimatsu, T., … Reh, T. A. (2017). Stimulation of functional neuronal regeneration from Müller glia in adult mice. Nature, 548(7665), 103–107.

Jusuf, P.R., Haverkamp, S., and Gru¨ nert, U. (2005). Localization of glycine receptor alpha subunits on bipolar and amacrine cells in primate retina. J. Comp. Neurol. 488, 113–128.

Kijas, J. W., Cideciyan, A. V., Aleman, T. S., Pianta, M. J., Pearce-Kelling, S. E., Miller, B. J., … Acland, G. M. (2002). Naturally occurring rhodopsin mutation in the dog causes retinal dysfunction and degeneration mimicking human dominant retinitis pigmentosa. Proceedings of the National Academy of Sciences of the United States of America, 99(9), 6328–6333. http://doi.org/10.1073/pnas.082714499

Klapoetke, N. C., Murata, Y., Kim, S. S., Pulver, S. R., Birdsey-Benson, A., Cho, Y. K., et al. (2014). Independent optical excitation of distinct neural populations. Nat. Methods 11, 338–346. doi: 10.1038/nmeth.2836

Lagali PS, Balya D, Awatramani GB, Münch TA, Kim DS, Busskamp V, Cepsko CL and Roska B. (2008) Light-activated channels targeted to ON bipolar cells restore visual function in retinal degeneration. *Nature Neuroscience Volume 11, Number 6, June 2008*

Lakowski, J., Gonzalez-Cordero, A., West, E. L., Han, Y., Welby, E., Naeem, A., Blackford, S. J., Bainbridge, J. W., Pearson, R. A., Ali, R. R. and Sowden, J. C. (2015), Transplantation of Photoreceptor Precursors Isolated via a Cell Surface Biomarker Panel from Embryonic Stem Cell-Derived Self-Forming Retina. Stem Cells, 33: 2469-2482. doi:10.1002/stem.2051

Lampe, P. D. & Lau, A. F. Regulation of gap junctions by phosphorylation of connexins. Arch. Biochem. Biophys. 384, 205–215 (2000).

Lampe, P. D. & Lau, A. F. The effects of connexin phosphorylation on gap junctional communication. Int. J. Biochem. Cell Biol. 36, 1171–1186 (2004).

Lenzi, D. and von Gersdorff, H. (2001) Structure suggests function: the case for synaptic ribbons as exocytotic nanomachines. Bioessays 23, 831–840

Leskov, I. B., Klenchin, V. A., Handy, J. W., Whitlock, G. G., Govardovskii, V. I., Bownds, M. D., … Arshavsky, V. Y. (2000). The gain of rod phototransduction: Reconcillation of biochemical

and electrophysiological measurements. Neuron, 27(3), 525–537. http://doi.org/10.1016/S0896-6273(00)00063-5

Lin, B., Masland, R.H. and Strettoi, E. (2009) Remodeling of cone photoreceptor cells after rod degeneration in rd mice. Experimental Eye Research, Volume 88, Issue 3, March 2009, Pages 589-599

Lin, B., Martin, P.R., Solomon, S.G., and Gru¨ nert, U. (2000). Distribution of glycine receptor subunits on primate retinal ganglion cells: a quantitative analysis. Eur. J. Neurosci. 12, 4155–4170.

Lurtz, M. M. & Louis, C. F. Intracellular calcium regulation of connexin43. Am. J. Physiol. Cell Physiol. 293, 1806–1813 (2007).

Lyubarsky, A.L., Falsini, B., Pennesi, M.E., Valentini, P. and Pugh, E.N. (1999) UV- and Midwave-Sensitive Cone-Driven Retinal Responses of the Mouse: A Possible Phenotype for Coexpression of Cone Photopigments. Journal of Neuroscience 1 January 1999, 19 (1) 442-455; DOI: https://doi.org/10.1523/JNEUROSCI.19-01-00442.1999

Ma N., Streilein J.W. (1998) Contribution of microglia as passenger leukocytes to the fate of intraocular neuronal retinal grafts. Invest Ophthalmol Vis Sci.;39(12):2384–93.

Macé, E., Caplette, R., Marre, O., Sengupta, A., Chaffiol, A., Barbe, P., … Dalkara, D. (2015). Targeting Channelrhodopsin-2 to ON-bipolar Cells With Vitreally Administered AAV Restores ON and OFF Visual Responses in Blind Mice. Molecular Therapy, 23(1), 7–16. http://doi.org/10.1038/MT.2014.154

Machida, S. et al. 2000. "P23H Rhodopsin Transgenic Rat: Correlation of Retinal Function with Histopathology." Investigative Ophthalmology and Visual Science 41(10): 3200–3209.

Marc RE, Jones BW, Anderson JR, Kinard K, Marshak DW, Wilson JH, et al. Neural reprogramming in retinal degeneration. Invest Ophthalmol Vis Sci. 2007; 48:3364–71. [PubMed: 17591910]

Marc, R.E., Jones, B.W., Watt, C.B. and Strettoi, E. (2003) Neural remodeling in retinal degeneration. Progress in Retinal Eye Research, Volume 22, Issue 5, September 2003, Pages 607-655.

Masland, Richard H. 2012. "The Neuronal Organization of the Retina." Neuron 76(2): 266–80. http://dx.doi.org/10.1016/j.neuron.2012.10.002.

Mataruga A, Kremmer E, Müller F. 2007. Type 3a and type 3b OFF cone bipolar cells provide for the alternative rod pathway in the mouse retina. J Comp Neurol 502:1123–1137.

Maya-Vetencourt JF, Ghezzi D, Antognazza MR, Colombo E, Mete M, Feyen P, Desii A, Buschiazzo A, Di Paolo M, Di Marco S, Ticconi F, Emionite L, Shmal D, Marini C, Donelli I, Freddi G, Maccarone R, Bisti S, Sambuceti G, Pertile G, Lanzani G and Benfenati F. (2017) A fully organic retinal prosthesis restores vision in a rat model of degenerative blindness. Nature Materials, Vol16, June 2017.

Mazzoni F, Novelli E, Strettoi E. 2008. Retinal ganglion cells survive and maintain normal dendritic morphology in a mouse model of inherited photoreceptor degeneration. J Neurosci 28:14282–14292.

Mendes, H. F., Van Der Spuy, J., Chapple, J. P., & Cheetham, M. E. (2005). Mechanisms of cell death in rhodopsin retinitis pigmentosa: Implications for therapy. *Trends in Molecular Medicine, 11*(4), 177–185. https://doi.org/10.1016/j.molmed.2005.02.007

Menger, N., Pow, D.V., andWa¨ ssle, H. (1998). Glycinergic amacrine cells of the rat retina. J. Comp. Neurol. 401, 34–46.

Milam A.H., Jacobson S.G. Photoreceptor rosettes with blue cone opsin immunoreactivity in retinitis pigmentosa. Ophthalmology. 1990; 971620- 1631

Molnar, A., Hsueh, H.A., Roska, B., and Werblin, F.S. (2009). Crossover inhibition in the retina: circuitry that compensates for nonlinear rectifying synaptic transmission. J. Comput. Neurosci. 27, 569–590.

Moreno, A. P., de Carvalho, A. C., Verselis, V., Eghbali, B. & Spray, D. C. Voltage-dependent gap junction channels are formed by connexin32, the major gap junction protein of rat liver. Biophys. J. 59, 920–925 (1991).

Moreno, A. P., Rook, M. B., Fishman, G. I. & Spray, D. C. Gap junction channels: distinct voltage-sensitive and -insensitive conductance states. Biophys. J. 67, 113–119 (1994).

Morgans, C.W., Zhang, J., Jeffrey, B.G., Nelson, S.M., Burke, N.S., Duvoisin, R.M., and Brown, R.L. (2009). TRPM1 is required for the depolarizing light response in retinal ON-bipolar cells. Proc. Natl. Acad. Sci. USA 106, 19174– 19178.

Morrow EM., Furukawa T., Raviola E. and Cepko CL. (2005) Synaptogenesis and outer segment formation are perturbed in the neural retina of Crx mutant mice. BMC Neuroscience 2005. 6:5, https://doi.org/10.1186/1471-2202-6-5.

Nakase, T. & Nasus, C. C. G. Gap junctions and neurological disorders of the central nervous system. Biochim. Biophys. Acta 1662, 149–158 (2004).

Nikonov, S.S., Kholodenko, R., Lem, J. and Pugh, E.N. (2006) Physiological Features of the S- and M-cone Photoreceptors of Wild-type Mice from Single-cell Recordings. DOI: 10.1085/jgp.200609490 | Published March 27, 2006

Ohtsuka, T., Takao-Rikitsu, E., Inoue, E., Inoue, M., Takeuchi, M., Matsubara, K., … Takai, Y. (2002). Cast: a novel protein of the cytomatrix at the active zone of synapses that forms a ternary complex with RIM1 and munc13-1. The Journal of Cell Biology, 158(3), 577–590. http://doi.org/10.1083/jcb.200202083

Pang, J., Dai, X., Boye, S.E., Barone, I., Boye, S.L., Mao, S., Everhart, D., Dinculescu, A., Liu, Li, Umino, Y., Lei, Bo, Chang, Bo, Barlow, R., Strettoi, E., Hauswirth, W.W. 2011. “Long-Term Retinal Function and Structure Rescue Using Capsid Mutant AAV8 Vector in the Rd10 Mouse, a Model of Recessive Retinitis Pigmentosa.” Molecular Therapy 19(2): 234–42. https://www.sciencedirect.com/science/article/pii/S1525001616323802#bib10.

Parsons, T. and Sterling, P. (2003) Synaptic ribbon: conveyor belt or safety belt? Neuron 37, 379–382

Paulus, Y.M., Jain, A., Gariano, R.F., Stanzel, B.V., Marmor, M., Blumenkranz, M.S., Palanker, D. 2008. “Healing of Retinal Photocoagulation Lesions.” Investigative Ophthalmology and Visual Science 49(12): 5540–45.

Peracchia, C. Calcium effects on gap junction structure and cell coupling. Nature 271, 669–671 (1978).

Peracchia, C., Sotkis, A., Wang, X. G., Peracchia, L. L. & Persechini, A. Calmodulin directly gates chemical channels. J. Biol. Chem. 275, 26220–26224 (2000).

Peracchia, C., Wang, X., Li, L. & Peracchia, L. L. Inhibition of calmodulin expression prevents low-pH-induced gap junction uncoupling in Xenopus oocytes. Pflugers Arch. 431, 379–387 (1996).

Phillips, M. J., Otteson, D. C. and Sherry, D. M. (2010), Progression of neuronal and synaptic remodeling in the rd10 mouse model of retinitis pigmentosa. J. Comp. Neurol., 518: 2071-2089. doi:10.1002/cne.22322

Pittler S.J., Fliesler S.J., Fisher P.L., et al. In vivo requirement of protein prenylation for maintenance of retinal cytoarchitecture and photoreceptor structure. J Cell Biol. 1995;130(2):431–9.

Pugh, E. N., & Lamb, T. D. (1993). Amplification and kinetics of the activation steps in phototransduction. *BBA - Bioenergetics*, *1141*(2–3), 111–149. https://doi.org/10.1016/0005-2728(93)90038-H

Puthussery, T., Gayet-Primo, J., & Taylor, W. R. (2010). Localization of the calcium-binding protein secretagogin in cone bipolar cells of the mammalian retina. *Journal of Comparative Neurology*, *518*(4), 513–525. https://doi.org/10.1002/cne.22234

Puthussery, T., Gayet-Primo, J., Pandey, S., Duvoisin, R. M., and Taylor, W. R. (2009). Differential loss and preservation of glutamate receptor function in bipolar cells in the rd10 mouse model of retinitis pigmentosa. Eur. J. Neurosci. 29, 1533–1542. doi: 10.1111/j.1460-9568.2009.06728.x

Rakoczy, E. P., Kiel, C., McKeone, R., Stricher, F., & Serrano, L. (2011). Analysis of disease-linked rhodopsin mutations based on structure, function, and protein stability calculations. *Journal of Molecular Biology*, *405*(2), 584–606. https://doi.org/10.1016/j.jmb.2010.11.003

Raviola, E. & Dacheux, R. F. Excitatory dyad synapse in rabbit retina. Proc. Natl Acad. Sci. USA 84, 7324–7328 (1987).

Roque RS, Imperial CJ, Caldwell RB (1996) Microglial cells invade the outer retina as photoreceptors degenerate in Royal College of Surgeons rats. Invest Ophthalmol Vis Sci 37:196 –203.

Rose, B., Simpson, I. & Loewenstein, W. R. Calcium ion produces graded changes in permeability of membrane channels in cell junction. Nature 267, 625–627 (1977).

Sanyal S, Bal AK (1973) Comparative light and electron microscopic study of retinal histogenesis in normal and rd mutant mice. Z Anat Entwicklungsgesch 142: 219–238.

Sekirnjak, C., Hulse, C., Jepson, L. H., Hottowy, P., Sher, A., Dabrowski, W., et al. (2009). Loss of responses to visual but not electrical stimulation in ganglion cells of rats with severe photoreceptor degeneration. J. Neurophysiol. 102, 3260–3269. doi: 10.1152/jn.00663.2009

Sengupta, A., Chaffiol, A., Macé, E., Caplette, R., Desrosiers, M., Lampič, M., et al. (2016). Red-shifted channelrhodopsin stimulation restores light responses in blind mice, macaque retina and human retina. EMBO Mol. Med. 8, 1248–1264. doi: 10.15252/emmm.201505699

Shen, Y., Heimel, J.A., Kamermans, M., Peachey, N.S., Gregg, R.G., and Nawy, S. (2009). A transient receptor potential-like channel mediates synaptic transmission in rod bipolar cells. J. Neurosci. 29, 6088–6093.

Spray, D. C., Harris, A. L. & Bennett, M. V. Gap junctional conductance is a simple and sensitive function of intracellular pH. Science 211, 712–715 (1981).

Spray, D. C., Harris, A. L. & Bennett, M. V. Voltage dependence of junctional conductance in early amphibian embryos. Science 204, 432–434 (1979).

Stasheff, S. F. (2008). Emergence of sustained spontaneous hyperactivity and temporary preservation of OFF responses in ganglion cells of the retinal degeneration (rd1) mouse. J. Neurophysiol. 99, 1408–1421. doi: 10.1152/jn.00144.2007

Stasheff, S. F., Shankar, M., and Andrews, M. P. (2011). Developmental time course distinguishes changes in spontaneous and light-evoked retinal ganglion cell activity in rd1 and rd10 mice. J. Neurophysiol. 105, 3002–3009. doi: 10.1152/jn.00704.2010

Sterling, Peter, and Gary Matthews. 2005. "Structure and Function of Ribbon Synapses." Trends in Neurosciences 28(1): 20–29.

Strettoi, E., Dacheux, R. F. and Raviola, E. (1990), Synaptic connections of rod bipolar cells in the inner plexiform layer of the rabbit retina. J. Comp. Neurol., 295: 449-466. doi:10.1002/cne.902950309

Strettoi, E., Dacheux, R. F. and Raviola, E. (1994), Cone bipolar cells as interneurons in the rod, pathway of the rabbit retina. J. Comp. Neurol., 347: 139-149. doi:10.1002/cne.903470111

Strettoi, E., Raviola, E. and Dacheux, R. F. (1992), Synaptic connections of the narrow-field, bistratified rod amacrine cell (AII) in the rabbit retina. J. Comp. Neurol., 325: 152-168. doi:10.1002/cne.903250203

Strettoi, E. and Pignatelli, V. (2000), Modifications of retinal neurons in a mouse model of retinitis pigmentosa. PNAS September 26, 2000 97 (20) 11020-11025; https://doi.org/10.1073/pnas.190291097

Strettoi, E., Pignatelli, V., Rossi, C., Porciatti, V. and Falsini, B. (2003) Remodeling of second-order neurons in the retina of rd/rd mutant mice. Vision Research; Volume 43, Issue 8, April 2003, Pages 867-877. https://doi.org/10.1016/S0042-6989(02)00594-1

Strettoi, E., Porciatti, V., Falsini, B., Pignatelli, V. and Rossi, C. (2002) Morphological and Functional Abnormalities in the Inner Retina of the rd/rd Mouse. Journal of Neuroscience 1 July 2002, 22 (13) 5492-5504; DOI: https://doi.org/ 10.1523/JNEUROSCI.22-13-05492.

Taylor, W.R., and Smith, R.G. (2011). Trigger features and excitation in the retina. Curr. Opin. Neurobiol. 21, 672–678.

Tehan, B. G., Bortolato, A., Blaney, F. E., Weir, M. P., & Mason, J. S. (2014). Unifying Family A GPCR Theories of Activation. Pharmacology & Therapeutics, 143(1), 51–60. https://doi.org/10.1016/J.PHARMTHERA.2014.02.004

To, K.W., Adamian M., Jakobiec F.A., Berson E.L. Clinical and histopathologic findings in clumped pigmentary retinal degeneration. Arch Ophthalmol. 1996;114950- 955

tom Dieck, S. and Brandstätter, J. H. (2006) Ribbon synapses of the retina, Cell Tissue Res, 326:339–346, DOI 10.1007/s00441-006-0234-0

Toychiev, A.H., Ivanova, E., Yee, C.W. and Sagdullaev, B.T. 2013. "Block of Gap Junctions Eliminates Aberrant Activity and Restores Light Responses during Retinal Degeneration." The Journal of Neuroscience 33(35): 13972 LP-13977. http://www.jneurosci.org/content/33/35/13972.abstract.

Török, K., Stauffer, K. & Evans, W. H. Connexin 32 of gap junctions contains two cytoplasmic calmodulin- binding domains. Biochem. J. 326, 479–483 (1997).

Trenholm, S., Borowska, J., Zhang, J., Hoggarth, A., Johnson, K., Barnes, S., et al. (2012). Intrinsic oscillatory activity arising within the electrically coupled AII amacrine-ON cone bipolar cell network is driven by voltage-gated Na+ channels. J. Physiol. 590, 2501–25017. doi: 10.1113/jphysiol.2011.225060

Tulvatana W., Adamian M., Berson E.L., Dryja T.P. Photoreceptor Rosettes in Autosomal Dominant Retinitis Pigmentosa With Reduced Penetrance. Arch Ophthalmol. 1999;117(3):399–402. doi:10.1001/archopht.117.3.399

Van Essen, D.C. (2004). Organization of visual areas in macaque and human cerebral cortex. In The Visual Neurosciences, J.S. Werner, L.M. Chalupa, and C. Barnstable, eds. (Cambridge, MA: MIT Press).

Vardi N. 1998. Alpha subunit of Go localizes in the dendritic tips of ON bipolar cells. J Comp Neurol 395:43–52.

Venkatakrishnan, A. J., Deupi, X., Lebon, G., Heydenreich, F. M., Flock, T., Miljus, T., … Babu, M. M. (2016). Diverse activation pathways in class A GPCRs converge near the G-protein-coupling region. Nature, 536(7617), 484–487. https://doi.org/10.1038/nature19107

Wässle H, Puller C, Muller F, Haverkamp S. 2009. Cone contacts, mosaics, and territories of bipolar cells in the mouse retina. J Neurosci 29:106–117.

Wässle, H. (2004). Parallel processing in the mammalian retina. *Nature Reviews Neuroscience* volume 5, pages 747–757 (2004)

Wei, T., Kang, Q., Ma, B., Gao, S., Li, X., & Liu, Y. (2015). Activation of autophagy and paraptosis in retinal ganglion cells after retinal ischemia and reperfusion injury in rats. Experimental and Therapeutic Medicine, 9(2), 476–482.

Whitney I.E.; Raven M.A.; Ciobanu D.C.; Williams R.W.; Reese B.E. Multiple Genes on Chromosome 7 Regulate Dopaminergic Amacrine Cell Number in the Mouse Retina. Investigative Ophthalmology & Visual Science May 2009, Vol.50, 1996-2003. doi:10.1167/iovs.08-2556.

Witkovsky, P. & Dearry, A. Functional roles of dopamine in the vertebrate retina. Prog. Retin. Res. 11, 247–292 (1991).

Witkovsky, P. "Dopamine and retinal function." Doc Ophthalmol (2004) 108: 17. https://doi.org/10.1023/B:DOOP.0000019487.88486.0a

Wong, F. (1997). Investigating retinitis pigmentosa: A laboratory scientist's perspective. *Progress in Retinal and Eye Research*, *16*(3), 353–373. https://doi.org/10.1016/S1350-9462(96)00032-8.

Wu, S.M., Gao, F., and Maple, B.R. (2001). Integration and segregation of visual signals by bipolar cells in the tiger salamander retina. Prog. Brain Res. 131, 125–143.

Xin, D. & Bloomfield, S. A. Dark- and light-induced changes in coupling between horizontal cells in mammalian retina. J. Comp. Neurol. 405, 75–87 (1999).

Xin, D. & Bloomfield, S. A. Effects of nitric oxide on horizontal cells in the rabbit retina. Vis. Neurosci. 17, 799–811 (2000).

Zeiss CJ, Johnson EA (2004) Proliferation of microglia, but not photoreceptors, in the outer nuclear layer of the rd-1 mouse. Invest Ophthalmol Vis Sci 45:971–976.

Zeng HY, Zhu XA, Zhang C, Yang LP, Wu LM, Tso MO (2005) Identification of sequential events and factors associated with microglial activation, migration, and cytotoxicity in retinal degeneration in rd mice. Invest Ophthalmol Vis Sci 46:2992–2999.

Zweifel S.A., Engelbert M., Laud K., et al. Outer retinal tubulation: a novel optical coherence tomography finding. Arch Ophthalmol. 2009;127(12):1596–602.

10. ABBREVIATIONS, ACRONYMS AND SYMBOLS

Ab – antibody

AC – amacrine cell

ACSF – artificial cerebro-spinal fluid

AD – autosomal dominant

AMD – age-related macular degeneration

BC – bipolar cell

CaB5 – calcium binding protein 5

CAZ – cytomatrix of the active zone

CBC – cone bipolar cell

Csen – calsenilin

ER – endoplasmic reticulum

ERG – electroretinography/~gram

GABA – gamma aminobutyric acid

GC – ganglion cell

GCAP - Guanylate-cyclase activating protein 1

GCL – ganglion cell layer

GFAP – glial fibrillary acidic protein

GFP – green fluorescent protein

GluR – glutamate receptor

GPCR – G-protein coupled receptor

HC – horizontal cell

HCN4 – potassium/sodium hyperpolarization-activated cyclic nucleotide-gated channel 4

HPLC – high-performance liquid chromatography

ICCH – immunocytochemistry

IPL – inner plexiform layer

IS/OS – inner segment - outer segment

LFP – local field potential

MEA – multi-electrode array

NK3R – neurokinin B receptor

NO – nitric oxide

ONL – outer nuclear layer

OPL – outer plexiform layer

ORT – outer retinal tabulation

PBS – phosphate buffered saline

PDE – cGMP-phosphodiesterase

PI – post-induction

PKARIIβ – protein kinase A receptor subunit IIβ

PKCα – protein kinase C alpha

PR – photoreceptor

R* – activated rhodopsin or metarhodopsin II

RBC – rod bipolar cell

RCS – Royal College of Surgeon

RGC – retinal ganglion cell

RGS – regulator of G-protein signaling

rho – rhodopsin gene

RHO – rhodopsin protein

ROS – rod outer segments

RP – Retinitis Pigmentosa

RPE – retinal pigmented epithelium

SCGN - secretagogin

SD-OCT – spectral-domain optical coherence tomography

TEM – transmission electron microscopy

TVRM – Translational Vision Research Models

Tvrm4 – TVRM number 4 mice

WT – wild type

11. ACKNOWLEDGEMENTS

First and foremost, I owe endless gratitude to my tutor and supervisor, Dr. Enrica Strettoi, who supported my PhD studies from the first day to the last, provided me this extremely important and interesting PhD project, helped me developing my skills in countless laboratory techniques and introduced me to the most renowned and knowledgeable scientists of the retinal research field at the most reputed international conferences.

I am similarly grateful to the members of the Strettoi lab, my fellow PhD student, Martina Biagioni and our omniscient laboratory technician and research assistant, Elena Novelli, who provided technical and emotional support during this project.

I would like to express my gratitude to the switchBoard Innovative Training Network funded by the European Commission's Horizon 2020 program under the Marie Sklodowska Curie Actions for elevating our PhD program to the highest quality. Special thanks to our Scientific Coordinator, Prof. Thomas Euler and to our Project Manager, Dr. Michaela Bitzer, who have been working extremely hard on organizing and executing all the meetings and training events this project had to offer.

I would like to thank Prof. Karin Dedek for hosting me in her lab during my secondment in Oldenburg, for the brainstorming together with Prof. Ulrike Janssen-Bienhold and for suggesting me experiments focusing on dopaminergic amacrine cells based on my findings about gap junctions. At the same place I am grateful to Shubhash Chandra Yadav (Prof. Karin Dedek's switchBoard PhD student) for teaching me the basics of neurobiotin cell injections under visual control in mouse retinal whole-mounts.

I am similarly thankful to Dr. Günther Zeck, Prof. Thomas Euler and Dr. Timm Schubert for hosting me in their laboratories during my secondment in Reutlingen and Tübingen. I am also grateful to Prerna Srivastava (Prof. Thomas Euler's switchBoard PhD student) and Michael Power (PhD student in the Euler lab) for their demonstrations on glutamate and calcium imaging with two-photon microscopy and to Meng-Jung Lee (Dr. Günther Zeck's switchBoard PhD student) for her valuable collaboration with our lab doing MEA recordings.

I would like to thank Prof. Claudia Gargini and Dr. Ilaria Piano for granting access to their lab and devices during MEA recordings and their professional help in brainstorming and troubleshooting during the experiments.

I thank Antonio Falasconi very much for his time and energy in collaborating with me on the developing Tvrm4 mouse experiments and image acquisitions.

Last but not least, I am most grateful to my loving husband, Tamás Czimmermann, who has been encouraging me and supporting me in all possible ways during this PhD. I couldn’t have done this without him!